SLOSHING PHENOMENA IN WATER RESERVOIR TANKS DUE TO LONG PERIOD-LONG DURATION EARTHQUAKE GROUND MOTIONS

DOCTORAL DISSERTATION

SLOSHING PHENOMENA IN WATER RESERVOIR TANKS DUE TO LONG PERIOD-LONG DURATION EARTHQUAKE GROUND MOTIONS

Ali VAKILAZADSARABI

July 2014

博　士　論　文

SLOSHING PHENOMENA IN WATER RESERVOIR TANKS DUE TO　LONG PERIOD-LONG DURATION EARTHQUAKE GROUND MOTIONS

長周期，長継続時間地震動による貯水槽のスロッシング現象に関する研究

金沢大学大学院自然科学研究科

環境科学専攻

環境計画講座

Student registration No.: 1123142414

Name: Ali VAKILAZADSARABI

Supervisor: Prof. Masakatsu MIYAJIMA

SUMMARY

There are a large number of storage tanks around the world, most of which are used as water and oil storage facilities. Different configurations of liquid storage tanks have been constructed. However, ground supported, rectangular tanks are more numerous than any other type because of their simplicity in design and construction. These structures play an important role in municipal water supply and firefighting systems. They can be easily constructed in different sizes to fulfill the capacity requirements. Rectangular tanks may be made of either concrete or steel.

Many storage tanks are considered as essential facilities and are expected to be functional after severe earthquakes. This is partly due to the need for water to extinguish fires that usually occur during such earthquakes.

The structural design criteria of liquid containing structures against earthquake are different from those of general building structures. Tanks require serviceability limit states such as leakage, deflection, and durability limit, due to the nature of their use.

Only few guidelines are presently available for earthquake-resistant design of liquid storage tanks. In addition, parts of these guidelines are not in full consistency with the rest. Currently, ACI 350.3-06 standard in conjunction with ASCE 7-05 and ACI 371R-08 are used for seismic design of tanks. Most of the current codes and standards have adapted Housner's method (Housner, 1957; 1963) for seismic analysis and design of tanks. There are some debates that the corresponding available guidelines are inaccurate in terms of the seismic induced loads on the tank wall which can consequently affect the required section properties of the earthquake-resistant structural system.

Most of the current codes including ACI 350.3-06 assume a rigid wall boundary condition in estimating the hydrodynamic forces acting on the tank wall. However, tank wall flexibility could increase the hydrodynamic pressure significantly as compared to the rigid wall assumption. As a result, more investigation regarding the effect of wall flexibility on seismic behavior of cylindrical liquid-filled tanks seem essential.

The poor seismic performance of both steel and concrete ground-supported water tanks under earthquake ground motions has been observed in major past earthquakes. In regions with the high seismic intensity many tanks have been severely damaged and some have collapsed with terrible outcomes. For example, severe damages suffered during the 1933 Long Beach, 1952 Kern County, 1964 Alaska, 1964 Niigata, 1966 Parkfield, 1971 San Fernando,1978 Miyagi prefecture, 1979 Imperial County, 1983 Coalinga, 1994

Northridge and 1999 Kocaeli earthquakes which revealed a complex behavior of ground-supported liquid storage tanks during seismic motions (Rinne (1967), Shibata (1974), Kono (1980), and Sezen and Whittaker (2006)).

This weakness in seismic performance was also observed among water tanks. As, for example, one can refer to the poor performance of some water tanks having reinforced concrete shaft-type supports during the 2001 Bhuj (Rai (2002)) and the 1997 Jabalpur (Rai et al. (1997)) earthquakes in India. In the Bhuj earthquake, three elevated water tanks collapsed completely, and many more were damaged severely. Similar damage was also observed in the Jabalpur earthquake. Reviewing the available literature, one can say that little effort has been made to better identify the dynamic behavior of elevated tanks.

The reported damage due to previous seismic events could have happened due to the following three reasons:

1) Coupled motion of the tank shell and stored liquid due to the short-period component of the seismic wave. This behavior is referred to as bulging. Under such vibration, a large part of the stored liquid acts as inertial mass with a period much shorter than the sloshing natural period. Tank walls are expected to be subjected to considerable inertial force and dynamic fluid pressure as a result of this type of vibration.

2) Liquid sloshing due to the long-period component of the seismic wave. Sloshing response in tanks may have a long natural period of several seconds to a few tens of seconds. This phenomenon may result in highly localized pressure on the body of the tank, substantial uplifting pressure on the tank roof or may cause spillover of stored liquid in open top tanks. Sloshing response in tanks particularly depends on the tank geometry, dimensions and dynamic characteristics of the ground motion.

3) Loss of soil bearing capacity as a result of liquefaction which in turn could result in non-uniform settlement of the tank foundation.

The conventional method for earthquake-resistant design of water tanks is to increase the strength of the structure so that it can tolerate the design earthquake safely. As a result of this strengthening, higher seismic forces will be applied to the structure. Contrarily, the effect of seismic input can be significantly reduced using Menshin (earthquake reduction) method (Kumieda (1976), MITI (1980), and Aoyagi and Shiomi (1985)). The Menshin method is a technique for reducing the amplitude of seismic vibrations being exerted on the structure. Considering the large number and size of liquid storage tanks, any safe reduction in structural material results in economic benefit. In the Menshin technique, safety of the structure is ensured through adjusting the dynamic properties of the structure

properly. This could be implemented by either one or combination of the following methods:

1) “Natural period adjustment method” in which the seismic response of the structure is reduced by increasing its natural period far beyond the predominant periods of the input earthquake. This may be accomplished by either mounting the structure on certain flexible mounts such as elastomeric bearings or by making alterations in structural configuration/geometry leading to a more flexible structure design.

2) “Energy dissipation method” in which the input seismic energy is absorbed by means of energy absorbing devices attached to the structure. Devices such as lead-rubber bearings, viscous dampers, or friction dampers may be used for this purpose.

3) “Isolation method” in which the structure is decoupled from the ground by means of insulators. The structure may be free to slide easily if mounted on low friction pads. Isolation could be implemented using fluids (floating type), sliding plates, or different types of bearings.

To find out the real behavior of fluid-structure in tanks, appropriate evaluation of the dynamic characteristics of ground motion and structure is essential. It is also necessary to employ a highly accurate method of dynamic analysis. In this study rigorous finite element method (FEM) and smoothed particle hydrodynamics (SPH) to simulate the precise three-dimensional behavior of the tanks involving nonlinear behavior of devices is used. Using these techniques, one can therefore estimate the seismic response of tanks taking into account the long period-long duration ground motions in detail.

The main challenge in predicting the seismic behavior of liquid-filled structures are the identification of the vibration response of the tank taking into account the fluid-structure interaction (FSI). A dynamic study of such tanks must allow for the motion of the water relative to the tank, as well as the motion of the tank relative to the ground. In this study, different numerical techniques are employed for dynamic analysis of fluid domain.

For tanks which are closed and fully filled with water or are completely empty, the behavior of the tank may be well estimated as a one-mass system. However, usually the tanks are partially filled with water. In this case, the tank has a free water surface and thus, there will be the sloshing of the water free surface during a seismic motion, which makes the behavior of the tank-liquid system a complicated coupled problem. In this case, the dynamic behavior of the tank may be quite different. For certain proportions of the tank-liquid system, the response of the system is dominated by the sloshing of the water, on the other hand, there are other preparations that the sloshing may have minor contributions in

response. Therefore, an understanding of the seismic behavior of liquid-filled tanks requires an understanding of the hydrodynamic pressures and forces associated with the oscillating water. These pressures and forces depend on the characteristics of the ground motion, the properties of the contained liquid, and the geometrical and physical properties of the tank itself.

In this study, the numerical techniques are used to investigate the seismic response of ground-supported as well as water tanks during long period-long duration ground motions. The results of this research will provide some useful information regarding the actual behavior of sloshing phenomena in tanks under seismic motions. This study will also lead to some recommendations for more accurate seismic analysis and design of water tanks.

ACKNOWLEDGMENTS

None other than my advisor, Professor Masakatsu Miyajima, can top the list of people I would like to take the opportunity here to thank. He accepted me into his environment and guided me through with his unlimited patience and energy. His support, guidance, and advice have been invaluable and deserve a special recognition. Thank you for your continuous support and advice throughout the past years. It has been an extremely educational and rewarding experience. I have enjoyed the enthusiasm and energy that you have brought towards all aspects of my life at Kanazawa University. I have enjoyed working with you tremendously and I hope we will continue to do so for years to come.

I am also very grateful to my dear professors in the Earthquake Engineering laboratory; Dr. Ikemoto and Dr. Murata. It has been a privilege to have all of them participated in this important part of my life's work. You have been sources of inspiration and support in various stages of my dissertation. Without your suggestions, timely advice, and comprehensive understanding of various aspects of my problems, my work would not have taken this shape and direction.

I would like also to thank committee members of this dissertation: Professors Masakatsu Miyajima, Ryoko Ikemoto, Takehisa Saito and Toshikazu Ikemoto from Kanazawa University, and Professor Junji Kiyono from Kyoto University for their critical reading and helpful argue.

Special words of thanks apply to my dear friend, Mr. Yavar Ghasempour for his invaluable help in the FEM code analysis and my dear uncle Mr. Vahid Hamdipour for always taking time to discuss about my research, my results, and our lives.

Thanks are also to Kanazawa University and JGC Company for providing the financial support during my study in Kanazawa University.

My admiration and gratitude go out to my family for supporting my study and encouragement throughout my life. I am grateful for their unfailing love and support that has been very rewarding. I attribute my success to their reassuring love and sacrifice.

Thanks are also to Dr. Abdolhossein Fallahi and Dr. Mohammad Hossein Erami for introducing me to Professor Miyajima and supporting me during my studies in Kanazawa University.

STUDY OF SLOSHING PHENOMENA IN WATER RESERVOIR TANKS DUE TO LONG PERIOD-LONG DURATION EARTHQUAKE GROUND MOTIONS

TABLE OF CONTENTS

List of Figures

List of Tables

1. INTRODUCTION

1.1. General remarks

One of the critical lifeline structures which have become widespread using during the recent decades is liquid storage tanks. These structures are extensively used in water supply facilities, oil and gas industries and nuclear plants for storage of a variety of liquid or liquid-like materials such as oil, liquid natural gas (LNG), chemical fluids and wastes of different forms. Problems associated with liquid tanks involve many fundamental problems. The calculation of hydrodynamic forces on the wall of vibrating liquid tanks is an important issue of safeguarding the structural integrity of industrial tanks and vessels.

Sloshing phenomena have caused significant damages on these vital structures in previous seismic events. In addition, tanks rule is increasing on human life, so researchers attempt to set accurate analysis methods and safe design solutions for fluid tanks. This chapter delivers a brief review on outstanding relevant works, and by summarizing their results, concludes with some outlines for new studies followed by the present study.

In this chapter an extensive literature review on dynamic response of liquid containing structures is presented. In Section 1.2 seismic performance of liquid storage tanks and associated damage types suffered during actual seismic events is discussed. Section 1.3 reviews and summarizes the available literature on seismic response of liquid storage tanks. The significant contributions made by previous researchers are also explained. An overview on existing codes, standards, and guides used in design of liquid storage tanks along with a literature review on application of seismic isolation to liquid storage tanks are provided in Section 1.4.

1.2. Earthquake damage to liquid storage tanks

There are frequent reports regarding the damage to liquid storage tanks due to previous earthquakes in the literature. For instance, there were heavy damages to both concrete and steel storage tanks during the strong seismic events such as 1933 Long Beach, 1952 Kern County, 1964 Alaska, 1964 Niigata, 1966 Parkfield, 1971 San Fernando, 1978 Miyagi prefecture, 1979 Imperial County, 1983 Coalinga, 1994 Northridge, and 1999 Kocaeli earthquakes (Rinne (1967), Shibata (1974), Kono (1980), Manos and Clough (1985), and Sezen and Whittaker (2006)). Severe damage levels were also observed in elevated water tanks during the 1960 Chilean as well as the 1997 Jabalpur (Rai et al. (1997)) and 2001 Bhuj (Rai (2002) and Dutta et al. (2009)) earthquakes in India. During the Bhuj

earthquake, many elevated tanks suffered severe damages in terms of flexural cracks in the circumferential direction in their supporting shafts near the base. Three elevated water tanks located in the highest intensity shaking zones also collapsed. Anshel (1999) has also reported heavy damages to cylindrical buried concrete tanks due to the 1995 Kobe earthquake. An underground concrete tank was also damaged severely in the form of the collapse of the wall during the 1971 San Fernando earthquake (Jennings (1971)).

Failure mechanism of liquid storage tanks depends on different parameters such as construction material, tank configuration, tank type, and supporting mechanism. Reported damage to liquid containing structures (LCS) during past earthquakes fall into one or more of the following categories:

1) Buckling of the shell caused by excessive axial compression of the shell structure due to exerted overturning moment (elephant-foot buckling)

2) Deformation, cracks and leakage inside shell

3) Damage to the roof or the upper shell of the tank, due to sloshing of the upper portion of the liquid contained in tanks with insufficient free board provided between the liquid free surface and the roof

4) Spillover of the stored liquid

5) Failure of piping and other accessories connected to the tank because of the relative movement of the flexible shell

6) Damage to the supporting structure in elevated water tanks

7) Damage to the anchor bolts and the foundation system

8) Failure of supporting soil due to over-stressing

In the 1964 Niigata earthquake, several damage modes including damage modes 3 and 4 due to excessive sloshing, mode 8 due to liquefaction of the supporting soil as well as damage modes 7 and 5 became prominent.

In the 1964 Alaska and 1971 San Fernando earthquakes, the lower part of the side shell bulged all along the perimeter as a result of mode 1 (elephant-foot buckling). This buckling type damage generally happens due to the excessive overturning moment generated during the seismic event.

In cases where the tank contains hazardous materials, liquid spillover (damage mode 4) and fire subsequent to a major earthquake may result in even more severe damage than the earthquake itself. The extensive uncontrolled fire eruption during the Niigata earthquake at Showa Petroleum blazed for about 15 days, resulting in the main destruction of the plant and residential apartments (Niigata Nippo Co. (1964)). The

Niigata and Alaska earthquakes of 1964 resulted in considerable loss in the petroleum storage tanks. This significant loss attracted many practicing engineers and researchers to further investigate the seismic behavior of liquid storage tanks, especially when the stored liquid is a hazardous material such as petroleum.

As an example of damage mode 4, one can mention oil spill over into the harbor that happened to the Sendai Refinery of Tohoku Petroleum Company during the 1978 Miyagi earthquake (Hazardous Material Technology Standards Committee: Fire Defense Agency (1979)).

During the Northridge earthquake main lifeline facilities of the Los Angeles area experienced severe damage. Five steel tanks were also damaged in the San Fernando Valley area. Buckling was the prominent form of damage in all of the damaged tanks. Several other tanks also suffered roof collapse due to the excessive sloshing of the stored liquid (Lund (1996)).

It is important to note that the damage mode in concrete tanks is different from that of steel tanks. Elephant-foot buckling, anchorage system failure, and sloshing damage to the roof and upper shell of the tank are the most common damages in steel tanks (see Figure 1.1).

In tanks found in practice, full base anchorage is not always a possible or economical alternative. Therefore, many tanks are either unanchored or partially anchored at their base. If the tank is not rigidly anchored to the ground, the generated overturning moment due to earthquake may be large enough to result in lift-off of the tank base. As the tank base falls back down after lift-off, high compressive stresses are generated in the wall near the base leading to elephant-foot wall buckling. This mode of damage is more common in steel tanks since they are generally more flexible than concrete tanks.

Some studies show that base lift-off in tanks having flexible soil foundations does not cause high axial compressive stresses in the tank wall. As a result, unanchored tanks flexibly supported at their base are less susceptible to elephant-foot buckling mode, but are more susceptible to uneven settlement of the foundation (Malhotra (1995) and Malhotra (1997A)).

On the other hand, damage mode 2 is the most common type of damage in concrete tanks. Stresses caused by large hydrodynamic pressures together with the additional stresses resulted from the large inertial mass of concrete could cause cracking, leakage and ultimately failure of the tank. That is why the design criteria for concrete tanks are based on crack control.

It is worth noting that elevated water tanks are very susceptible to seismic excitations because of the concentrated large mass located at top of the shaft structure. As a result, strong lateral seismic motions may result in large tensile stresses on one side of the concrete shaft section which may eventually lead to severe cracking or even collapse of the concrete pedestal.

As mentioned before, many elevated tanks collapsed during the 1960 Chilean, 1997 Jabalpur and 2001 Bhuj earthquakes since insufficient reinforcement was provided in the shaft section.

(a) 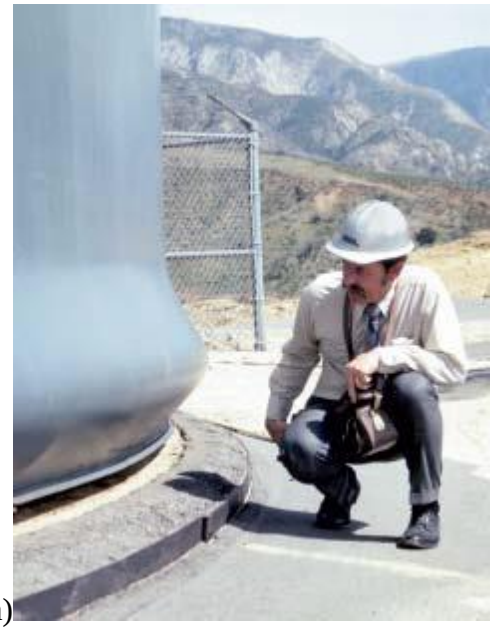 (b) 

(c) 

Fig. 1.1. Common damage modes: (a) Elephant-foot buckling, (b) Inelastic stretching of an anchor bolt at the tank base (c) Sloshing damage to the upper shell of the tank (adapted from Malhotra et al. (2000) and Malhotra (2000))

The significance of preventing such damages has led to a great deal of research to be carried out on dynamic behavior of such structures. These research studies could result in a better comprehension of the part of complicated behavior of liquid containing structures under long period seismic excitations.

1.3. A brief review of studies on response of water tanks subjected to sloshing phenomena

In the last four decades, many researchers have studied on the sloshing problem. And herein, studies with the most advantageous modeling methods and distinguished findings about the most influencing parameters of sloshing phenomena on fluid tanks are introduced. In addition, their most considerable assumptions, effective shortcomings and progressive results are presented.

1.3.1. Long period & long duration ground motions

Previously, most structures in earthquake-prone regions were low-profile structures, and so relatively short-period (1 s or shorter) ground motions, with which these structures might be resonant, were important. However, considering the increasing number of large structures, such as high-rise buildings, storage tanks, suspension bridges, offshore oil drilling platforms, and recent base-isolated structures, long-period (1 to 10 s or longer) ground motions have been increasingly important (e.g., Kanamori 1979; Fukuwa 2008). One of the worst examples of destruction caused by long period ground motion happen in Mexico City, close to another long period ground motion in this area the 1985 Michoacan earthquake (MW= 8.0; e.g., Beck and Hall 1986). The other one is the 2003 Tokachi-Oki earthquake (MW=8. 3) that occurred in Hokkaido, Japan (e.g., Koketsu et al. 2005).

The 2003 Tokachi-Oki earthquake was the first M 8-class event to be recorded by the Japanese nationwide strong ground motion seismograph networks, K-NET and KiK-net. It was thus the first time that large-amplitude long-period ground motions, which are a characteristic of large earthquakes, were recorded at a high station density in Japan. The resulting dataset makes it possible to study the detailed features of shaking, such as the spatial variation in amplitudes of long-period strong ground motions.

The most important procedures issued for this phenomenon considering long period-long duration ground motions are as follows:

Hanks (1975)

Hanks recovered 234 components of long-period ground motion in the source region of the 1971 San Fernando earthquake (MW=6.6), and the neighboring Los Angeles basin in California. He coined the term “long-period strong ground motion” in this paper (Zama

1993). Long-period ground motions are caused by the specific characteristics in the magnitude of the earthquake, epicenter location and geological structure through which seismic waves propagate. Large subduction-zone earthquakes and moderate to large crustal earthquakes can generate far-source long-period ground motions in distant sedimentary basins with the help of path effects. Near-fault long-period ground motions are generated, for the most part, by the source effects of forward rupture directivity. Far source long-period ground motions consist primarily of surface waves with longer durations than near-fault long-period ground motions.

Shima (1970)

The predominant period of long-period strong ground motion can vary between earthquakes, meaning that it is necessary to consider the source and path effects as well as local site effects in the prediction of predominant periods of such ground motions at a certain site. Far-source long-period ground motion was identified, for the first time in Japan, in seismograms of the 1968 Tokachi-Oki earthquake (MW=8.2) observed with large amplitudes and a predominant period of 2.5 s at Hachinohe, northeastern Japan. They were also observed by strong motion seismographs installed in the first super high-rise building in Japan. This building was located in Tokyo, 650 km from the earthquake source.

Trifunac and Brune (1970)

Trifunac and Brune observed long period ground motion in distant seismograms of the 1940 Imperial Valley earthquake (MS=7.1) in California. Both the Japanese and Californian authors attributed these far-source long-period ground motions of regional surface waves. The most obvious difference is the duration of ground motion. The far-source long-period ground motions continue for 1 min or longer, whereas the near-fault long period ground motions last only for 10 to 20 s.

Koketsu et al. (2005)

The worst example of destruction caused by long period ground motion occurred in Mexico City, 400 km from the 1985 Michoacan earthquake (MW= 8.0; e.g., Beck and Hall 1986). Another example is the 2003 Tokachi-Oki earthquake (MW=8.3) that occurred in Hokkaido, Japan.

Murata and Miyajima (2008)

Murata and Miyajima have considered that one of the causes of the unusual phenomena seems to be sloshing of water in receiving water tank. If sloshing of water in many

receiving water tanks occurred simultaneously, an abrupt increase in flow rate and a decrease in water pressure may be occurring. Occurrence of sloshing of water in receiving water tank depends on the dimensions of receiving water tank and the height of water in the tank. Murata and Miyajima have investigated dimensions of receiving water tank in a water distribution block of Osaka City and estimated the natural period of sloshing of the water. Figure 2.3 shows the cumulative percentage of natural periods of water in receiving water tank in case that the height of water is 3/4 and 1/2 of the height of the water tank. The height of water is variable and depends on the use of water. The natural period of sloshing is more than 1.0 second of more than 80% of the water tank in the direction of the long side of the water distribution block in Osaka City.

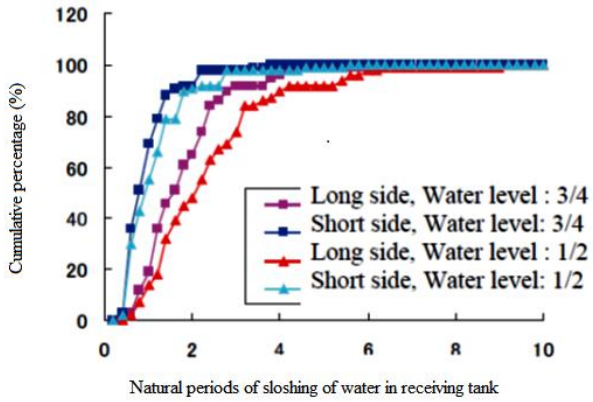

Fig. 2.3 Cumulative percentage of natural periods of water in receiving water tank

Ohta and Zama (2005)

The generation of long-period ground motion can be identified based on damage to large tanks. This damage is caused primarily by sloshing of the liquid inside the tanks. Because the excitation of liquid sloshing appears to require long duration seismic ground motion, it can be linked to far-source long-period ground motion. They documented 14 cases of tank damage because of liquid sloshing (Table 1.1).

Table.1.1.Tank damages due to liquid sloshing

Earthquake	Year	MW	Damage	Reference
Kanto	1923	7.9	6,000 t oil tank	Hirano (1982)
Long Beach	1933	6.2	Water tank	Steinbrugge (1970)
Kern County	1952	7.5	Oil tanks	Steinbrugge and Moran (1954)
Alaska	1964	9.2	Many oil tanks, fires	Rinne (1967)
Niigata	1964	7.6	Many oil tanks, fires	FDMA (1965)
Central Chile	1965	7.1	Oil tanks	Shibata (1974)
San Fernando	1971	6.6	Oil tanks	Shibata (1974)
Miyagi-oki	1978	7.4	Oil tanks	FDMA (1979)
Imperial Valley	1979	6.5	Oil tanks	Horoun (1983)
Coalinga	1983	6.2	Many oil tanks	Manos and Clough (1985)
Japan Sea	1983	7.7	Many oil tanks, fires	Yoshiwara et al. (1984)
Kocaeli	1999	7.6	Many oil tanks, fires	JSCE (2000)
Chi-Chi	1999	7.7	Oil tanks	Yoshida et al. (2000)
Tokachi-oki	2003	8.3	Many oil tanks, fires	Ohta and Zama (2005)

1.3.2. Response of ground-supported tanks

A comprehensive research work on dynamic behavior of liquid-filled tanks has been carried out both theoretically and experimentally. Initial studies involved analytical investigation of the dynamic response of liquid containing structures having rigid wall and supported on rigid foundations. Extensive study of the dynamic behavior of liquid containing structures started in the late 1940's.

Jacobsen (1949) and Ayre (1951)

Jacobsen and Ayre studied the dynamic response of cylindrical tanks subjected to horizontal ground motions. They estimated the effective hydrodynamic masses and mass moments for the accelerated contained liquid.

Housner (1963)

In the early 1960s, Housner proposed a useful idealization for obtaining liquid response of rigid rectangular and cylindrical water tanks fully anchored to the rigid foundation and subjected to horizontal ground motion. The liquid was assumed to be incompressible and inviscid. This method is probably one of the most well-known procedures available in the literature. However, attention should be drawn to the effect of tank wall flexibility which is not considered in this simplified technique. Housner separated the tank hydrodynamic response into "impulsive" motion, in which the liquid is assumed to be rigidly attached to the tank and moves in unison with the tank shell, and "convective" motion, which is characterized by long-period oscillations and involves vertical displacement of the fluid free surface. Under seismic motions, impulsive water undergoes the same acceleration as

the ground. This component is believed to have a significant contribution to the base shear and base moment. In this study, Housner developed simple equations to approximate the hydrodynamic pressures in the tanks using lumped mass approach.

Many current standards and guides such as ACI 350.3-06 and ACI 371R-08 have adapted Housner's method with some modifications which were the results of subsequent studies by other researchers for seismic design of liquid storage tanks. As mentioned before Housner's method is not capable of accounting for the effect of tank wall flexibility. Therefore, as an approximate method ACI 350.3-06 accounts for wall flexibility by determining the oscillating water mass components from the rigid tank solution and only using the amplified pseudo acceleration corresponding to the fundamental natural frequency of the system instead of the ground acceleration. This approximation may be unduly inaccurate for values of H/R (liquid depth/tank radius) greater than 1 (Veletsos (1984)).

Edwards (1969)

Edwards (1969) for the first time suggested a finite element method to be employed for estimating the seismic response of deformable liquid storage tanks. A cylindrical liquid storage tank with the height to diameter ratio of less than one was analyzed using the finite element technique. The proposed FEM was capable of accounting for the coupled interaction between the stored liquid and the elastic tank shell.

Epstein (1976)

Using Housner’s model, Epstein produced design curves for calculating the overturning moment due to hydrodynamic pressures in both rectangular and cylindrical storage tanks.

Veletsos (1974) and Yang (1976)

Veletsos and Yang showed that the flexibility of the tank shell could have a significant effect on dynamic forces induced by horizontal ground motion in liquid-filled cylindrical containers. It was concluded that the flexibility of the walls of such tanks has a substantial effect on the impulsive component of the response. Veletsos and Yang (1977) modified this method by using Flugge's shell theory (Flugge, 1960) in combination with the Rayleigh-Ritz procedure to calculate the natural frequencies of the liquid-shell system. Both shell analysis and the simpler beam-type analysis were carried out.

Hunt and Priestley (1978)

The dynamic behavior of horizontally accelerated liquid storage tanks containing inviscid liquid was further investigated by Hunt and Priestley. Both rectangular and cylindrical configurations were examined. The results of the study led to the derivation of

mathematical equations regarding the contained fluid motion under dynamic excitations. The displacement of liquid free-surface was measured experimentally for a cylindrical water tank tested on a shaking table and subjected to both sinusoidal and seismic excitations. The predicted theoretical results were in close agreement with those obtained through experiment.

Clough (1977)

Clough for the first time performed a series of experimental tests on large-scale thin-walled liquid storage tanks. The obtained hydrodynamic pressures were much larger than those proposed by Housner's analytical method. The difference in pressures was believed to be due to the tank wall flexibility effect. Several other numerical and analytical studies taking into account the interaction between the flexible shell and the containing liquid were conducted among which significant contributions were made by Haroun (1980) and Barton and Parker (1987).

Haroun and Housner (1981)

Haroun and Housner studied the behavior of deformable liquid storage tanks using modal superposition analysis. In this study, the tank shell was modeled by finite elements and the fluid domain was treated mathematically using the boundary solution technique.

They also developed a mechanical model capable of including the effect of wall deformability. The proposed three-degree-of-freedom (DOF) mechanical model involved three equivalent lumped masses corresponding to the convective component contributed by the sloshing of the liquid, the impulsive component which varies in unison with the horizontal ground acceleration, and the short period component contributed by the deformable wall vibrations. The latter component is only present in flexible liquid containers. In a tank with the rigid wall boundary condition, only the first two components need to be considered. The study also showed that the tank wall deformability may result in the hydrodynamic pressures several times larger than those experienced in rigid wall tanks. Based on this study, design charts for estimating the equivalent lumped masses of the proposed mechanical model were derived. It was assumed that the liquid contained in the tank was incompressible and had irrotational flow.

Balendra et al. (1982)

Balendra et al presented a finite element analysis of an annular cylindrical tank with an axisymmetric elastic dome, using a FE code. The fluid inside the tank was considered as inviscid and incompressible. However, sloshing of the fluid was neglected.

Minowa (1980)

Minowa further studied the tank wall flexibility effect and the corresponding hydrodynamic pressure exerted on the tank shell. He also performed experimental studies on the dynamic behavior of rectangular liquid-filled tanks.

Haroun (1983)

Haroun also performed a series of experimental investigations, including forced and ambient vibration tests on flexible ground-supported cylindrical tanks. In order to determine the mode shapes of vibrations and corresponding natural frequencies, three full scale water storage tanks were tested. This study led to a better understanding of the dynamic behavior of liquid storage tanks.

Haroun (1984)

Haroun evaluated the dynamic response of rectangular concrete liquid storage tanks using the classical potential flow approach assuming a rigid wall boundary condition. The fluid was assumed to be homogeneous, incompressible and inviscid. The tank was assumed to be subjected to the simultaneous action of horizontal and vertical components of earthquake. Bending moments developed in the walls of rectangular liquid-filled tanks due to seismic excitation at their base were calculated. As a result of this study, theoretical equations to evaluate the internal moments in the tank wall were derived and numerical values of moment coefficients to be used in seismic design of rectangular tanks were tabulated.

Haroun and Tayel (1985)

Haroun and Tayel employed the finite element technique for investigating the dynamic behavior of cylindrical liquid storage tanks having elastic wall and subjected to vertical seismic excitations. The proposed method was based on the superposition analysis technique using the axisymmetrical, free vibration modes of the tank-liquid system. The axial and radial components of the wall displacement together with the resulting stresses were calculated. In obtaining the dynamic response of the tanks, the effect of liquid sloshing was ignored.

Veletsos and Tang (1990)

Veletsos and Tang studied the dynamic behavior of liquid containing tanks resting on flexible foundations through rigid base mats. The results of the study indicated that the translational and rocking vibrations of the tank base resulted in the extended impulsive period and also larger effective damping. They had previously concluded that soil-

structure interaction reduces the hydrodynamic effects in tanks subjected to vertical excitations.

Park et al. (1992)

Park et al used a coupled boundary element-finite element method (BEM-FEM) to study the dynamic behavior of concrete rectangular tanks. The dynamic response of the tanks was obtained using the time-history analysis method. Both impulsive and convective components were included.

Gupta (1995)

Coupled free vibration dynamics of cylindrical liquid storage tanks were studied by Gupta. The vibration study of the container was made possible using Flugge's exact equations of motion. The hydrodynamic pressure associated with the contained liquid was obtained using the velocity potential approach. The obtained results compared well with those calculated by Haroun and Housner method.

Kim et al. (1996)

Kim et al. used Rayleigh-Ritz method to study the dynamic response of a flexible rectangular liquid storage tank. In this study, the effect of sloshing component of the contained liquid was neglected.

Dogangun et al. (1997 and 2004)

The dynamic response characteristics of rectangular fluid containers were further studied by Dogangun et al. He used analytical methods as well as finite element method using the modified structural analysis program SAPIV to evaluate the dynamic response. The fluid domain was modeled by displacement-based fluid elements. Effect of tank wall flexibility on dynamic behavior of tanks was also investigated. The proposed model was capable of including the effects of fluid compressibility and free-surface sloshing motion. The obtained FE results were compared with those obtained through boundary-finite element method (BEMFEM) and the requirements of Eurocode-8.

Koh et al. (1998)

Koh et al. proposed a coupled BEM-FEM technique, including free-surface sloshing vibration, to investigate the dynamic behavior of three dimensional rectangular water storage tanks under horizontal ground motions. In their study, finite element method was employed to model the solid wall while the indirect boundary element method was used to model the fluid domain.

Chen and Kianoush (2005)

In a study by Chen and Kianoush a new procedure called sequential method for estimating the hydrodynamic pressures in rectangular tanks was introduced. In this method, fluid and structure domains are coupled through applying the results from the first analysis as loads or boundary conditions for the second analysis. The study was performed in a two dimensional space and the effect of tank wall flexibility was also included. However, the effect of fluid sloshing was not taken into account.

Virella (2006)

Virella investigated the natural periods, mode shapes, and dynamic response to horizontal ground excitations of cylindrical tanks partially filled with a liquid. The finite element package ABAQUS was used to perform the computations. The contained fluid was modeled using two different techniques: the added mass formulation and acoustic fluid elements based on linear wave theory. The considered tanks had the height to diameter ratios from 0.40 to 0.95. No sloshing waves were considered in the study. It was concluded that the response of a tank-liquid system under horizontal excitation can be precisely estimated by considering just the fundamental mode. Furthermore, it was verified that the tanks with a height to diameter ratios larger than 0.63 have the fundamental modes similar to the first mode of a cantilever beam. For the shortest tank considered in the study (H/D = 0.4), the fundamental mode was a bending mode.

Kianoush and Chen (2006)

The dynamic behavior of rectangular containers under vertical seismic excitations was also investigated in a later study by Kianoush and Chen in a two-dimensional space. It was concluded that the vertical ground excitation could cause a significant seismic response in rectangular concrete tanks and therefore such effect should be considered in design.

Kianoush et al. (2006)

A new approach for seismic analysis of rectangular liquid storage tanks in time domain taking into account the effects of both impulsive and convective components was introduced by Kianoush et al. The method was able to solve the coupled liquid-filled tank problem in three-dimensional space.

Ghaemmaghami et al. (2010)

Ghaemmaghami et al investigated the seismic behavior of both concrete rectangular and cylindrical liquid storage tanks in three-dimensional space. The containers were assumed to be fixed to the rigid ground. Both impulsive and sloshing components of response were

considered. The tank models were analyzed in time domain under the horizontal and vertical components of a real earthquake record. Fluid-structure interaction effects were taken into account incorporating wall flexibility. The study indicated that the effect of vertical excitation on the seismic response of the liquid tanks could be significant when considered individually, however it was of less significance when the horizontal and vertical earthquake components were applied together. This was valid for both rectangular and cylindrical tanks.

1.3.3. Numerical models

During the time, studies on the event will be continued by issuance some numerical models to find out the most effective parameters, their way of influence and also evaluation of the procedures by comparing their, calculated and corresponding observed values due to real cases or experimental tests. And based on these findings, later researchers will try to issue more accurate analytical models and this improvement way will continue alternatively between analytical and numerical models until getting into a reasonably exact one and finally, the principle established for considering the event. Modelling of sloshing, as an imprecise and complicated engineering events, has a similar unfinished evolution history and herein we will have a brief review of the attempts done in this way which has started by Morse and Fesbach in 1953, and continued by many individuals all around the world.

By using high performance computers in conducting numerical models used in analytical models, it is possible to simulate the fluid-structure interaction as accurate and complicated elements. Hence, researchers are able to investigate the fluid sloshing behavior after taking place the large deformation. However, analysis of sloshing phenomena due to long duration ground motion needs too much time and digital memory. Therefore, some researchers tried to introduce some solutions to overcome this problem by introducing some effective techniques without considerable deficiency in accuracy of study results. Methods used for numerical modeling of sloshing phenomena is discussed in the next section, meanwhile introducing studies on the parametric behavior of fluid structure interaction. And herein, we introduce most recent attempts in this way for modeling of fluid structure interaction considering long duration of seismic motion.

Recent advances in computational methods and computer power make it possible for numerical methods to be applied to study large motion problems of free surface flow. Since analytical methods are restricted to small motions of the sloshing fluid, the numerical

solution algorithms, which take into account accurately the all source of nonlinearity of the sloshing problem have been developed over the years. In these methods, fluid motion inside the container have been represented with either Laplace, Euler wave or Navier-Stokes equations which have been solved employing Traditional numerical methods are mesh based, such as Finite Difference Method (FDM), Boundary Element Method (BEM), Finite Volume Method (FVM) and Finite element Method (FEM). The main common feature of these methods is that computation is based on a pre-defined mesh.

1.3.3.1. Boundary Element Method (BEM)

Among the numerical methods, the BEM is often used to analyze nonlinear free surface problems. An important feature of the BEM is that only the boundary has to be discretized in order to carry out the integrations. Because the interior of a solution domain is not discretized, there is a much less approximation involved in representing the solution variables, making data generation much easier (Fenner, 1983). However, the coefficient matrix in BEM is generally fully populated with non-zero terms, and is not symmetric. It has been pointed out by Bettess (1981) that for simple elements, the FEM is more efficient than BEM in which the mesh is the FEM mesh with internal nodes and elements removed.

Faltinsen (1978), Nakayama and Washizu (1981)

Faltinsen and Nakayama and Washizu simulated large amplitude sloshing in 2D rectangular tanks using BEM.

Grilli and Svendsen (1990)

Grilli and Svendsen examined the corner problems and investigated accuracy in the BEM simulation of nonlinear wave flows.

Koh et al. (1998)

Koh et al. proposed a coupled BEM-FEM scheme to study the fluid-structure interaction during liquid sloshing in a 3D rectangular tank. The tank structure was modeled by FEM while the fluid domain by BEM. Experiments were conducted to validate the proposed numerical scheme. Good agreement in terms of the free surface elevations and hydrodynamic pressures was obtained.

Dutta and Laha (2000)

Dutta and Laha analyzed the small amplitude liquid sloshing using a low-order boundary element method.

Gedikli and Erguven (2003)

Gedikli and Erguven adopted variational BEM to investigate the effect of a rigid baffle on the natural frequencies of the liquid in a cylindrical tank.

Zhang et al. (2004)

Zhang et al. developed a fully nonlinear 3D numerical wave tank base on a higher order BEM in the time domain. Numerical examples were presented to show the good performance of their mixed-Eulerian-Lagrangian scheme.

Huang et al. (2010)

Huang et al. developed a time-domain Green function based BEM to simulate liquid sloshing in tanks. Experiments were conducted to validate the numerical simulation results.

1.3.3.2. Mesh-based methods

There has been a considerable amount of work using mesh-based methods in the simulation of liquid sloshing. Most of the early studies on liquid sloshing problems were based on linear wave theory. Free surface elevation was assumed to be sufficiently small so that the nonlinear effects could be neglected. Abramson (1996) used a linear theory to simulate small amplitude sloshing in a container. Solaas and Faltinsen (1997) adopted a perturbation theory to investigate sloshing in 2D tanks of general shape.

1.3.3.2.1. Finite Difference Method (FDM)

The FDM is also widely used in the study of liquid sloshing problems. The most attractive feature of FDM is that it is relatively easy to implement. Its basic form is, however, restricted to handle regular shapes and simple boundaries. To handle complicated geometries, FEM is more straightforward to apply (Bathe, 1996).

Chen et al. (1996)

Chen et al. developed an FDM to simulate large amplitude liquid sloshing in 2D container due to seismic load.

Chen and Chiang (2000)

Chen and Chiang used time-independent FDM to study sea-wave induced sloshing in a floating tank. The fluid was assumed to be inviscid, incompressible and irrotational. The coupled interaction effect of sloshing fluid and tank motion was investigated by the FDM.

Kim et al. (2004)

Kim et al. applied the FDM in simulating violent sloshing flows in 2D and 3D prismatic tanks. The impact pressure on tank ceiling was studied. Numerical solutions were compared with existing experimental data for which favorable agreement was achieved.

Frandsen and Borthwick (2003)

Frandsen and Borthwick developed fully nonlinear FDM solutions based on inviscid flow assumption. The sloshing motions were studied in 2D tanks under both horizontal and vertical external excitations.

Chen and Nokes (2005)

Chen and Nokes developed a novel time dependent FDM for simulation of 2D sloshing motion in a tank. A fully nonlinear model was developed where fluid viscosity was included. The numerical solution of 2D waves was compared with other published results and good agreement was obtained. The FDM with SURF scheme was applied to simulate liquid sloshing.

Liu and Lin (2008)

Liu and Lin studied 3D liquid sloshing in rectangular tanks using FDM. Volume of Fluid (VOF) was used to capture the free surface.

Wu and Chen (2009)

Wu and Chen developed a 3D time-independent FDM to study sloshing waves in a square-base tank under coupled surge-sway motions. Five types of waves under various excitation angles and a wide range of excitation frequencies were presented.

1.3.3.2.2. Finite Element Method (FEM) and Finite Volume Method (FVM)

The FEM has been extensively used in the study and simulation of the liquid sloshing problems. The FVM is widely used in computational fluid dynamics where the solution favors simpler and lower order approximation within each cell (Bucchignani et al., 2004; Ahmadi et al., 2007; Greaves, 2007). Bucchignani (2004) studied 2D sloshing in rectangular tank using FVM based on potential flow. Zhang et al. (2005) developed a FVM code for the numerical simulation of free surface flow in a container. Recently, Ming and Duan (2010) investigated liquid sloshing in rectangular tank using FVM based on unstructured grid. A high order VOF method was adopted in their study to capture the free surface.

Finite element and finite volume analysis can account for complex geometry. On the other hand, finite element solution can be time consuming and expensive. In addition, if

local nonlinear effects such as overturning and breaking waves are considered, mesh-based methods like FEM, FVM and FDM meet difficulties in simulating waves involving discontinuity of liquid motion. To solve this problem, different interface capturing methods have been proposed by many investigators. Updating of the free surface is a key factor in the identification of the flow domain as well as in the application of free surface boundary conditions. The error accumulated in the free surface tracking as time progresses may cause numerical instability in the sloshing response (Fletcher, 1991; Chen et al., 1996).

Ikegawa (1974)

Ikegawa analyzed sloshing liquid under a single component of horizontal excitation using FEM.

Nakayama and Washizu (1980)

Nakayama and Washizu used FEM to analyze nonlinear sloshing of liquid in a 2D rectangular tank subjected to pitching excitations.

Wu et al. (1998)

Wu et al. gave a broad account of both 2D and 3D sloshing problems based on FEM. In their paper, the potential flow assumption, where the viscosity of the fluid was neglected, was made.

Biswal et al. (2003)

Biswal et al. developed a finite element formulation to investigate the vibration modes of liquid in a liquid-filled cylindrical tank. But their results were limited to cylindrical tanks; also wave breaking was not included in their work. FEM was used to model both the fluid and structure domain. A mixed- Eulerian-Larangian approach was developed. Ideal fluid was assumed. The results were provided for a cylindrical container using a 2D finite element approach.

Bermudez et al. (2003)

Bermudez et al. used FEM to compute sloshing modes in a container with an elastic baffle. Linear velocity potential formulation in the frequency domain was adopted in their work.

Cho and Lee (2004)

Cho and Lee simulated a large amplitude liquid sloshing in 2D tanks using fully nonlinear FEM.

Mitra and Sinhamahapatra (2005)

Mitra and Sinhamahapatra studied the coupled slosh dynamics of liquid in containers using pressure based FEM. The analysis was, however, restricted to linear problems where the small amplitude wave was assumed.

Wang and Khoo (2005)

Wang and Khoo studied nonlinear sloshing in a rectangular container under random excitations. FEM solutions were obtained using the fully nonlinear potential wave theory. The spectra of random waves and forces were investigated. The nonlinear effects of the random waves were studied and typical nonlinear features of the waves were captured.

Eatock Taylor et al. (2008)

Eatock Taylor et al. proposed a coupled FE and BE model to study nonlinear transient waves in numerical wave tanks. A mixed Eulerian-Lagrangian formulation was implemented in quadratic iso-parametric elements. Wave overturning was not captured in their numerical model.

1.3.3.2.3. Free surface capturing method used in mesh-based methods

The most well-known approaches to capture the free surfaces are VOF (volume of fluid), PIC (particle-in-cell), and MAC (marker-and-cell) methods.

Hirt and Nicholls (1981)

Hirt and Nicholls developed the VOF method in capturing the moving boundaries of fluids. VOF method solves an additional partial differential equation for the volume fraction at each time step besides the conservation equations. This method can define sharp interfaces and is robust. Nevertheless, tracking and reconstruction of free surfaces remain complicated and difficult, especially in three dimensions (Qian et al., 2006).

Osher and Sethian (1988)

Osher and Sethian proposed a Level-Set method to deal with moving boundaries. This method also needs to solve an additional level-set function except for the conservation equations.

The PIC scheme uses particles on the free surfaces and FDM to solve the governing equations (Harlow, 1963). Another similar approach, MAC method, is based on Lagrangian concepts and can treat overturning waves and reentry inception with simple logic. Marker particles which move with the fluid are used in MAC method to track the movement of free surfaces (Harlow and Welch, 1965). MAC has been widely used to solve complex computational fluid dynamic problems (Johnson, 1996).

Mikelis and Journee (1984)

Mikelis and Journee simulated 2D liquid sloshing using the MAC method. A series of experiments were conducted on scaled tanks in their work. The measured pressure was compared with their numerical transient solution and reasonable agreement was achieved.

Armenio and La Rocca (1996)

Armenio and La Rocca studied the sloshing of water in rectangular containers with the filling depths of liquid in shallow water hypotheses numerically with a modified form of MAC method. Experiments were carried out to verify the performance of the numerical solutions.

Though PIC and MAC are flexible and robust, they are quite complicated in programming and need additional storage required for locating the marker particles, and the additional programming complexity to locate the cells containing the free surface. It significantly increases the computational effort, especially in 3D cases (Griebel et al. 1998).

All of the above free surface capturing methods can properly compute the instantaneous free surface displacement. However, they all require complex computer programming in order to treat the time varying free surface boundary and update the computational mesh. Furthermore, the problem of numerical diffusion arises owing to the discretization of the advection terms in the Navier-Stokes equations in the mesh-based methods using Eulerian grids.

Generally, mesh-based methods are proficient when the sloshing amplitude is small, where several assumptions can be made to help solve the problem. Though, mesh-based methods have difficulties in simulating waves relating discontinuity of liquid motion. These methods may suffer from mesh distortion in problems with extremely large fluid motion if no additional effort of free surface capturing scheme, such as VOF method, is introduced. Even with some free-surface tracking techniques incorporated, mesh-based methods using Eulerian formulations suffer from the problem of numerical diffusion. In addition, tracking of free surfaces requires a complex and time consuming algorithm to update the rapidly changing nonlinear boundary. Furthermore, many aforementioned works about liquid sloshing problems are limited to cylindrical tanks because most of the storage tanks are of cylindrical shape. Little research has been reported on liquid sloshing in rectangular tanks in the context of large motions.

1.3.3.3. Meshless methods

In recent years, a new generation of numerical methods has been developed, i.e. meshless (mesh-free) methods that outperform conventional mesh-based methods in dealing with discontinuous motion. Meshless methods have been found to have advantages in dealing with problems for large-amplitude free surface flows, moving interfaces, large motion and complex and deformable boundaries. Liquid sloshing with the possibility of wave breaking belongs to the class of large motion problems with a free surface. In particular, meshless methods have good potential in liquid sloshing problems when the sloshing amplitude is large, especially with possible breaking of free surface. The main idea of meshless methods is to obtain numerical solutions of partial differential equations through a set of particles instead of meshes. Since no numerical meshes are needed, multi-scale resolution problems can be modeled with relative ease in meshless methods through adjusting the particle distribution densities over the solution domain. The particles have a natural ability to represent the union and the fragmentation behavior of breaking waves, especially when they are used to simulate free-surface sloshing. Furthermore, the problem of numerical diffusion in mesh-based methods does not arise in Lagrangian formulated particle methods. Therefore, with great potential to simulate breaking wave phenomena, meshless methods have recently concerned increasing attention.

Liszka and Orkisz (1980)

Liszka and Orkisz proposed a Generalized Finite Difference (GFD) method for structural problems.

Chew et al. (2006)

Chew et al. proposed an Arbitrary Lagrangian-Eulerian (ALE) formulation of GFD method and applied it in vortex flow and flows past moving bodies.

Kuhnert and Tiwari (2007)

Kuhnert and Tiwari presented a meshless method for two-phase incompressible flows named finite pointset method. Nevertheless, neither of these methods has been applied in the study of incompressible free surface flow problems.

Liu et al. (2005)

Liu et al. developed a Lagrangian particle method named finite particle method (FPM) and applied it to modeling incompressible free surface flow problems. Nevertheless, the same approach of imposing the incompressibility condition was adopted in these studies.

Onate et al. (1996)

Onate et al. proposed a meshless method called the Finite Point Method using a Lagrangian formulation to solve fluid mechanics problems.

Idelsohn et al. (2001)

Idelsohn et al. generalized Onate idea with finite-element type approximations. They later proposed a new method called the Particle Finite Element Method (PFEM) using the same meshing technique (Idelsohn et al., 2004). The PFEM method was tough to solve fluid-structure interaction problems with moving free surfaces. However, extra effort was needed to generate a new mesh at each time step, and this made the method inefficient of computation.

Koshizuka and Oka (1996)

A particle method with more direct modeling of incompressible fluid was suggested by Koshizuka and Oka named the Moving Particle Semi-implicit (MPS) method, it assumes a particle number density in the computation of density parameter. The incompressibility condition is imposed by solving the Poisson equation of pressure.

1.3.3.3.1. Smoothed Particle Hydrodynamic (SPH)

In the SPH method, the incompressible flow condition is simulated as the limit of the compressible Navier–Stokes equations with some stiff equation of state (Monaghan, 1988). The compressibility is adjusted by changing the numerical speed of sound in the equation of state, which helps to control density fluctuation to some pre-defined ratio. The incompressible limit is obtained by choosing a very large speed of sound in the equation of state in SPH. However, the large value of the speed of sound restricts the time step to be very small due to the Courant–Friedrichs–Lewy condition (Courant et al., 1967). Furthermore, the compressibility adjustment is case-dependent and it has to be calibrated for every specific fluid dynamic problem.

Monaghan (1988, 1994)

Another group of meshless methods using particles to describe the motion of the fluid based on the Lagrangian formulation. The first idea of this approach was proposed by Monaghan for the dealing of astrophysical hydrodynamic problems. The method was called Smooth Particle Hydrodynamics (SPH). Many other researchers later generalized this method to solve fluid mechanical problems.

Shao and Lo (2003)

Shao and Lo developed an enhanced SPH to simulate Newtonian flows with a free surface. They tested the method with a typical 2D dam break example.

Souto-Iglesias et al. (2004)

Souto-Iglesias et al simulated sloshing in the anti-roll tanks using SPH. Later, they studied the sloshing moment amplitudes in a rectangular tank under different rolling frequencies using SPH and experiments were conducted for validation of the numerical solutions.

Delorme et al. (2009)

Delorme et al. explored the impact pressure in shallow water sloshing under forced rolling motion numerically and experimentally using SPH. Also, they concerned traveling waves and breaking waves under resonant sloshing condition. A modified SPH scheme was also proposed to study the density effect of the impact pressure. Good agreement in terms of free surface shape and global dynamic of the flow was shown between experimental and numerical in their results.

The more complete literature review and detailed investigations of sloshing phenomena from basic experimental and theory to advanced analytical studies gathered in the work of Ibrahim.

1.4. Codes and standards

In this section a brief review of various codes and standards available for seismic design of liquid containing structures is presented. International Building Code, IBC (2011) is one of the most comprehensive and preferred codes currently used in the United States. In the last revision of this code, the ASCE 7-10 (2010) standard is referred to for seismic design of common liquid storage tanks. Inside ASCE 7-10, the input ground motion is defined as a response spectrum corresponding to the Maximum Considered Earthquake (MCE) which represents an earthquake with a 2% probability of exceedance in a 50-year period (equivalent to a recurrence interval of approximately 2500 years).

Currently, there are no direct guidelines for structural design of environmental structures in Canadian design standards. However, useful guidelines may be found in a variety of other codes and standards such as ACI 350.3-06 (2006), New Zealand Standard NZS 3106 (2010), European Eurocode-8 (2006), and British Standard BS 8007 (1987), among which ACI 350.3-06 is the most comprehensive and widely adopted one.

ACI 350.3-06 standard reported by the American Concrete Institute, Committee 350 is presently used as an obligatory document for seismic design of reinforced concrete liquid storage tanks in North America. Supplementary guidelines regarding the analysis and design of elevated concrete and composite steel-concrete water storage tanks may be found in ACI 371R-08 (2008).

The Committee 350 was formed by the American Concrete Institute (ACI) in 1964 as a technical board responsible for providing guidelines for the design of environmental engineering structures. In 2001, ACI published the first standard for the design of environmental engineering concrete structures in North America (ACI 350-01 and ACI 350.3-350.3R-01). In that standard, two different methods of design (working stress method and modified ultimate strength method) were proposed. The design methods were calibrated in such a way to provide comparisons, but not necessarily identical designs.

The current revision of the Code (ACI 350.3-06) is based on the ultimate strength design method. In this standard, an equivalent mechanical model based on the Housner's method (Housner (1963)) has been incorporated by which the resultant seismic forces acting on the walls of rigid containers can be estimated.

Two different standards intended for the design of pre-stressed concrete liquid storage tanks were published by the American Water Work Association (AWWA); AWWA D110 (1995), and AWWA D115 (1995). The guidelines regarding the design of welded steel liquid storage containers were provided in AWWA D100 (2005).

The American Petroleum Institute (API) published two standards; API 650 (1998), and API 620 (1998) for the design of tanks used in the petroleum industry.

American Society of Civil Engineers (ASCE) provided two publications including useful guidelines regarding the seismic design of storage tanks used in the nuclear industry; ASCE 4-98 (1998), and ASCE 58 (1980). Tanks used in the nuclear industry should meet more stringent design requirements compared to those used in other industries because of the potential hazard of radioactive materials to public safety.

Most of the standards, including ACI 350.3-06, AWWA D100, AWWA D110, and API 650 have employed the Housner's mechanical model (Housner (1963)) with some modifications for determining the seismic forces associated with the accelerated contained liquid. In NZS 3106 (2010), the mechanical model proposed by Veletsos and Yang (1977) is used for seismic analysis of rigid tanks while the model developed by Haroun and Housner (1981B) is used for deformable liquid storage tanks.

In Eurocode-8 (2006) the dynamic analysis of rigid circular tanks is performed using Veletsos and Yang's model (1977). The models developed by Veletsos (1984) and Haroun and Housner (1981B) together with the approach proposed by Malhotra et al. (2000) are used for dynamic analysis of flexible circular tanks. Housner's method (1963) is recommended for seismic evaluation of rigid rectangular tanks, while no practical approach is assigned for flexible rectangular containers.

In seismic design codes, the seismic response values corresponding to the impulsive and convective parts are combined using an appropriate combination method. All codes and Standards except the Eurocode-8, recommend SRSS (Square Root of Sum of Squares) rule to be used for combining the impulsive and convective seismic effects. Eurocode-8 suggests an absolute summation combination rule.

Different standards specify different damping values to be considered for impulsive component. However, all codes and standards agree on the damping ratio of 0.5% to be used for convective component. ACI 350.3-06, ASCE 7-05, AWWA D100, AWWA D110, AWWA D115, and API 650 recommend a damping ratio of 5% for impulsive component for all tank types. In Eurocode-8, a damping ratio of 5% is proposed for the impulsive component of concrete tanks while 2% damping is specified for steel tanks. As a result of different damping ratios associated with impulsive and convective liquid components, different response spectra corresponding to these components are provided in LCS design codes and standards.

In NZS 3106 (2010), the appropriate damping ratio for the impulsive component is determined based on the tank geometry, tank aspect ratio, tank material, and shear wave velocity in foundation soil.

In Japanese recommendation code (2010) seismic load can be obtained by the modified seismic coefficient method or by modal analysis, and the sloshing oscillation of a contained liquid is obtained from the velocity response spectrum, although; the velocity response spectra in the range of longer periods are not yet fully clarified, and it is considered to be a valid conservative estimate. The seismic design method adopted in this recommendation is the allowable stress method modified by the ratio of the horizontal load-carrying capacity in the structure to the short-term allowable yield strength. Furthermore the effects of tank flexibility and vertical excitation are taken into account, however the issues of sloshing, is not adequately considered.

1.5. Objectives and scope

The main focus of the current study is to evaluate the performance of ground-supported rectangular as well as liquid-filled water tanks under long period-long duration seismic loading. Different types of analysis, including time history are performed using the general numerical analysis code. Furthermore, the effects of a wide range of parameters including tank wall flexibility, sloshing of the water free surface of these tanks are addressed.

In order to investigate the effect of earthquake frequency content on dynamic behavior of such structures, some different ground motions having different frequency contents ranging from low to high are used.

In addition, to investigate the accuracy of code provisions in seismic analysis and design of liquid containing structures, a comparison between the calculated FE results and those proposed by current practice is made.

Through this research, a detailed parametric study is also carried out on water tanks. The tank geometry parameters used for the study covers a range of tank capacities and aspect ratios found in practice today. Based on the results of this study, graphs corresponding to the hydrodynamic pressure distribution are produced which can be easily employed in design applications for water tanks.

Furthermore, two different techniques are investigated; the first is Coupled Eulerian Lagrangian (CEL) and the second one is Smoothed Particle Hydrodynamics (SPH); the results of these two techniques compared together.

In summary, the main objectives of this research are as follows:

1) Perform a comprehensive study on the dynamic behavior of rectangular ground supported water tanks and determine the deciding factors based on the obtained results.

2) Understand the effect of a broad range of parameters on dynamic behavior of liquid containing structures such as: tank geometry aspect ratio, the sloshing of the liquid free surface, wall flexibility, and etc.

3) Investigate the effect of ground motion frequency content on dynamic response of water tanks.

4) Simulate fluid-structure interaction problems in tanks with different geometries.

5) Verify the proposed FE models by comparing the calculated results with those obtained through an exact analytical solution and/or other experimental studies reported in the literature.

6) Develop a parametric model capable of creating any FE model of a 3D liquid filled tank with varying parameters such as the shell thickness, tank dimension, tank height, and liquid depth.

8) Carry out an extensive parametric study on the dynamic response of water tanks and provide hydrodynamic pressure distribution graphs to be used in seismic design of water tanks.

The scope of this study is summarized as follows:

1) The tanks are assumed to be rigidly anchored to the rigid ground such that no sliding or uplift may occur. As a result, the effect of soil-structure interaction is not considered.

2) The tank walls are considered to be of constant thickness.

3) In dynamic analysis of water tanks, only the effect of horizontal ground motion in two directions is considered.

5) The fluid is assumed incompressible and inviscid.

6) In FE modeling of the tanks, all structural materials are assumed to behave as linear elastic.

1.6. Research significance

The FE method used in this study has several advantages over previous studies carried out on liquid containing structures. One of the main advantages of the current method is using two new arisen techniques to estimate the real behavior of water in tanks due to long period-long duration seismic motions.

In this research, study of liquid sloshing effects in tanks with complex geometries is made possible. The results of this study show that the proposed finite element techniques are capable of accounting for the fluid-structure interaction with liquid containing structures. The suggested FE model is verified by comparing the obtained results with well proved analytical and experimental results available in the literature.

The other parameter which is ignored in the current practice is the effect of base fixity. The natural period of vibration of the tank-liquid system and as a result the hydrodynamic forces could be affected by different conditions at the base. This is an important factor not studied adequately in the literature and therefore needs more investigation. Regarding the seismic analysis and design of water tanks the need for such study is even more.

However, using the rigorous technique introduced in this research, studying the effect of fluid-structure interaction in tanks has been made possible and practical guidelines to overcome these modeling difficulties are addressed.

Concerning the dynamic response of ground-supported water tanks there are areas in the literature that need to be further investigation. Kianoush and Chen (2006) studied the combined effect of horizontal and vertical ground accelerations in rectangular liquid storage tanks; however, no study has been carried out to consider the effect of long period-long duration ground motions for rectangular tanks.

The effect of earthquake frequency contents on the dynamic behavior of liquid-filled tanks need to be investigated by selecting input ground motions having low, intermediate and high frequency contents and performing a series of rigorous time-history analyses.

In addition, very few studies can be found in the literature regarding the seismic behavior of liquid-filled rectangular tanks. The need for proposing a thorough method capable of considering all deciding parameters and assessing the relative importance of such effects on the overall seismic response of rectangular tanks seems essential.

During this study, effort has been made to develop a detailed three-dimensional FE model in order to eliminate the inaccuracies associated with such simplifications in dynamic analysis of tanks.

1.7. Thesis layout

This dissertation delivers the findings of an investigation of sloshing phenomena in tanks due to long period – long duration ground motions.

The outline of this thesis involves six chapters defined according to the objectives and scope of the research.

The first chapter presents a summary of the previous research studies carried out on response of liquid containing structures considering the effect of long period-long duration ground motions. An overview on existing codes, standards, and guides used in design of liquid storage tanks is also provided in this chapter.

Chapter 2 deals with the finite element formulation of three-dimensional liquid containing structures. A discussion on how to consider the fluid-structure coupling effect in finite element modeling of liquid containing structures is made. In addition, the corresponding equations of motion of liquid domain accounting for both the impulsive and sloshing components of the response are addressed.

The dynamic behavior of rectangular water tanks due to harmonic motions is discussed in Chapter 3. The validity of current practice in seismic analysis of liquid-filled rectangular containers is also investigated. Furthermore, the accuracy of current practice in predicting the dynamic behavior of water tanks is studied. In the second part of the chapter, the

effect of earthquake frequency content on the seismic behavior of liquid-filled conical elevated tanks is studied.

Chapter 4 discusses the results of a comprehensive parametric study carried out in liquid filled tanks using the finite element techniques. Effects of important parameters including sloshing of liquid free surface, tank wall flexibility, ground acceleration and tank aspect ratio are addressed in this chapter. A wide spectrum of tank capacities and geometries typically found in practice today is covered in this parametric study. Based on the results of this parametric study, pressure distribution graphs corresponding to impulsive and convective components are created by carrying out spectral analyses on a large number of tanks with different capacities. It is shown that the proposed pressure graphs can be utilized conveniently with high level of accuracy in design applications for liquid-filled tanks.

In Chapter 5, conclusions and some suggestions for future work are presented. The thesis ends with a list of references and three appendices. In the first appendix, details of the lamina fluid theory discussed in Chapter 3 are presented. The second appendix provides the input text command files for the tank's parametric model and the post-processors used in Chapters 3 and 4.

References

[1] Aquelet, N., Souli, M., Gabrys, J., 2003, Olovsson, L. A new ALE formulation for sloshing analysis, *Struct. Eng. Mech.* **16**, 423–440.

[2] Belytschko, T., Liu, W.K., Moran, B,2000, Nonlinear finite elements for continua and structures, Wiley, New York.

[3] Ghosh, S., Kikuchi, N,1991, An arbitrary Lagrangian-Eulerian finite element method for large deformation analysis of elastic-viscoplastic solid, *Comput. Meth. Appl. Mech. Engng*. **86**, 127–188.

[4] Benson, D.J, 1997, A mixture theory for contact in multimaterial eulerian formulations, *Comput. Meth. Appl. Mech. Eng.* **140**, 59–86.

[5] Chen, B.F., Chiang, H.W, 1999, Complete 2D and Fully Nonlinear Analysis of Ideal Fluid in Tanks, *J. Eng. March. ASCE* **125,** 70–78.

[6] Chen, B.F, 2005,Viscous Fluid in Tank under Coupled Surge, Heave, and Pitch Motions, *Journal of Waterway, Port, Coastal, and Ocean Engineering ASCE* **131**, 239– 256.

[7] Chen, Y.H., Hwang, W.S., Ko, C.H, 2007, Sloshing Behaviors of Rectangular and Cylindrical Liquid Tanks Subjected to Harmonic and Seismic Excitations, Earthquake Engineering and Structural Dynamics **36**, 1701– 1717.

[8] El-Zeiny, A, 1995, Nonlinear Time-Dependent Seismic Response of Unanchored Liquid Storage Tanks, Ph.D. Dissertation, Department of Civil and Environmental Engineering, University of California, Irvine.

[9] Fischera, F.D., Rammerstorferb, F.G, 1999, A Refined Analysis of Sloshing Effects in Seismically Excited Tanks, Int. J. *Press. Vessels Piping* **76**, 693–709.

[10] Hatayama, K, 2008, Lessons from the 2003 Tokachi-oki, Japan, earthquake for prediction of long-period strong ground motions and sloshing damage to oil storage tanks, Springer Science Business Media B.V. J Seismol 12, 255-263.

[11] Housner, G.W, 1954, Earthquake pressures on fluid containers. 8th Technical Report under Office of Naval Research, *California Institute of Technology*, Pasadena, California.

[12] Ibrahim, R.A, 2005, Liquid Sloshing Dynamics: Theory and Applications, Cambridge University Press, New York, USA.

[13] Iwaharai, T, 2008, Safety assessment of underground tank against long-period strong ground, The 14th *World Conference on Earthquake Engineering*, Beijing, China.

[14] Koketsu, K., Hiroe Miyake, H, 2008, A seismological overview of long-period ground motion, Springer Science Business Media B.V. J Seismol 12, 133-143.

[15] Liu, D., Lin, P, 2008, A numerical study of three-dimensional liquid sloshing in tanks, *J. Comput. Phys*. **227**, 3921–3939.

[16] Longatte, E., Bendjeddou, Z., Souli, M, 2003, Application of Arbitrary Lagrange Euler Formulations to Flow-Induced Vibration problems, *J. Press. Vessel Technology* **125,** 411–417.

[17] Manos, G.C, 1986, Dynamic response of a broad storage tank model under a variety of simulated earthquake motions. Proc. 3rd U.S. Nat. Conf. on Earthquake Engrg., Earthquake Engineering Research Institute, E1 Cerrito, Calif., 2131–2142.

[18] Mitra, S., Upadhyay, P.P., Sinhamahapatra, K.P, 2008, Slosh Dynamics of Inviscid Fluids in Two-Dimensional Tanks of Various Geometry Using Finite Element Method, Int. J. *Num. Methods Fluids* 56, 1625–1651.

[19] Murata, K. and Miyajima, M.2007, Influence of Receiving Water Tank Sloshing on Water Distribution

[20] Panigrahy, P.K., Saha, U.K., Maity, D., 2009. Experimental studies on sloshing behavior due to horizontal movement of liquids in baffled tanks, *Ocean Engineering*, **36**, 213–222.

[21] Ozdemir, Z., Souli, M., Fahjan, Y.M, 2010, FSI methods for seismic analysis of sloshing tank problems, *M´ecanique & Industries*, **11**, 133–147.

[22] Souli, M., Ouahsine, A., Lewin, L, 2000, ALE formulation of fluid-structure interaction problems, *Comput. Methods Appl. Mech. Eng*. **190**, 659–675.

[23] Souli, M., Zolesio, J.P, 2001, Arbitrary Lagrangian-Eulerian and free surface methods in fluid mechanics, *Comput. Methods Appl. Mech. Eng*. **191,** 451–466.

[24] Tanaka, Motoaki, Sakurai, Ishida, Tazuke, Akiyama, Kobayashi and Chiba, 2000, Proving Test of Analytical Method on Nonlinear Response of Cylindrical Storage Tank Under Severe Earthquakes, *Proceedings of 12th World Conference on Earthquake Engineering (12 WCEE)*, Auckland, New Zealand.

[25] Vakilazadsarabi, A, Miyajima, M, Murata, K, 2012, study of Sloshing phenomena due to long period ground motions, *Proceedings of 14th World Conference on Earthquake Engineering (14 WCEE)*, Lisbon, Portugal.

[26] Vakilazadsarabi, A, Miyajima, , 2014, Sloshing of Tanks due to Long Period-Long Duration Ground Motions, International Journal of Civil Engineering Research (IJCER), (article in press).

[27] Veletsos, A.S, Yang, J.Y, 1977, Earthquake response of liquid storage tanks. *Advances in Civil Engineering Through Engineering Mechanics, Proceedings of the Engineering Mechanics Division Specialty Conferences*, ASCE, Raleigh, North Carolina, 1–24.

[28] Young, D.L, 1982, Time-dependent multi-material flow with large fluid distortion, Numerical Methods for Fluids Dynamics, K.W. Morton, M.J. Baines (eds.), Academic Press, New-York.

[29] Zama, S, 1996, Regionality of long-period ground motion using JMA strong motion displacement records, *Eleventh World Conference on Earthquake Engineering*.

2. Numerical modeling of water-tank interaction

2.1. General remarks

Interaction of water-tank to apply support and load transmission continuum for tank is one of the most important issues in analyses of sloshing phenomena in tanks and has an essential effect on the exactitude of modeling and accuracy of results. As discussed in the first chapter, during the last decade, studies on fluid-structure interaction for modeling sloshing in water tanks, especially rectangular shape, had considerable progress and recently have led to some reasonable analytical equations confirmed by comprehensive numerical models, experimental tests or comparison to previous real seismic events.

Generally the fluid hydrodynamic pressure in tanks can be divided into two distinct parts. One is directly proportional to the ground acceleration and is caused as a result of fluid motion in unison with the tank. The second is convective pressure, which is due to sloshing at the liquid free surface. As a result, the liquid dynamic behavior inside closed tanks can be approximated by an equivalent model capable of taking into account the effects of both liquid components. This equivalence criterion is met by equating the resulting forces and moments acting on the tank wall between the actual model and its mechanically equivalent model.

In this chapter the fluid-structure interaction problem is formulated using the finite element techniques (CEL and SPH). Firstly, basic equations of motion in fluid dynamics were formulated. The remaining task to be addressed in this chapter is to solve these equations using an appropriate method capable of accurately simulating the actual behavior of liquid containers under dynamic loadings. Here, first the general equations of motion are derived for MDOF structures discretized as systems with a finite number of degrees of freedom. Then, an overview of how the fluid-structure coupling effect is accounted for in the proposed FE technique along with the corresponding equations of motion of fluid domain is presented.

In order to obtain the seismic response history of liquid tanks, the discretized structural equations and the fluid domain equations of motion have to be considered simultaneously as coupled sets of equations. The main objective of this chapter is to address this issue using FE method.

This chapter also provides a brief discussion on the problems associated with boundary conditions at fluid/structure interface and free surface of the fluid. Moreover, the element

types and meshing patterns used for FE modeling of the tank models are explained. The general purpose FE analysis software is used for dynamic analysis of liquid tank models.

2.2. Introduction of fluid-structure governing equations

The governing equations for fluid flow are the Navier-Stokes equations: conservation of mass (Equation 2.1), momentum-equation (Equation 2.2) and energy-equation (Equation 2.3). These equations are not solvable in an analytical way.

$$\frac{\partial \rho}{\partial t} + \nabla.(\rho v) = 0 \tag{2.1}$$

$$\rho \frac{\partial v}{\partial t} + \rho v.\nabla(v) = \nabla.s + f \tag{2.2}$$

$$\rho \frac{\partial e}{\partial t} + \rho v.\nabla(e) = s:\nabla(v) + f.v \tag{2.3}$$

The parameters in these equations are as follows:

- f is the external force density.
- v is the velocity vector
- The total Cauchy stress s is given by:

$$s = -p.I + \mu(\nabla(v) + \nabla(v)^T) \tag{2.4}$$

where p is the pressure and μ represents the dynamic viscosity by applying initial boundary conditions, these equations completely tracking the flow. For the sloshing problem, two different regions on the boundary of the domain are distinguished (Fig. 2.1):
The velocity is prescribed on $\partial\Omega_f^1$: $.v(t) = g(t)$
The velocity isn't prescribed, but the traction boundary condition is assumed to be imposed on $\partial\Omega_f^2$: $.s.n = h(t)$

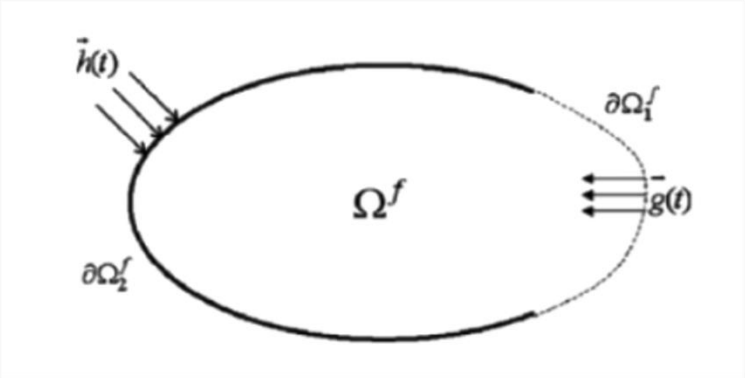

Fig. 2.1.Fluid domain

When computers became powerful enough to solve large sets of equations, a lot of numerical sloshing models were developed. The Navier-Stokes equations were formulated in a discrete form and solved numerically.

2.3. Material definitions

In the CEL and SPH analysis, two types of material are used. First, there is the structural material of the container. This can be metal, concrete or a composite material for example. These materials are modelled as an elastic material, with given density ρ, stiffness E and poisson ratio of υ.

The fluid -water- is modelled based on the equation of state (EOS). This means the fluid is considered to be in thermodynamic equilibrium at all times.

An example of an EOS is the ideal-gas law. By giving the temperature T and the density ρ, the pressure is known by using $p = \rho RT$, and the internal energy is specified by $i = C_v T$.

To define a fluid in code, the density ρ, the wave velocity in the material c = P RT and the dynamic viscosity μ are specified using the $U_s - U_p$ formulation for the EOS; the fluid is considered incompressible. When the fluid is incompressible, no relation exists between the energy equation on one hand and the mass conservation and momentum equations on the other hand. The energy equation must only be solved when temperature variations are taken into account, but this is not considered in this case.

The equation of state gives the pressure as a function of the density and the internal energy: $p = f(\rho, i)$. It is possible to eliminate the internal energy *i* and eventually obtain an $pH = f(\rho)$ relationship, which is called the Hugoniot-curve. pH is called the Hugoniot pressure. It can only be obtained experimentally.

Normally, the $U_s - U_p$ formulation of EOS is used to simulate shocks in solid materials. Now it is used to define fluid materials. The Hugoniot curve is approximated using following expressions:

$$U_s = c_0 + sU_p \tag{2.5}$$

$$p = \frac{\rho_0 c_0^2 \mu}{(1-s\mu)^2}\left(1 - \frac{\Gamma_0 \mu}{2}\right) + \Gamma_0 \rho_0 i \tag{2.6}$$

U_s is the linear shock velocity, U_p the particle velocity. Γ_0 and s are parameters of the approximation. To model fluids, these parameters are set to zero: $\Gamma_0 = 0$ and s = 0. Eventually, we the following expression for the equation of state is obtained:

$$p = c_0^2 \rho \mu \tag{2.7}$$

When defining a viscosity of the material, it is treated as a Newtonian fluid, meaning the viscosity depends only on the temperature. This is the default setting in the using code. As the temperature is constant during the analysis, so the viscosity also is.

The velocity of the air is not higher than 100 m/s, so the Mach-number does not exceed 0.3. When only low Mach numbers occur, air can be treated as an incompressible gas. Furthermore, when air is modelled using the ideal-gas EOS, the energy equation has to be taken into account, resulting in an increase of calculation time.

To conclude, the parameters for each of the fluids used in the model are given in Table 2.1.

Table 2.1.Values of parameters used to model water and air

	Water	Air
$\rho[kg/m^3]$	986	1.2
$c_0[m/s]$	48.5	344
$\mu[Pa.s]$	0.001	1.8E-05
Γ_0	0	0
s	0	0

2.4. Explicit dynamic analysis

In order to simulate sloshing events, a dynamic analysis is needed. In the using code, CEL and SPH techniques, calculations are performed using a dynamic explicit method, due to the nonlinear nature of the governing equations. This explicit method is characterized by two important properties. First, an explicit integration rule is applied, and second, a lumped mass matrix is used.

The equations of motion of an object are integrated using an explicit central difference integration scheme:

$$\dot{u}^{(i+1/2)} = \dot{u}^{(i-1/2)} + \frac{\Delta t^{(i+1)} + \Delta t^{(i)}}{2} \ddot{u}^{(i)} \tag{2.8}$$

$$u^{(i+1)} = u^{(i)} + \Delta t^{(i+1)} \dot{u}^{(i)} \tag{2.9}$$

$\dot{u}$ is the velocity, and $\ddot{u}$ is the acceleration. The kinematic state of the body is updated, using the values of $\dot{u}$ at $(i - 1/2)$, and $\ddot{u}$ at (i), making it an explicit method. $(i - 1/2)$ and $(i + 1/2)$ are called intermediate states.

To calculate the acceleration $\ddot{u}$ at the beginning of each increment, Newton's second law is applied:

$$\ddot{u}^{(i)} = M^{-1}.(F^{(i)} - I^{(i)}) \tag{2.10}$$

In this equation, M represents the lumped mass matrix, F is the applied load vector, and I is the internal force vector. The inverse of the mass matrix is tri-axial, which makes the explicit method calculating fast. When compared with an implicit method, the explicit method generally needs more increments to complete a calculation. But in an implicit method, a global set of equations must be solved each increment, while here this is not the case because of the tri-axial inversed mass matrix, so neither iterations nor a tangent stiffness matrix is needed.

2.5. Stable increment time

The increment time is based only on the highest natural frequency occurring in the model. When using an implicit method, the time increment is based on the needed accuracy and the convergence of the calculations. This means that the calculation cost of an extra increment is cheaper using an explicit method.

The stable increment time for each element is determined using Equation 2.11

$$\Delta t = \frac{2}{\omega_{max}^{element}} \tag{2.11}$$

To estimate the increment time for the whole model, the minimum of the increment time for all elements is chosen. This implies a very conservative estimate. It can also be formulated in terms of a characteristic element dimension L_e and the dilatational wave speed in the material c_d:

$$\Delta t = min(\frac{L_e}{c_d}) \tag{2.12}$$

L_e depends on the maximum eigen frequency of the element, which means the stable increment time is smaller when a stiffer material is used. Expressions for L_e exist for every element type available in software. To control high-frequency oscillations, an amount of damping is automatically introduced. The stable time increment becomes:

$$\Delta t = \frac{2}{\omega_{max}^{element}} (\sqrt{1 + \xi^2} - \xi) \tag{2.13}$$

The fraction of critical damping in the highest mode ξ is determined by:

$$\xi = b_1 - b_2^2 \frac{L_e}{c_d} min(0, \dot{\epsilon}_{vol}) \tag{2.14}$$

Here $\dot{\epsilon}_{vol}$ represents the volumetric strain rate, b_1 and b_2 are bulk viscosity scaling factors. The damping actually reduces the stable time increment. Normally, an algorithm that automatically an estimate the highest eigenfrequency is implemented in using code, the

maximum value of the eigen frequency is updated every time step. However, when using fluids in a model, the software does not use a global estimation, but an element-by-element one. From this data, the stable increment time is calculated automatically. If desired, a smaller increment can be chosen, but this is not of use in the models that are discussed here.

2.6. Application to CEL

2.6.1. Contact interactions

General contact is applied to account for the interaction between the Lagrangian part and the Eulerian domain. The contact formulation is based on an immersed boundary method. This means the Lagrangian part occupies void in the Eulerian domain. A rough friction constraint applies to the contact interaction. Mechanically, this implies that the friction coefficient $\mu_{fric} = \infty$. Once the surfaces make contact and undergoes rough friction, the contact should remain closed. As a consequence, a layer of fluid remains attached to the Langrangian part. The contact interaction is implemented using a penalty based method. The using code calculates the contact interaction twice. The second time the calculation is performed, the surface that previously was the master surface, now becomes the slave surface and vice versa. Eventually a weighed average is taken in order to calculate the contact for that particular step. Implementing a penalty based method makes the model stiffer, because artificial springs are implemented between the slave and master surface. This could implicate that the stable time increment decreases, rising the calculation time needed. The software automatically prevents this, thus limiting the stable time increment.

When the deformation of the structure is also taking into account, contact algorithms must be developed to calculate the contact forces applied from the fluid to the structure and vice versa. An explicit method is used to update the nodal forces at the interface each time step to calculate the contact forces. To stay in contact with the structure, fluid nodes must follow the structure at the interface. Souli and Zolesio and Rabier and Medale present a coupling algorithm where remeshing is not applied. Only small fluid motions are allowed in order to prevent mesh distortion, as this would lead to incorrect results. When modeling fluids with such a mesh, the mesh gets severely distorted due to the large deformations of the water, as can be seen in Fig. 2.11(a). A remeshing method is needed, which is very CPU-time consuming.

An often-used algorithm that addresses these issues is the Euler-Langrange coupling. One example of such an algorithm can be found in Aquelet et al., in which the structure is

modeled with a Langrangian mesh. The mesh follows the deformation of the structure. Because the deformation is relatively small, no severe mesh distortion occurs. The fluid is modeled in an Eulerian mesh, in which the mesh is fixed in space. The fluid flows through the mesh, and distortion does not occur.

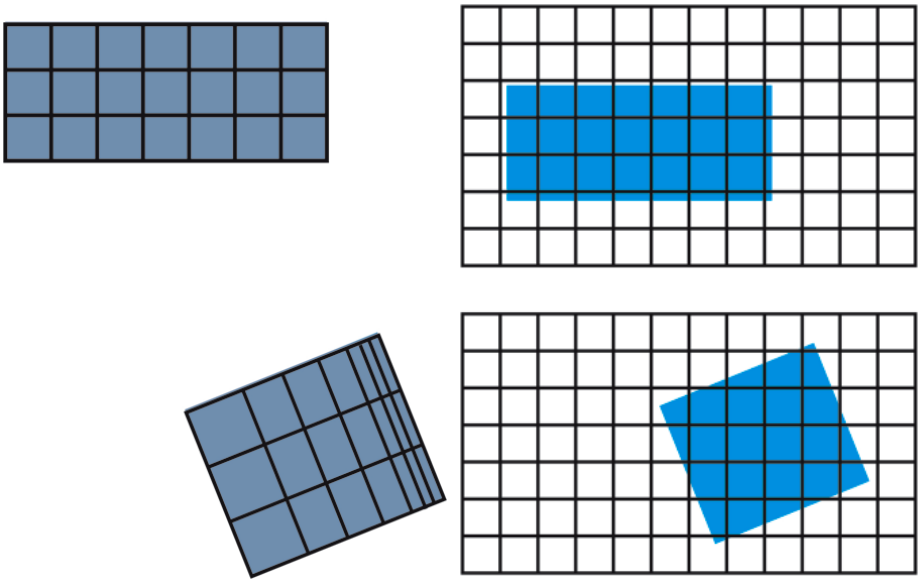

Fig. 2.2 (a) Lagrangian mesh (b) Eulerian mesh

To model the contact interface, two conditions are applied: an impenetrability condition (Equation 2.15) and a traction condition (Equation 2.16) to make sure that momentum is conserved across the interface.

$$s^s . n^s + s^f . n^f = 0 \tag{2.15}$$

$$\dot{d} = v^s . n^s + v^f . n^f = (v^s - v^f) . n^s \leq 0 \tag{2.16}$$

In this equation:

- ^{s} denotes the structural domain, and ^{f} denotes the fluid domain
- d is the penetration vector
- s is the total Cauchy stress
- n is the normal on the domain boundary

The interaction itself can be modeled in different ways. One surface (either fluid or structural) is the master surface, the other one is the slave surface, containing the slave nodes. Kinematic contact, where fluid and structure have the same velocity, makes sure momentum is conserved, but violates the energy equation. Another possibility is to apply the penalty based method. A penalty is a resisting force to the slave node, depending on its penetration through the master node. To satisfy equilibrium, an opposite force is

applied to the nodes of the master element. In Aquelet [22] an expression for the forces is proposed:

$$F_s = -k.d \tag{2.17}$$

$$F_m^i = N_i.k.d \tag{2.18}$$

N_i is a shape function at node i. This can be interpreted as springs with stiffness k placed between the slave nodes and the contact surface, see Fig. 2.11. The stiffness depends on the bulk modulus K of the master material, the surface area A of the master element and the volume V of the master element:

$$k = p_f \frac{KA}{V} \tag{2.19}$$

where p_f is scale factor for the interface stiffness. It must satisfy $0 \leq pf \leq 1$.

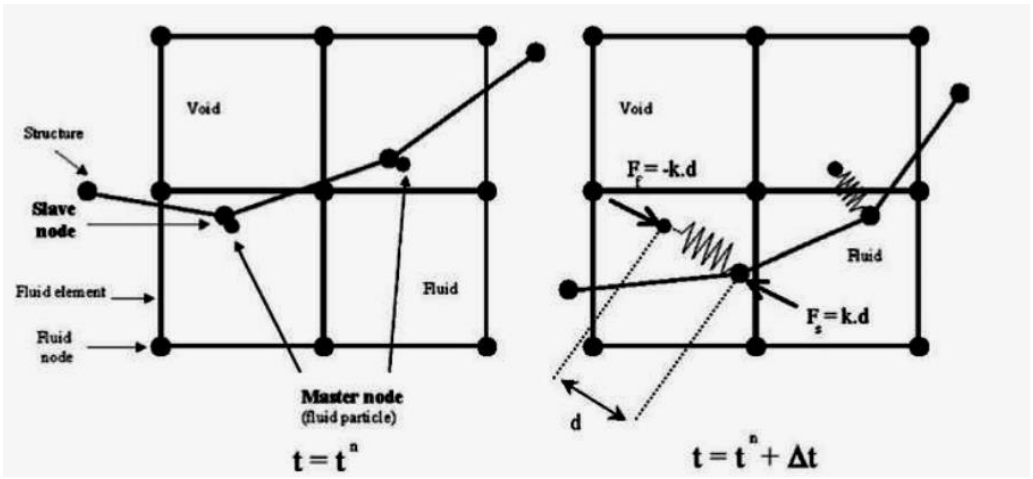

Fig. 2.3. Contact algorithm

Contact between different fluids in an Eulerian domain does not need to be defined, as it occurs by default. Because of the kinematic assumption that a single strain field is applied to the materials present in one element, the interaction is rough.

2.6.2 Volume of Fluid Method (VOF)

When using an Euler-Lagrange coupling, the fluid is modeled with a fixed mesh. The location of the free surface cannot be calculated by looking at the displacement of the nodes. Therefore, a different approach is needed to determine the free surface; several methods exist:

In the level-set free surface tracking method, the distance function $\emptyset(x,t)$ is introduced to know the distance of the surface x from its initial position at t=0. The interface corresponds to $\emptyset(x,t) = 0$. The problem with this model is that mass is not conserved.

The most popular model is the Volume of fluid model (VOF). The volume fraction F is the fractional volume of a cell occupied by the fluid, and has a value between zero and one. Every cell has its own VOF. Cells with F = 0 or F = 1 are called pure cells; when $0 \leq F \leq 1$, the cell is called a mixed cell. The VOF-method was first introduced by Hirt and Nichols. It has two important characterizing properties: The way the interface is reconstructed and the way it is propagated. As explained later on in this section, several methods exist to reconstruct the interface. Based on the obtained interface and the velocity fluxes at the different surfaces of each cell, fluid is moved from a donor cell to an acceptor cell. Only the value of the VOF in surrounding cells is needed to calculate the VOF in cell. This makes it easy to divide the calculations in parallel processes.

Rider identifies 4 steps to calculate the VOF, as shown in Fig. 2.12. In the first step, the volume is divided in discrete parts using a mesh. Next, the free surface is discretized. Now the material fluxes can be calculated. In the final step, the volumes are integrated to a new time level.

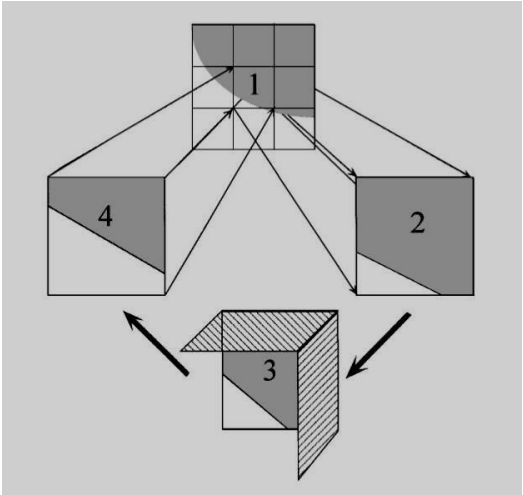

Fig. 2.4. Steps taken to calculate Volume Fraction F

Two ways of reconstructing the surface are much used nowadays. First, there is the Simple Linear Interface Calculation method (SLIC), where the interface is always parallel to one of the coordinate axes. As can be seen in Fig. 2.13(a), this method is not very accurate.

A more sophisticated method is the Piecewise Linear Interface Reconstruction method (PLIC), as can be seen in Fig. 2.13 (b). To reconstruct the interface, it is divided by a line in a certain number of discrete partitions equal to the number of phases present in the cell. The line is a linear approximation of the curved interface. Also, a discontinuity between the different lines is allowed. This method is very accurate when the curvature of the

interface is small, but even when the fluid surface has a large curvature it remains robust. This is important, especially when modelling events which can contain droplets, because infinite curvatures may appear when these droplets reconnect.

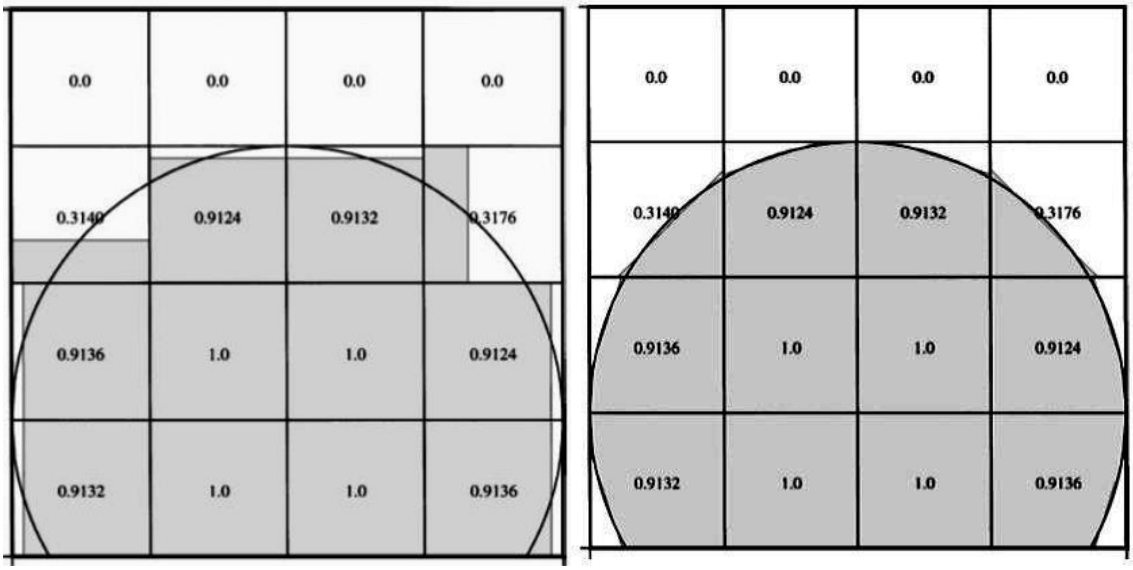

Fig. 2.5. Comparison between the SLIC and PLIC surface reconstruction algorithms

The advection equation that governs F for an incompressible fluid can be written as follows:

$$\frac{\partial F}{\partial t} + u.\nabla F \rightarrow \frac{\partial F}{\partial t} + \nabla.(u.F) = 0 \tag{2.20}$$

where u is the flow field. This equation shows that volume is conserved along a streamline.

The fluxes through a cell face can be calculated using:

$$\partial F = u.nA\partial t \tag{2.21}$$

with A the cell surface and ∂t the time step.

When these fluxes are calculated, the VOF is updated from level n to n + 1:

$$F^{n+1} = F^n + \frac{\partial F_e + \partial F_n - \partial F_w - \partial F_s}{\partial x \partial y} \tag{2.22}$$

The indices n, e, s and *w* stand for north, east, south and west, representing the fluxes through the different faces of a cell in two dimensions. Away from the free surface, the net flux becomes zero. Around the free surface the calculation of the fluxes becomes more complicated, a method to do so can be found in Hurt and Nichols. There are however some major drawbacks to this method. First of all, conservation of mass may be violated when rounding F when $F \leq 0$ or $F \geq 1$. This is especially the case for the

lower-order methods like SLIC. To address these problems, a local height function was introduced. A detailed description is given by Gerrits. The local height function h is defined in each surface cell, and gives the height of the surface in a column of three cells each. The direction of the local height function is defined as the direction most normal to the free surface.

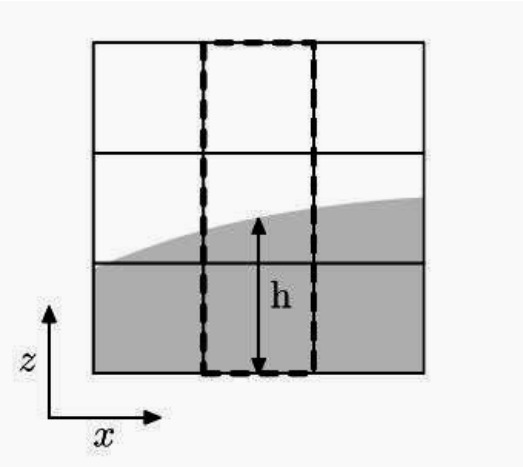

Fig. 2.6. Local height function h

Normally, when the fluxes at the boundaries are calculated, the individual values of the VOF are updated. Here the local height function *h* is updated instead. Afterwards, the VOF is calculated from the height of the fluid in each column. No underflow or overflow of the column can appear, so this method is strictly mass conserving. As a conclusion, it can be stated that the introduction of the local height function definitely improves the performance of the VOF algorithm.

In the initial time step, the initial volume occupied by the water must be determined. This can be done using a predefined field for the material assignment. The Eulerian domain must be divided in different sections to be able to do this. A volume fraction between 0 and 1 can be assigned to a chosen section of the domain. It is important to include a certain region filled with void. When the Langrangian part moves through the Eulerian domain, the Eulerian elements occupied by the lagrangian part become filled with void. Assigning at least one layer of void, results in the formation of a free surface. This is especially important when the lagrangian part is positioned outside of the Eulerian domain in the initial state of the model. But even when this is not the case, including void makes sure that water can be pushed out of the Eulerian element by the impacting body.

2.6.3. Boundary conditions and loads

In fact, boundary conditions are related to the problem, not to the description employed. Thus, the same boundary conditions employed in Eulerian or Lagrangian descriptions are implemented in the CEL formulation, that is along the boundary of the domain, kinematical and dynamical conditions must be specified. Generally, this is described as:

$$\begin{cases} \vec{v} = \overrightarrow{v_D} & on\ \ \Gamma_D \\ \vec{n}.\vec{\sigma} = t & on\ \Gamma_N \end{cases} \tag{2.23}$$

where $\overrightarrow{v_D}$ and t are the prescribed boundary velocities and tractions respectively; n is the outward unit normal to Γ_N, and Γ_D and Γ_N are the Derichle and Neumann different subsets respectively, which explain the piecewise smooth boundary of the target domain. Usually, stress conditions on the boundaries represent the natural boundary conditions, and therefore, they are directly considering in the weak form of the momentum conservation equation. If part of the boundary is composed of a material surface whose position is unknown, and then a mixture of both conditions is required. The CEL formulation allows an accurate tracking of material surfaces.

In a customary Lagrangian analysis nodes are fixed within the material, and elements distort as the material distorts. Lagrangian elements are always totally full of a single material, so the material boundary overlaps with an element boundary.

By contrast, in an Eulerian analysis, nodes are fixed in space, and material flows through elements that do not distort. Eulerian elements may not always be totally full of material; several may be partially or completely void. Therefore, the Eulerian material boundary must, be computed during each time increment and generally does not correspond to an element boundary. The Eulerian mesh is typically a simple rectangular grid of elements created to cover well beyond the Eulerian material boundaries, giving the material space in which to move and deform. In fact, if some Eulerian material passes outside the Eulerian mesh domain, it is lost from the simulation. Eulerian material can interact with Lagrangian elements through Eulerian–Lagrangian contact. Volume fraction data are computed for each Eulerian material in an element. Within each time increment, the boundaries of each Eulerian material are reconstructed using these data. The interface reform algorithm approaches the material boundaries within an element as simple planar surfaces; considering that the Eulerian method is applied only to three-dimensional elements. This assumption produces a simple, estimated material surface that may be discontinuous between neighboring elements. Therefore, accurate determination of a

material’s location within an element is possible only for simple geometries and fine mesh resolution is required in most Eulerian analyses.

The material representing the water can flow during the analysis, and the mesh does not need to conform to the topology of the materials; in fact, a simple rectangular grid typically provides the best results.

An Eulerian section assignment defines the materials that may be present in the mesh over the progression of the analysis, and an initial condition specifies which materials are present in each element at the beginning of the analysis. The initial condition effectively determines the initial topology of the materials in the model. The water inside the tank has been included into the model by defining an Eulerian initialized with water. In this numerical analysis the Eulerian material is tracked as it flows through the mesh by computing its Eulerian volume fraction (EVF). Each Eulerian element is designated a percentage, which represents the portion of that element filled with a material. If an Eulerian element is completely filled with a material, its EVF is 1; if there is no material in the element, its EVF is 0. Contact between Eulerian materials and Lagrangian materials is enforced using a general contract that is based on a penalty contact method. A general contact algorithm does not enforce contact between the Lagrangian elements and the Eulerian elements. The Lagrangian elements can move through the Eulerian mesh without resistance until they encounter an Eulerian element filled with material (EVF $\neq 0$). The water inside the tank has been included into the model by defining an Eulerian initialized with water. The tank structure can be modeled using traditional nonlinear Lagrangian elements. The Eulerian-Lagrangian contact formulation is based on the enhanced immersed boundary method. A great benefit of this method is there is no need to generate a conforming mesh for the Eulerian domain. A rough property is introduced into a mechanical surface model governing the interaction of the contact surfaces.

2.6.4. Mesh

There is only one element available in the code, element library to mesh an Eulerian part, called EC3D8R. 'E' stands for Eulerian, 'C3D8' means it's a three-dimensional brick with 8 nodes, and 'R' indicates reduced integration is applied. It is based on a langrangian element (C3D8R), but with added controls to be able to handle multiple materials in one element, and to support the transport phase in the calculation of the volume fraction.

The default formulations for the element are applicable for a wide range of problems, both dynamic and quasi-static, but are not very efficient. To optimize the control element

of the high-rate dynamic event, hourglass control is used, which is an artificial numerical stiffness applied to a single element. Otherwise, the linear element's behavior is not stiff enough.

When applying reduced integration, only the linear varying part of the incremental displacement is used to calculate the increment of physical strain. The remaining part of the incremental displacement is called the hourglass field, and can be expressed in hourglass modes. It may occur that these hourglass modes get excited, resulting in severe mesh distortion without any resisting stress. To prevent this, there are several methods of hourglass control. In this model, viscous hourglass control is appropriate, because it the most efficient approach for very dynamic simulations. Three parameters can be adjusted: The displacement hourglass scaling factor s, and the linear and quadratic bulk viscosity scaling factors b_1 and b_2.

2.6.4.1 Displacement hourglass scaling factors

A viscoelastic approach of the Kelvin-type is governed by the following Equation:

$$Q = s\left[(1-\alpha)Kq + \alpha C\frac{dq}{dt}\right] \tag{2.24}$$

Here, q is an hourglass mode, magnitude, and Q is the force or moment related to q. K represents the hourglass stiffness, and is calculated automatically by software. C is the linear viscous coefficient. The first term on the right hand side, determines the elastic behavior, while the second term accounts for the viscous behavior. α is a scaling factor to model the balance between elastic and viscous control. Because a pure viscous hourglass control is chosen, α equals one. Equation 2.24 becomes:

$$Q = sC\frac{dq}{dt} \tag{2.25}$$

The Eulerian elements do not move in space, so we can apply s = 0, resulting in Q = 0.

2.6.4.2. Bulk viscosity scaling factors b_1 And b_2

Bulk viscosity introduces damping in the model. It can be adjusted for the whole model in each time-step. By doing this for the Eulerian element in the section controls, the adjustment is only valid in the Eulerian domain. The bulk viscosity parameters for the Lagrangian part are set to a default value. For the Eulerian domain, both, b_1 and b_2 are set to zero. This can be explained as follows:

The linear bulk viscosity scaling factor b_1 is used to damp ringing of the highest element frequency in the model, which would give oscillations in the stable time increment. The damping introduces a bulk viscosity pressure given by the following expression:

$$p_{bv1} = b_1 \rho c_d L_e \dot{\epsilon}_{vol} \tag{2.26}$$

This pressure has a linear relation with the volumetric strain rate $\dot{\epsilon}_{vol}$. The quadratic viscosity scaling factor b_2 is related to a pressure that smears possible shock fronts across different elements in order to prevent they should collapse under extremely high velocity gradients.

$$p_{bv2} = \rho \, (b_2 \rho L_e \dot{\epsilon}_{vol})^2 \tag{2.27}$$

Again, because the Eulerain mesh is not moving, this damping is not necessary and can be set to zero. This increases the stable time increment, reducing calculation time. The pressure associated with the damping is purely a numerical aid, and makes no difference in the obtained pressure at the nodes.

2.6.4.3. Mesh size

Of course, the mesh of the Eulerian domain must be small enough to capture the impact pressure and the boundary layer around the impacting object. Considering the advice of code support and relying on the knowledge present in the last works, an Eulerian mesh element size of 10 mm was chosen. Moreover, the element size of the lagrangian mesh a must have the same order of magnitude in order to prevent numerical leaking, where the fluid leaks into the lagrangian part.

2.7. Application to SPH

Smoothed particle hydrodynamics (SPH) is a numerical method which is part of the family of mesh-less mesh-free methods. It was proposed by Gingold and Monaghan (1977) primarily for astrophysical problems. This method is based on Lagrangian method wherever the coordinates move with fluid, and the resolution of the method can be adjusted regarding inconstant such as density. There are many purposes for which both the Eulerian-Lagrangian and the smoothed particle hydrodynamics methods can be used. In many Eulerian-Lagrangian analyses the material to void ratio small and, therefore, the calculative effort might be excessively high. In such these cases the smoothed particle hydrodynamics method can be useful. For these methods you do not define nodes and elements as you would normally define in a finite element analysis; instead, only a

collection of points are necessary to represent a given body. In smoothed particle hydrodynamics these nodes are commonly referred to as particles or pseudo-particles.

For the application of SPH into incompressible flow (such as water) the continuity equation can be written in two forms:

$$\rho_a = \sum_b m_b w_{ab} \tag{2.28}$$

or by:

$$\frac{d\rho_a}{dt} = \sum_b m_b v_{ab} \,.\nabla_{ab} w_{ab} \tag{2.29}$$

where a is the particle of interest, b is the neighboring particle by particle a, ρ is the particle density, m is the particle mass, w is the kernel function and v_{ab} is the velocity difference of particles a and b. w_{ab} is the kernel function which has the features of symmetric, normalization, monotonic, and compact support. Equation (2.28) preferred because it shows a less boundary insufficiency error than equation (2.29).

The SPH momentum equation is shown in equation (2.30) which Π_{ab} is the viscosity term.

$$\frac{dv_a}{dt} = -\sum_b m_b \left(\frac{p_a}{\rho_a^2} + \frac{p_b}{\rho_b^2} + \Pi_{ab}\right)\nabla_a w_{ab} \tag{2.30}$$

For water simulations, Cleary (1998) viscosity model is chosen because in this model angular momentum assuming smoothing length h remains constant:

$$\Pi_{ab} = -\frac{\xi}{\rho_a \rho_b} \frac{4\mu_a \mu_b}{(\mu_a + \mu_b)} \frac{v_{ab} r_{ab}}{r_{ab}^2} \tag{2.31}$$

where μ is the dynamic viscosity of the fluid and numerical calibration yields $\xi = 4.9633$ (Cleary, 1998).

The force per unit mass appearing from a boundary particle in a fluid particle within a close domain is:

$$\vec{f} = \vec{n} R(\eta) \rho(\xi) \tag{2.32}$$

where $\vec{n}$ is the normal of the boundary particle. η is the normal distance from the fluid particle in the boundary particle. ξ is the distance from the distance between the fluid particle and the boundary particle projected on the tangent of the boundary particle. The Tait equation of state is expressed as follows:

$$P = B\left[\left(\frac{\rho}{\rho_0}\right)^{\gamma} - 1\right] \tag{2.33}$$

where B is the reference pressure defined as $B = CS_0^2 \rho_0/\gamma$. Based on experimental data, Cole suggested B=3047 MPa and $\gamma = 7.15$ for water. (Table.2.1)

2.7.1. Boundary conditions

When a fluid particle is coming close to a closed boundary, it is supposed to be blocked. A water particle near a wall still has the density and other quantities of water. Three boundary condition theories are used in the SPH method, which are ghost boundary condition, repulsive boundary condition and dynamic boundary condition. The ghost boundary condition was proposed by Randles and Libersky (1996). In this method the properties, including particle position, vary with each time step to prevent particles from penetrating through the boundaries. Based on the repulsive boundary condition, fluid particle can never cross a solid boundary (Monaghan 1994; Monaghan and Kos; Rogers and Dalrymple 2008). The dynamic boundary particles; which are applied in this research, were proposed by Dalrymple and Knio (2000) and developed by Crespo et al. (2007). The boundary particles share the same properties as the fluid particles. They have to satisfy the same equations of state, continuity and energy equations.

In this method the water is modeled using continuum pseudo-particle. As the internally determined connectivity is permitted to change every increment, the method robustly handles the severe deformations associated with the sloshing water. The smoothed particle hydrodynamics method implemented in this research uses a cubic spline as the interpolation polynomial and is based on the classical smoothed particle hydrodynamic theory as mentioned before. The pseudo-particles are spaced in a relatively uniform fashion every 5mm in all directions. These particle elements utilize the existing functionality to reference element-related features such as materials, initial conditions, distributed loads, and conception.

There are no edges connecting the points as these points (pseudo-particles) do not require the definition of multiple-node element connectivity, as is the case in the traditional finite element representation on the left. An alternative to directly defining particle elements is to define conventional continuum finite elements and automatically convert them to particle elements at the beginning of the analysis or during the analysis.

Smoothed particle hydrodynamics is a fully Lagrangian modeling scheme permitting the discretization of a prescribed set of continuum equations by interpolating the properties directly at a discrete set of points distributed over the solution domain without the need to define a spatial mesh. The method's Lagrangian nature, associated with the absence of a

fixed mesh, is its main strength. Difficulties associated with fluid flow and structural problems involving large deformations and free surfaces are resolved in a relatively natural way.

At its core, the method is not based on discrete particles (spheres) colliding with each other in compression or exhibiting cohesive-like behavior in tension as the word particle might suggest. Rather, it is simply a clever discretization method of continuum partial differential equations. In that respect, smoothed particle hydrodynamics is quite similar to the finite element method. SPH uses an evolving interpolation scheme to approximate a field variable at any point in a domain. The value of a variable at a particle of interest can be approximated by summing the contributions from a set of neighboring particles, denoted by subscript *j*, for which the "kernel" function, *W*, is not zero

$$f(x) \approx \sum \frac{m_j}{\rho_j} f_j W(|x - x_j|, h) \tag{2.34}$$

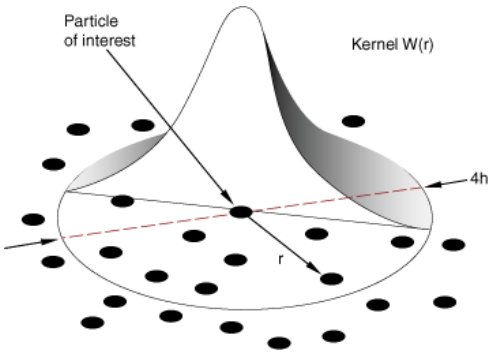

Fig. 2.7.Kernel function.

The smoothing length, *h*, determines how many particles influence the interpolation for a particular point.

The method can use any of the materials available in Abaqus/Explicit (including user materials). You can specify initial conditions and boundary conditions as for any other Lagrangian model. Contact interactions with other Lagrangian bodies are also allowed, thus expanding the range of applications for which this method can be used.

The method is less accurate in general than Lagrangian finite element analyses when the deformation is not too severe than coupled Eulerian-Lagrangian analyses in higher deformation regimes. If a large percentage of all nodes in the model are associated with smoothed particle hydrodynamics, the analysis may not scale well if multiple CPUs are used.

2.7.2. Artificial viscosity

Artificial viscosity in smoothed particle hydrodynamics has the same meaning as bulk viscosity for finite elements. Similar to other Lagrangian elements, particle elements use linear and quadratic viscous contributions to dampen high frequency noise from the computed response. In rare cases when the default values are not appropriate, you can control the amount of artificial viscosity included in a smoothed particle hydrodynamic analysis.

Initial conditions pertinent to mechanical analyses can be used in a smoothed particle hydrodynamic analysis.

2.7.3. SPH kernel interpolator

By default, the smoothed particle hydrodynamic method implemented in this code uses a cubic spline as the interpolation polynomial.

The implementation is based on the classical smoothed particle hydrodynamic theory as outlined in the references below. You also have the option of using a mean flow correction configuration update, commonly referred to in the literature as the XSPH method (see Monaghan, 1992), as well as the corrected kernel of Randles and Libersky, 1997, also referred to as the normalized SPH (NSPH) method.

2.7.4. Computing the particle volume

There is currently no capability to automatically compute the volume associated with these particles. Hence, you need to supply a characteristic length that will be used to compute the particle volume, which in turn is used to compute the mass associated with the particle. It is assumed that the nodes are distributed uniformly in space and that each particle is associated with a small cube centered at the particle. When stacked together, these cubes will fill the overall volume of the body with some minor approximation of the free surface of the body. The characteristic length is half the length of the cube side. From a practical perspective, once you have created the nodes, you can use the half-distance between two nodes as the characteristic length. Alternatively, if you know the mass and density of the part, you can compute the volume of the part and divide it by the total number of particles in the part to obtain the volume of the small cube associated with each particle. Half of the cubic root of this small volume is a reasonable characteristic length for this particle set.

2.7.5. Smoothing length calculation

Even though particle elements are defined in the model using one node per element, the smoothed particle hydrodynamic method computes contributions for each element based on neighboring particles that are within a sphere of influence. The radius of this sphere of influence is referred to in the literature as the smoothing length. The smoothing length is independent of the characteristic length discussed above and governs the interpolation properties of the method. By default, the smoothing length is computed automatically. As the deformation progresses, particles move with respect to each other and, hence, the neighbors of a given particle can (and typically do) change. Every increment recomputed this local connectivity internally and computes kinematic quantities (such as normal and shear strains, deformation gradients, etc.) based on contributions from this cloud of particles centered at the particle of interest. Stresses are then computed in a similar fashion as for reduced-integration brick elements, which are in turn used to compute element nodal forces for the particles in the cloud based on the smoothed particle hydrodynamic formulation.

By default, using code computes a smoothing length at the beginning of the analysis, such that the average number of particles associated with an element is roughly between 30 and 50. The smoothing length is kept constant during the analysis. Therefore, the average number of particles per element can either decrease or increase during the analysis depending on whether the average behavior in the model is expansive or compressive, respectively. If the analysis is mostly compressive in nature, the total number of particles associated with a given element might exceed the maximum allowed and the analysis will be stopped. By default, the maximum number of allowed particles associated with one element is 140.

2.7.6. Interactions

Bodies modeled with particles can interact with other finite element meshed bodies via contact. The contact interaction is the same as any contact interaction between a node-based surface (associated with the particles) and an element-based or analytical surface. Both general contact and contact pairs can be used. All interaction types and formulations available for contact involving a node-based surface are allowed, including cohesive behavior. Different contact properties can be assigned via the usual options. By default, the particles are not part of the general contact domain similar to other 1-node elements (such as point masses). The default contact thickness for particles is the same value

specified as the characteristic length on the section definition; thus, for contact purposes, particles behave as spheres with radii equal to the radius of a sphere inscribed in the small cube associated with the particle volume as described above.

You should not specify a contact thickness of zero for the nodes associated with PC3D elements or contact may not be resolved robustly. The recommended approach is to use the default or specify a reasonable contact thickness.

Interaction between different bodies all modeled with PC3D elements is allowed. However, this interaction is meaningful only in cases when the colliding smoothed particle hydrodynamic bodies are made of the same fluid-like material, such as a water drop falling in a bucket partially filled with water. In solids-related applications, such as modeling a bullet perforating an armor plate, one of the bodies must be modeled using regular finite elements.

Contact interactions cannot be defined between particles and Eulerian regions.

2.7.7. Elements

These one node elements fill only the space initially occupied by the water just before the impact. Therefore, fewer elements are needed when compared to the number of Eulerian elements in the CEL method. These elements do not have faces or edges associated with them. Also a node-based surface associated with the water pseudo-particle is included in the contact domain to model the interaction between the water and the tank.

The smoothed particle hydrodynamic method is implemented via the formulation associated with continuum particle elements (PC3D). These 1-node elements are simply a means of defining particles in space that model a particular body or bodies. These particle elements utilizes the existing functionality in using code to reference element-related features such as materials, initial conditions, distributed loads, and visualization.

These elements define a similar fashion as define point masses. The coordinates of these points lie either on the surface or in the interior of the body being modeled, similar to the nodes of a body meshed with brick elements. For more accurate results, you should strive to space the nodal coordinates of these particles as uniformly as possible in all directions.

An alternative to directly defining PC3D elements is to define conventional continuum finite element types C3D8R, C3D6, or C3D4 and automatically convert them to particle elements at the beginning of the analysis or during the analysis. The smoothed particle hydrodynamic method implemented in software uses a cubic spline as the interpolation polynomial and is based on the classical smoothed particle hydrodynamic theory as

outlined in the references below.

The smoothed particle hydrodynamic method is not implemented for two-dimensional elements. Asymmetry can be simulated using a wedge-shaped sector and symmetry boundary conditions. There are no hourglass or distortion control forces associated with PC3D elements. These elements do not have faces or edges associated with them.

2.7.8. Limitations of SPH method

Smoothed particle hydrodynamic analyses are subject to the following limitations:

- They are less accurate in more general than Lagrangian finite element analyses when the deformation is not too severe and the elements are not distorted. In higher deformation regimes coupled Eulerian-Lagrangian analyses are also generally more accurate. The smoothed particle dynamic method should be used primarily in cases when the conventional finite element method or the coupled Eulerian-Lagrangian method has reached their inherent limitations or are prohibitively expensive to perform.
- When the material is in a state of tensile stress, the particle motion may become unstable leading to the so-called tensile instability. This instability, which is strictly related to the interpolation technique of the standard smoothed particle dynamic method, is especially noticeable when simulating the stretched state of a solid. As a consequence, particles tend to clump together and show fracture-like behavior.
- Mass distribution inside a body defined by particle elements is somewhat different when compared to the mass distribution of the same body defined by continuum elements, such as C3D8R elements. When particle elements are used, the volume of all particles in that body is the same. Consequently, the nodal mass associated with all particles in that body is the same. If the nodes are not placed in a regular cubic arrangement, the mass distribution is somewhat inexact, particularly at the free surface of the body being modeled.
- Surface loads cannot be specified on PC3D elements. However, distributed loads, such as pressure, can be applied to other finite element surfaces that can apply a pressure onto the particle elements via contact interactions.
- Bodies modeled with particles that were not defined using the same section definition do not interact with each other. Hence, you cannot use smoothed particle hydrodynamics to model the mixing of bodies with dissimilar materials.

- Within a given body (part) defined via one solid section definition, gravity loads and mass scaling cannot be specified selectively on a subset of elements referenced by this definition. Instead, the two features must be applied to all the elements in the element set associated with the solid section definition.

Smoothed particle hydrodynamic computations are distributed across parallel domains in most cases; however, they are all performed by a single domain (with a single processor) for models with any of the following characteristics (which will often dramatically degrade parallel scalability):

- Progressive element conversion
- Multiple solid sections for PC3D elements
- Normalized kernel specified as a section control
- Predefined field variable (including temperature) dependence of material properties

Smoothed particle hydrodynamic analyses are subject to the following limitations if multiple CPUs are used:

- Contact output is not supported for smoothed particle hydrodynamic slave nodes.
- The element history output is not supported.
- Energy history output other than for the whole model is not supported.
- Dynamic load balancing cannot be activated.

2.7.9. Using section controls for specifying other SPH formulation parameters

The smoothing length (units of length) for precise control of the radius of influence associated with a given particle can be specified separately. Alternatively, it is possible to scale the default smoothing length by specifying a dimensionless smoothing length factor. By default, the smoothing length is kept constant throughout the analysis. You can specify a variable smoothing length that will increase or decrease during the analysis depending on the divergence of the velocity field, which is a measure of compressive or expansive behavior.

By default, the maximum number of particles associated internally with a PC3D element cannot exceed 140, and in this research it is chosen as 8 because of considering the long duration ground motions. You can modify this number; however, a large value leads to larger memory requirements and, in most cases, to a significant degradation in performance.

You can specify a mean velocity filtering coefficient that is used for the modified coordinate updates for particles. A zero value for this coefficient (default) leads to the classical SPH method. Also a nonzero value for this coefficient leads to the XSPH method.

By default, the SPH kernels satisfy the zero-order completeness requirement. A first-order complete, corrected (normalized) kernel is also available, which is sometimes referred in the literature as the normalized SPH (NSPH) method. In high-deformation solid mechanics analyses the use of this kernel may lead to more accurate results.

2.8. Summary

The equation of motion for a typical structural MDOF system subjected to external dynamic forces was derived. The procedure for coupling the fluid and structural domains in finite element modeling of the liquid tanks was discussed for two techniques were employed in this research. The equations of transferring the structural motion and the hydrodynamic pressure between the structure and the fluid were developed.

The finite element formulation for the coupled system of liquid tanks in the time domain was described. In deriving these formulations, appropriate boundary conditions available in typical liquid tanks were applied. In addition, problems, advantages and disadvantages associated with performance of the CEL and SPH methods were discussed. Using the proposed finite element techniques, the effects of both impulsive and convective parts and their corresponding effects can be taken into account. The proposed techniques are general and can be employed for any tank configurations, or any direction of seismic excitation. This method can account for all aspects of structural and fluid components in the time domain.

Some important properties of the elements and particles used in this study for numerical modeling of sloshing phenomena in tank models were described in this chapter.

References

[1] Souli, M. and Zolesio, J.P.: Arbitrary Lagrangian-Eulerian and free surface methods in fluid mechanics. Computer methods in applied mechanics and engineering, 191:451-466, 2001.

[2] Rabier, S. and Medale, M.: Computation of free surface ows with a projection fem in a moving mesh framework. Computer methods in applied mechanics and engineering, 192:4703-4721, 2003.

[3] Aquelet, N, Souli, M., and Olovsson, L.: Euler-Lagrange coupling with damping effects: Application to slamming problems. Computer methods in applied mechanics and engineering, 195:110-132, 2006.

[4] Gingold, R. A., and J. J. Monaghan, "Smoothed Particle Hydrodynamics: Theory and Application to Non-Spherical Stars,"Royal Astronomical Society, Monthly Notices, vol. 181, pp. 375–389, 1977.

[5] Johnson, J., R. Stryk, and S. Beissel, SPH for High Velocity Impact Calculations," Computer Methods in Applied Mechanics and Engineering, 1996.

[6] Libersky, L. D., and A. G. Petschek, High Strain Lagrangian Hydrodynamics, Journal of Computational Physics, vol. 109, pp. 67–75, 1993.

[7] Monaghan, J., "Smoothed Particle Hydrodynamics," Annual Review of Astronomy and Astrophysics, 1992.

[8] Munjiza, A., and K. R. F. Andrews, "NBS Contact Detection Algorithm for Bodies of Similar Size," International Journal for Numerical Methods in Engineering, vol. 43, pp. 131–149, 1998.

[9] Randles, P. W., and L. D. Libersky, "Recent Improvements in SPH Modeling of Hypervelocity Impact," International Journal of Impact Engineering, 1997.

[10] Swegle, J. W., and S. W. Attaway, "An Analysis of Smoothed Particle Hydrodynamics," Sandia National Lab Report SAND93–2513, 1994.

[11] Wendland, H., "Piecewise Polynomial, Positive Definite and Compactly Supported Radial Functions of Minimal Degree,"Advances in Computational Mathematics, 1995.

3. Sloshing in water reservoir tanks due to harmonic motions

3.1. General remarks

Sloshing is the motion of a liquid with a free surface in a partially filled liquid container. The phenomenon is often associated with many engineering problems. The basic analysis of liquid sloshing involves the estimation of hydrodynamic pressure distribution, free surface elevations and the natural frequencies of the system. These parameters have a significant effect on the dynamic stability and performance of the tanks induced by motions. The high pressures and impact forces created can result in serious implications such as structural deformation within the walls, fatigue of the membrane layer or even structural failure in severe cases. Sloshing is related to the continuously changing free surface. It is difficult to simulate the free surface, especially when nonlinear phenomena such as breaking waves and overturned wave are considered. In this regard, sloshing experiment is essential for understanding and verification of numerical simulating results.

In this chapter, water sloshing in rectangular tank under lateral excitation is first investigated experimentally. Rectangular tanks are designed to investigate the different aspects of sloshing behavior. Parameters such as water depth and excitation frequencies are varied to study their effects on sloshing. Numerical simulations of typical sloshing cases are then performed using the SPH and CEL methods and the results are compared with the experimental results.

3.2. Experimental setup

3.2.1. Experimental facilities

Fig.3.1 shows the experimental setup. A rectangular tank was mounted on a shake table which was subjected to lateral displacement excitation. The tank made of Plexiglas was partially filled with water. The free surface elevation of water was measured using wave gauges. A pressure sensor was used to measure water pressure on one side wall (see Figure 3.5 for details). A hydraulic actuator generates horizontal motion of the shake table. Its displacement was measured by a displacement transducer mounted on the shake table. All the output signals from the shake-table, wave gauges and pressure sensor were sent to a digital oscilloscope where data can be acquired and stored. The dynamic motion of the fluid was recorded by a high speed camera located in front of the tank.

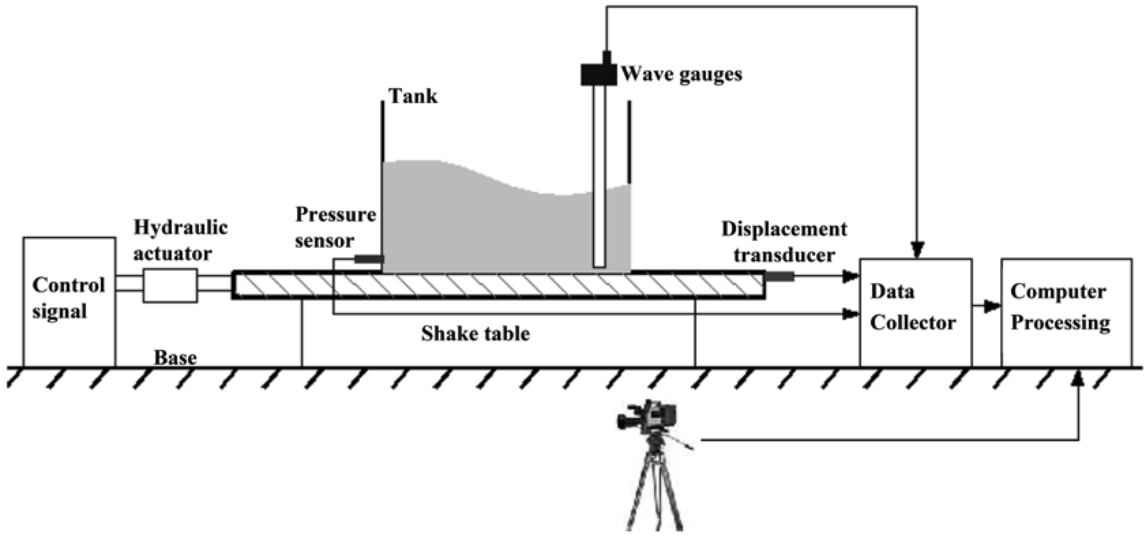

Fig.3.1. Experimental apparatus and working principle

3.2.2. Water Tank

The water tank used in the sloshing experiments is schematically shown in Figure 3.2. The tank with length L and height H was filled with water up to the filling depth *d*. A wave probe was placed 10 mm from the right wall to measure the free surface elevation (η) near that corner. The pressure sensor was located at the corner of the tank bottom, which is shown in the figure.

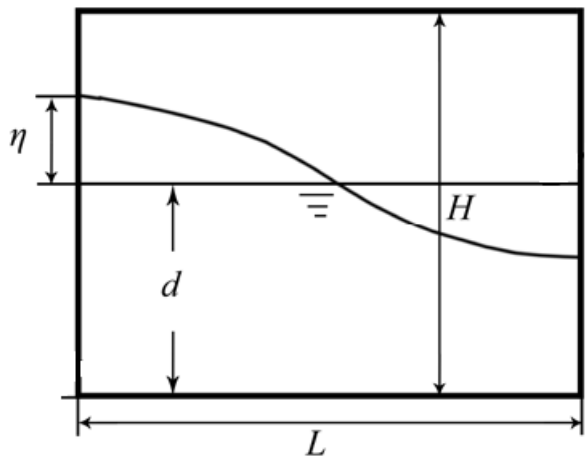

Fig.3.2. Definition of parameters for liquid sloshing in a rectangular tank

3.2.3. Shake table

A 1.5 m x 1.5 m shake table driven by a hydraulic actuator is used in the sloshing experiments. The shake table can only generate unidirectional lateral excitation.

In order to ensure that the excitation from the shake table can be fully transmitted to the

tank, the rectangular tank has to be tightly fastened on the shake table. This is done by anchoring the tank against two square steel tubes that are bolted tightly against the shake table (Figure 3.3).

Fig.3.3. Fixing tools of rectangular tank on the shake table

3.2.4. Wave probes

Wave probes were installed to measure the free surface elevation of the sloshing waves. The wave probes worked based on the principle of linear variation of capacitance with water surface change. A capacitor is formed from insulated wire held taut by a supporting rod, with water serving as a "ground" (see Figure 3.4). The capacitance of the wire changes according to the water surface displacement. Hence, the wave height is obtained by detecting the change in capacitance of the wire. The wave probe should be installed vertically for accuracy.

Calibration is necessary to obtain conversion coefficient between voltage and water level. Calibration is performed in a deep water bucket, by mounting wave probe on an adjustable stand which allows it to be adjusted up and down. The readings are taken at intervals of 10 mm from 10 cm to 23 cm of the water height.

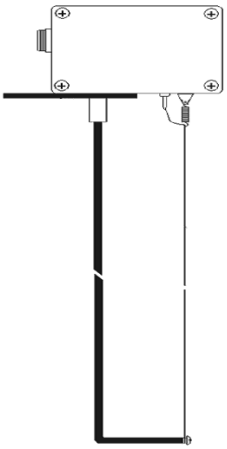

Fig.3.4. Schematic Diagram and picture of wave probe

3.2.5 Pressure sensor

Pressure sensor was installed on the two side walls at near the bottom of the tank. It was used to measure the hydrodynamic pressure response during sloshing.

Calibration was carried out to obtain the different voltage readings corresponding to the different water pressures. As shown in Figure 3.5, the pressure sensor was mounted at the bottom of a container for calibration. A bubble level was used to make sure the container was standing vertically. Pressure readings were collected from varying the water level.

Fig. 3.5. Tank with pressure sensor mounted

3.2.6 High speed camera

A high speed camera was set up at about 1 m in front of the experimental tank for image capture and connected to a data processor. The camera could record the wave profiles at a maximum frame rate of 500 fps and provided a graphical view of water sloshing. DC lighting was used to provide the necessary brightness. The images taken were selectively

digitized to derive the free surface profiles.

3.2.7. Other considerations

Precautions were taken to ensure better accuracy of results during the experiments. Firstly, the water surface was ensured to be stationary before the shake table was started. Secondly, the tank was placed and fastened to align with the motion of the shake table. The inner surface of the tank was also made smooth to reduce the boundary layer effect and minimize 3D effects of sloshing waves. Thirdly, connecting cables were arranged so as not to cross one another and sufficient lag lengths were reserved to avoid cable being stretched when the shake table moved.

3.3. Sloshing experiments and comparison with numerical and analytical solutions

Liquid sloshing in a tank is a highly nonlinear phenomenon in which the free surface profiles can be considered as a composition of several wave modes. The superposition of the modes depends on the liquid depth, tank geometry and external excitations.

For a rectangular tank, the natural frequency of the fluid can be estimated from linear theories (Su et al., 1982) by the following equation,

$$\omega_0 = \sqrt{g\frac{m\pi}{L}tanh\left(\frac{m\pi}{L}d\right)} \tag{3.1}$$

Where d is the depth of water in the tank, L the length of the tank, m the mode number and g the acceleration due to gravity.

As seen from the above equation, there exist an infinite number of natural frequencies. However, only the fundamental frequency (m=1) is significant for marine engineering application (Su et al., 1982). In our experimental study only the first natural frequency of the first sloshing mode is considered.

It should be noted that resonant sloshing is an ideal scenario difficult to achieve in experiments due to the accuracy in the natural frequency of sloshing. Furthermore, Hill (2003) and Chen and Nokes (2005) pointed out that the first natural frequency is shifted due to the nonlinearity of sloshing and the effect of the viscosity of the fluid. The accuracy of the calculation of the real natural frequency is further decreased by the precision of the parameters used in Eq. (3.1) which were measured during experiments. Therefore, in the following resonant sloshing case, the excitation frequency is close to but is not necessarily exact the natural frequency of liquid sloshing.

In our experiment study, the shake table displacement is sinusoidal and governed by

$\chi(t) = \chi_0 \sin(\omega_d t)$, where χ_0 is the amplitude of excitation and ω_d the excitation frequency. Initially we used the excitation acceleration for t≥0, as many investigators adopted it such as Faltinsen (1978) and Wu et al. (1998). For the shake table given an initial condition with a non-zero velocity, there will be a big initial impulse occurring in a very short time. Ideally, the initial conditions of the shake table should be, $u_{t=0} = 0$, $v_{t=0} = 0$ and $a_{t=0} = 0$.

Tap water is used in the experiments and the property of water, including viscosity is considered in numerical simulation.

3.3.1. Analytical formulations for sloshing in tank subjected to harmonic motion

A tank problem with sloshing liquid is generally regarded as an initial boundary value problem. The sloshing of irrotational flow of an incompressible and inviscid fluid within a container is treated by potential flow theory in which the motion of the fluid inside a tank governed by the Laplace equation:

$$\nabla^2 \phi = 0 \tag{3.2}$$

where ϕ represents the velocity potential function of fluid. It is possible to split the total velocity potential function, ϕ, into a fluid disturbance potential function, $\tilde{\phi}$, and a tank potential function, ϕ_0, which defines the motion of the tank, that is:

$$\phi = \tilde{\phi} + \phi_0 \tag{3.3}$$

The tank is excited in the lateral direction using the following sinusoidal function with a driving frequency ω_d:

$$\chi(t) = \chi_0 \, sin(\omega_d t) \tag{3.4}$$

where χ_0 represents the harmonic external force amplitude. The tank potential function defines the motion of the tank and computed by the following equation:

$$\phi_0 = -\chi_0 \omega_d \, cos(\omega_d t) x \tag{3.5}$$

Graham and Rodriguez (1974) solved the three dimensional velocity potential:

$$\tilde{\phi}(x, y, z, t) = \sum_{m=0}^{\infty} \sum_{n=1}^{\infty} \alpha_{mn}(t) \, cos\left(\frac{2m\pi x}{L}\right) cos\left(\frac{2n\pi y}{l}\right) cosh[k_{mn}(z + h)] \tag{3.6}$$

where L and l are the tank width and breadth, respectively, $k_{mn} = \pi \sqrt{\left(\frac{(2m)^2}{L^2}\right) + \left(\frac{(2n)^2}{l^2}\right)}$, m and n are positive integers. The corresponding free-surface natural frequency is:

$$\omega_{mn}^2 = gk_{mn}tanh\ (k_{mn}h) \tag{3.7}$$

The wave height, η can be written in the form:

$$\eta(x, y, t) = \frac{1}{g}\frac{\partial \phi}{\partial t} \tag{3.8}$$

It measured from the undisturbed liquid surface at equilibrium, and pressure can be defined in terms of velocity potential function as follows:

$$\mathrm{p(x, y, z, t)} = -\rho\frac{\partial \phi}{\partial \mathrm{t}} \tag{3.9}$$

where ρ is the mass density of the liquid.

3.3.2. Experiments of sloshing waves in the filling tank

Depending on the liquid filling height in the tank, the sloshing waves can be in the form of a standing wave, a traveling wave or a bore (Wu et al., 1998). Armenio and La Rocca (1996) have found that these three types of wave scenario may all appear depending on the ratio of filling depth over tank length, i.e. d/L. In this section, experiments are designed to observe the free-surface elevation under relative to filling depth where $d/L \leq 0.5$ since Chen et al. (2008) and Loyd's Register (2005) has found out that the sloshing is most severe when the filling depth (d) is from nearly 50% to 70%H, where H is the tank height.

Experiments and numerical simulations at partial filling levels in a tank were investigated by many researchers, indicating that the sloshing motion in a tank at the low-filling level is quite different from that experienced at the high-filling level (Ibrahim, 2005). In the low-filling case, a more distinct wave motion is observed in the tank compared with standing wave in high filling level. At the low-filling level, where the filling height is less than 20 percent of tank width (for lateral motion) or length (for longitudinal motion), a phenomenon known as a bore can be observed in the tank (Huang and Hsiung, 1996). The phenomenon can have some practical implications for the carriers. When tank motion is large, the front of the hydraulic run-up becomes steeper, developing a breaking wave. If the bore hits the bulkhead before breaking, large impact pressure can occur and damage the tank. The uniform velocity of the traveling wave also results in a large drag force on the lower part of the pump tower and its supporting system, which is an additional load on the system that must be considered when designing storage tanks on the carriers. Armenio and La Rocca (1996) have reported that, depending on the ratio of fluid depth to breadth of tank, a combination of standing wave, traveling waves and a bore may exist.

The same observation was made by Wu et al. (1998) using a FEM simulation. Therefore, it is of interest to see the CEL and SPH perform in simulating sloshing waves in relatively shallow filling depth.

In this study, a tank with dimension 0.6 m (L) x 0.36 m (H) x 0.3 m (B) is used. The filling depth of the tank is 0.23 m with the ratio $d/L = 0.38$. The first natural frequency is calculated by Eq. (3.1) according to the tank dimensions and filling condition. Resonant sloshing is 6.54 rad/s considered with external excitation frequency close to the first natural frequency of the sloshing system. The excitation amplitude used in this study is 0.4 m/s^2.

Typical wave profiles at several time instants are shown in Figure 3.6. Good agreement is observed between the numerical solutions and experimental results.

The long time simulation of this example is performed and the time history of the free surface elevation is shown in Figure 3.7 and Figure 3.9. The pressure contours at different time instants are shown in Figure 3.8 and Figure 3.10. The pressure field of the liquid is smooth and stable. Furthermore, when the wave peaks reach the wall, the pressure around the wall is as expected larger that the hydrostatic pressure.

With the parameters of the tank and, three different cases are considered with different excitation frequencies. The frequency ratios of the excitation frequency (ω_d) to the natural frequency (ω_0) of the sloshing system examined in this section are =1.0, 0.77, 0.39 respectively.

3.3.3. Free surface profiles

The sloshing event inside a 3D tank subjected to harmonic motion is investigated with fully nonlinear fluid-structure interaction algorithm based on CEL approach and SPH methods implemented in this paper. The free surface profiles of the rectangular tank model obtained from experimental and numerical studies are compared at an arbitrary instant for each loading case.

The tank is modeled as 3D in the shape of rectangles in the numerical simulations both CEL and SPH methods. Rigid solid elements are used for tank walls and Eulerian mesh for the fluid domain in CEL method and Lagrangian particles to simulate fluid in SPH method are used. The Eulerian meshes of the CEL consist of 81920 Eulerian elements with the dimension of 0.01m and the solid Lagrangian mesh consist of 12560 elements with the dimension of 0.01 m in all directions. Also in SPH method the numbers of particles consist are 41400 particles. The water assumed that was incompressible and

invoiced elastic fluid material. Boundary condition of experimental analysis and numerical analysis was chosen to be same. The slosh event simulated for this water tank system in 60 seconds using a velocity time history. The Eulerian mesh motion is engaged to allow the Eulerian mesh to move in space to surround the water tank. The simulation carried out on a Windows/x86-64 platform with 8 CPUs. The simulations took about 230 hours to solve for one analysis.

The comparison of the results of the studies is shown in Fig.3.6 at three different times of 20.15 s, 50.50 s and 50.65 s for the situation of when the amplitude and frequency of the applied harmonic acceleration are 0.4 m/s^2, 0.4 Hz, 0.8 Hz, and resonant frequency respectively. This figure shows that the free surface profile obtained from an experimental study matches with the numerical analysis.

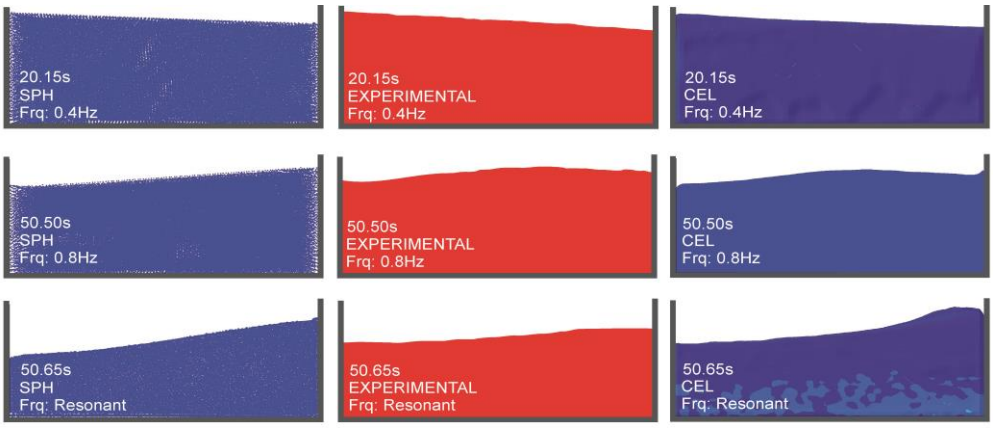

Fig.3.6. Free surface profiles of SPH, Experimental and CEL models under sinusoidal excitation with amplitude of 0.4 $m.s^{-2}$ at different times.

3.3.4. Sloshing wave height and pressure

Water displacement inside the tank subjected to harmonic motion is studied in this part considering the nonlinear interaction of water and rigid tank based on CEL and SPH approaches. These numerical results are compared with the related results of experimental and analytical formulations. Shaking table results are reference solution for this problem. The physical properties and boundary conditions of model are same as the last part. In numerical methods the time step size is 0.01 s throughout the simulation.

Both resonance and non-resonance loading case are considered. Taking into account the first fundamental sloshing frequency obtained from Eq. (3.7) as $\omega_0 = 6.547\ \text{rad.}\,s^{-1}$, the excitation frequency of the first case was taken by $\omega = 0.383\ \omega_0$ and second non-resonance loading case was taken by $\omega = 0.766\ \omega_0$. The third loading case is intended

to simulate sloshing phenomena under resonant frequency, therefore the excitation frequency is taken as the same as first fundamental frequency. The amplitudes of the horizontal harmonic excitations are $0.4\ \mathrm{m.s^{-2}}$ for all cases. The time history response of free surface elevation is measured at three locations which were near left (i.e. x = −0.3) and right (i.e. x = 0.3) ends of the tank.

In case of non-resonant frequency motion, the numerical solution of sloshing by the proposed methods (CEL and SPH) is in an acceptable agreement with the reference solution and analytical formulation in terms of displacement of water surface. Corresponding to the frequency of 0.4 Hz, figure 3.10 shows the time history response of free surface elevations at two measurement locations (i.e. x = −0.3, 0 and 0.3 m) that is extended to 60 s. The maximum sloshing amplitude at x = -0.3 m is measured as 0.052 m from the CEL solution and 0.051 from the SPH solution, whereas, it is obtained as 0.053 m from both the analytical formulation and experimental data. The minimum free surface elevation is obtained as 0.050 m, 0.051 m, 0.054 m and 0.048 from experimental, analytical, CEL and SPH methods, respectively. In both cases, the numerical results are quite close to the experimental ones.

3.3.4.1 Resonant water sloshing with $\omega_d/\omega_0 = 1$

When the frequency of the external excitation is close to the natural frequency of the sloshing system, resonant sloshing occurs. The time history of the free surface elevation at P1 is shown in Figure 3.7. One can see in the figure that the wave amplitude increases with time until steady state is reached.

The CEL and SPH methods are first used to simulate the case and the time history of the free surface. In this case that is extended to 10 s, Figure 3.7 presents the wave height increases continuously for all solution types at the near left and right end of the tank. The comparison of four solution methods shows that analytical study overestimates surface amplitudes. Numerical and experimental results are highly consistent in terms of peak level timing, shape and amplitude of sloshing wave. The free surface displacement time histories obtained from experimental and numerical studies show that the upward sloshing wave amplitudes are always superior to the downward ones. This phenomenon is a sign of a nonlinear behavior of sloshing and caused by the suppression effect of the tank base on waves with downward amplitude. Although the gravity effects exist for upward and downward fluid motion, the downward motion of fluid is obstructed by the tank bottom. The ratio of positive amplitude to absolute negative amplitude increases as the fluid depth decreases. This is cannot be perceived from the analytical solution because it

is derived based on linearized assumptions.

As can be seen in the figure, the CEL and SPH method can reasonably simulate the overall free surface elevations, although there is some phase difference as compared to the experimental results. This may be due to the small difference of the excitation frequency assumed in the numerical methods from the actual excitation frequency in the experiment. The overall sloshing trend and wave profile can reasonably be modeled with the numerical methods. The general sloshing phenomenon of liquid in the tank is represented fairly well by numerical and agrees with the experimental results.

Nevertheless, as mentioned in the last Chapter, the pressure fluctuation in the SPH method is severe. We can see that the pressure distribution in the liquid is not smooth. A large number of particles with zero pressure value occur inside the fluid domain below the free surface. This greatly affects the pressure field and thus inaccurate pressure distribution is obtained.

Nevertheless, in the SPH method, the high frequency pressure fluctuation still appears in the time signal of pressure. The pressure fluctuation obtained by the original SPH method is very large with amplitude of fluctuation up to 2-3 times of the actual pressure value.

The pressure history at P_2 is shown in Figure 3.8. The comparison of the pressure solution with experimental result shows excellent agreement. Due to enforcement of the incompressibility condition for all the fluid particles, there are only some minor fluctuations of the pressure values when the sloshing amplitude becomes large. It can be easily improved by imposing some artificial compressibility of the fluid, as introduced by Hu and Kashiwagi (2004) and Khayyer and Gotoh (2009). In our study, we do not implement this since the fluctuation is so minor that it can be neglected. A little phase difference is observed after 6 s. This difference is likely due to the frequency ratio used in the experiment is not exactly the same as the one assumed in the numerical model.

To show the improvement achieved by CEL over the SPH, the pressure solutions are plotted together in Figure 3.8 in comparison with the experimental result. The tremendous improvement of the pressure history in the proposed CEL shows the capability of the CEL method in simulation water sloshing.

In the case of resonant frequency that is extended to 10 s, Fig.3.7 presents the wave height increases continuously for all solution types at the near left and right end of the tank. The comparison of four solution methods shows that analytical study overestimates surface amplitudes. Numerical and experimental results are highly consistent in terms of peak level timing, shape and amplitude of sloshing wave. The free surface displacement

time histories obtained from experimental and numerical studies show that the upward sloshing wave amplitudes are always superior to the downward ones. This phenomenon is a sign of a nonlinear behavior of sloshing and caused by the suppression effect of the tank base on waves with downward amplitude. Although the gravity effects exist for upward and downward fluid motion, the downward motion of fluid is obstructed by the tank bottom. The ratio of positive amplitude to absolute negative amplitude increases as the fluid depth decreases. This is cannot be perceived from the analytical solution because it is derived based on linearized assumptions.

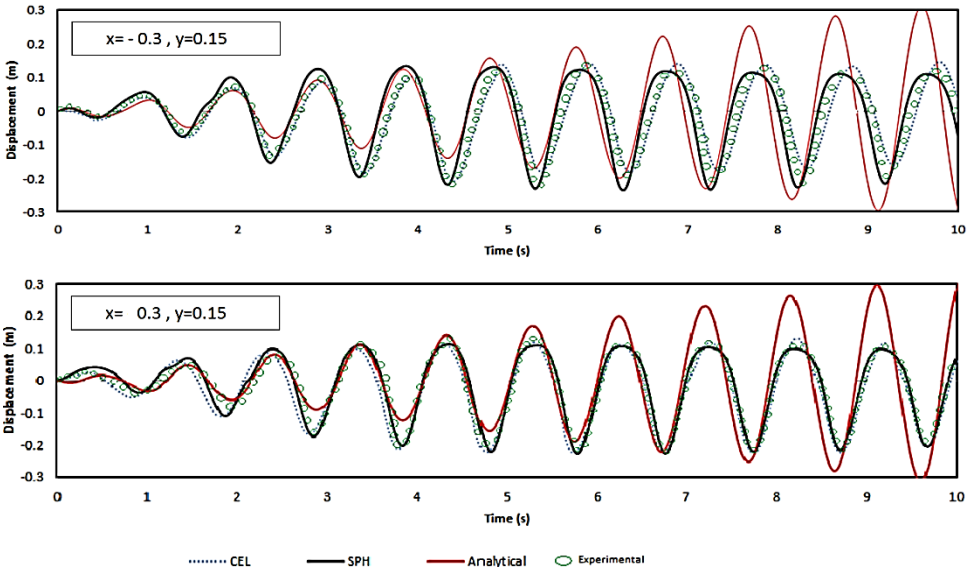

Fig.3.7. Time histories of sloshing wave height two end points obtained by CEL, Analytical, SPH and experimental methods with the frequency of 1.042 Hz (Resonant frequency)

For resonant frequency loading case, nonlinear sloshing action at the free surface causes small amplitude oscillations in pressure time histories and it seems that the SPH method does not work properly in the first 3 seconds because of structure of particles; but the analytical method reflects only hydrostatic pressure effect at the same point without any fluctuation. Pressure response at the two edges of the tank is almost symmetric with respect to vertical axis passing in the middle of the tank. Although peak level timing of pressure time histories obtained by analytical and numerical methods is perfectly consistent, pressure obtained from analytical study at the right and left sides of the tank continuously increases over time in an unbounded manner. Although because of hitting the water with roof of the tank, it doesn't allow to increase after some seconds in experimental and numerical simulations. However, pressure observed by numerical model

oscillates between the same negative and positive values after 20 s. Therefore, it can be concluded that analytical method is not reliable for resonant frequencies due to the boundless response.

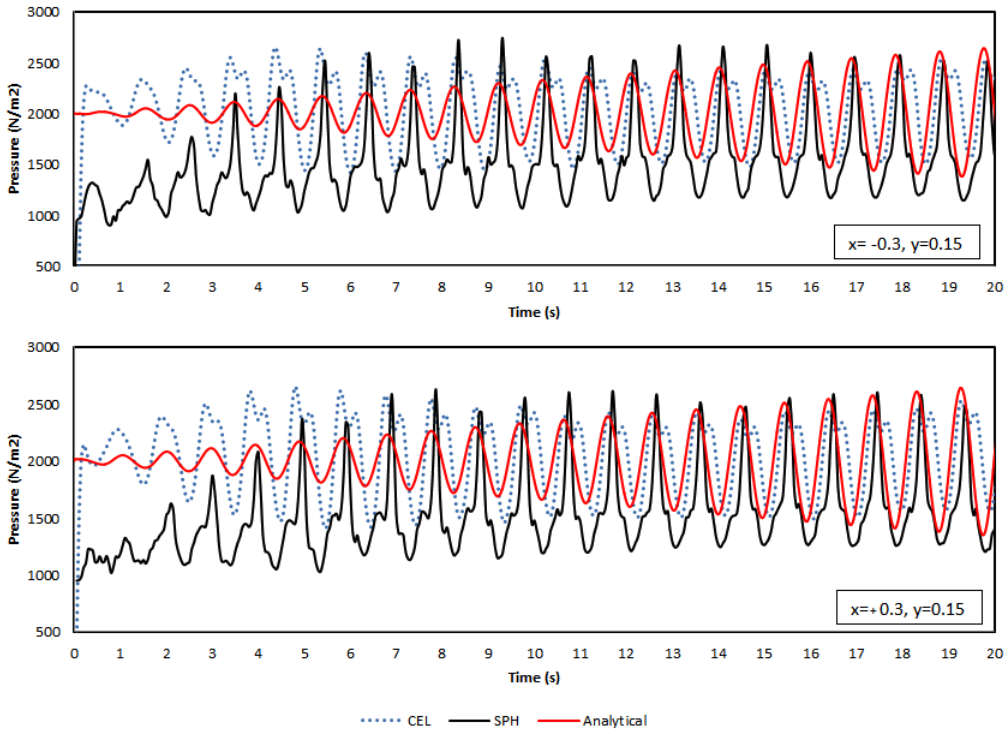

Fig. 3.8. Pressure time histories at two end location of the tank wall obtained by CEL, Analytical and SPH methods with a frequency of 1.042 Hz (Resonant frequency)

3.3.4.2 Water sloshing with $\omega_d/\omega_0 = 0.766$ and $\omega_d/\omega_0 = 0.383$

Taking into account the first fundamental sloshing frequency obtained from Eq. (25) as $\omega_0 = 6.547\ \text{rad.s}^{-1}$, the excitation frequency of the first case was taken by $\omega_d = 0.383\ \omega_0$ and second non-resonance loading case was taken by $\omega_d = 0.766\ \omega_0$. The third loading case is intended to simulate sloshing phenomena under resonant frequency, therefore the excitation frequency is taken as the same as first fundamental frequency. The amplitudes of the horizontal harmonic excitations are $0.4\ \text{m.s}^{-2}$ for all cases. The time history response of free surface elevation is measured at three locations which were near left (i.e. x = −0.3) and right (i.e. x = 0.3) ends of the tank.

In case of non-resonant frequency motion, the numerical solution of sloshing by the proposed methods (CEL and SPH) is in a acceptable agreement with the reference solution and analytical formulation in terms of displacement of water surface.

Corresponding to the frequency of 0.4 Hz, figure 3.10 shows the time history response of free surface elevations at two measurement locations (i.e. x = −0.3, 0 and 0.3 m) that is extended to 60 s. The maximum sloshing amplitude at x = -0.3 m is measured as 0.052 m from the CEL solution and 0.051 from the SPH solution, whereas, it is obtained as 0.053 m from both the analytical formulation and experimental data. The minimum free surface elevation is obtained as 0.050 m, 0.051 m, 0.054 m and 0.048 from experimental, analytical, CEL and SPH methods, respectively. In both cases, the numerical results are quite close to the experimental ones.

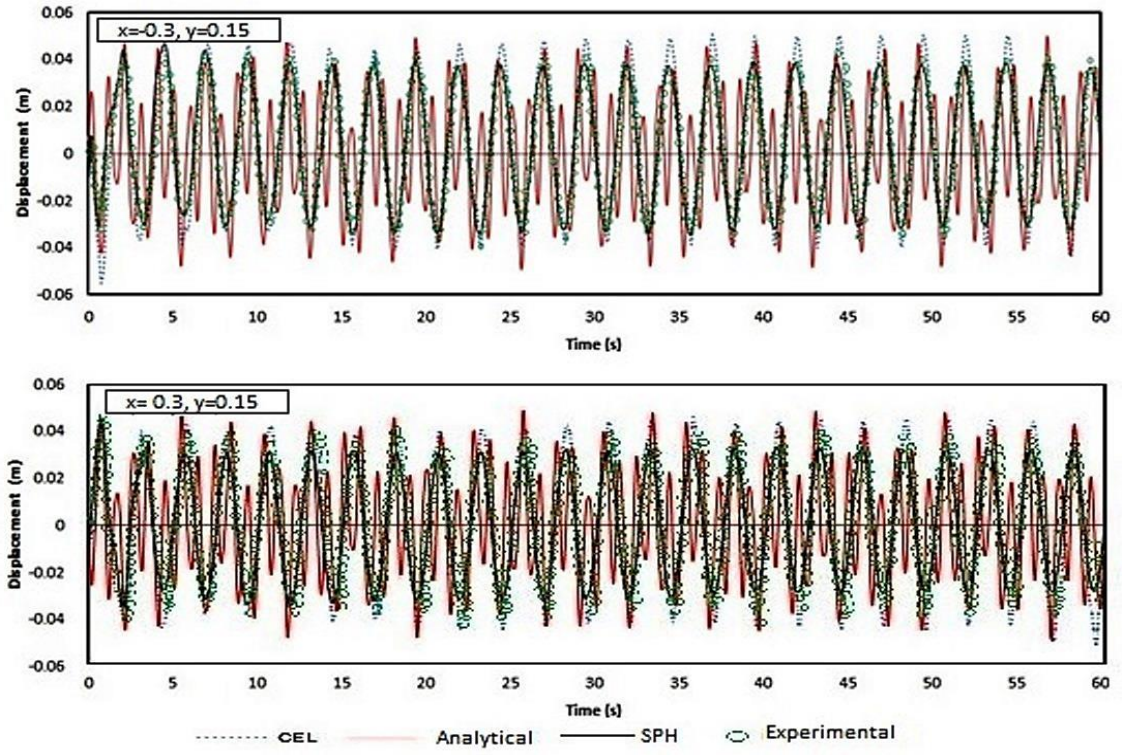

Fig. 3.9. Time histories of sloshing wave height two end points obtained by CEL, Analytical, SPH and experimental methods with the frequency of 0.4 Hz

Corresponding to the frequency of 0.8 Hz, figure 3.11 shows the time history response of free surface elevations at two measurement locations (i.e. x = −0.3, 0 and 0.3 m) that is extended to 60 s. The maximum sloshing amplitude at x = -0.3 m is measured as 0.079 m from the CEL solution and 0.077 from the SPH solution, whereas, it is obtained as 0.069 m for the analytical formulation and 0.073 m for the experimental data. The minimum free surface elevation is obtained at 0.081 m, 0.061 m, 0.091 m and 0.088 from experimental, analytical, CEL and SPH methods, respectively. In both cases, the

numerical results are close to the experimental ones, but the result of analytical analysis a little far from others.

Pressure time histories, including hydrodynamic pressure, detected at two locations which are on the left (x = −0. 3) and right (x = 0.3) sides of the tank about 0.01 m above the base are plotted in Figures 3.10 and 3.11 for non-resonant (0.4 and 0.8 Hz) and figure 3.9 for resonant frequency motions, respectively. Since the pressure was not measured in the experimental study, only analytical and numerical results are compared. Although the hydrostatic pressure field is generated by increasing the gravity gradually in the first second of the analysis there is a high frequency oscillation region in pressure response in the first 5 s of the analysis. For non-resonant frequency motion, there is a small phase difference in pressure time histories observed by analytical and numerical methods at the left and right sides of the tank. For non-resonant frequency motion, the contribution of hydrodynamic pressure to total pressure response is very small value.

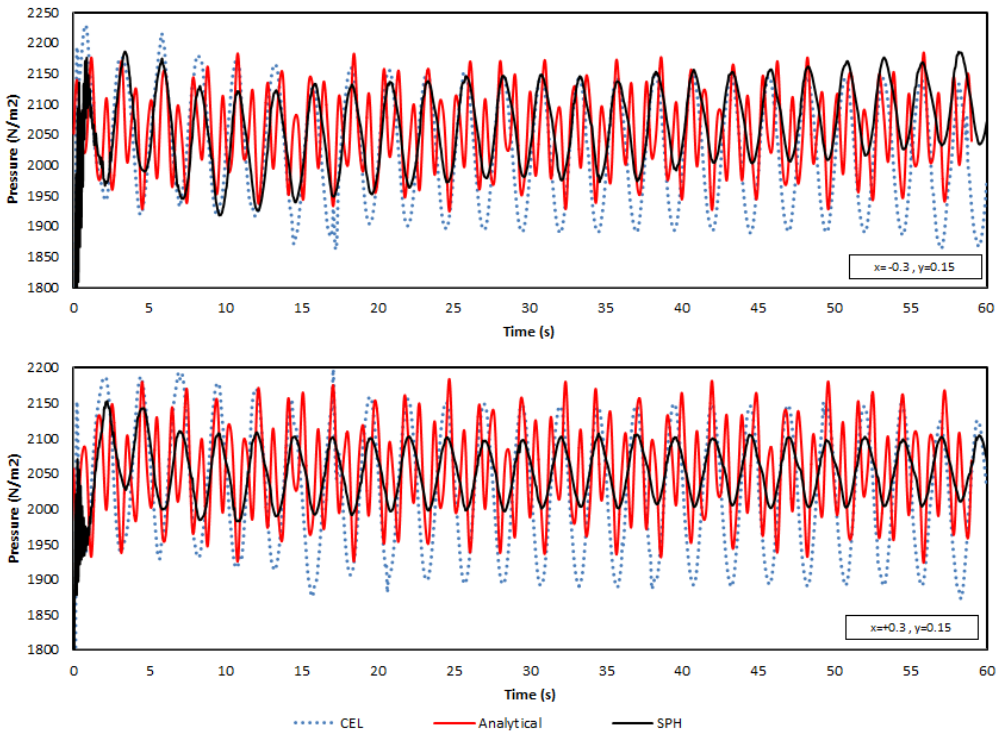

Fig. 3.10. Pressure time histories at two end location of the tank wall obtained by CEL, Analytical and SPH methods with the frequency of 0.4 Hz

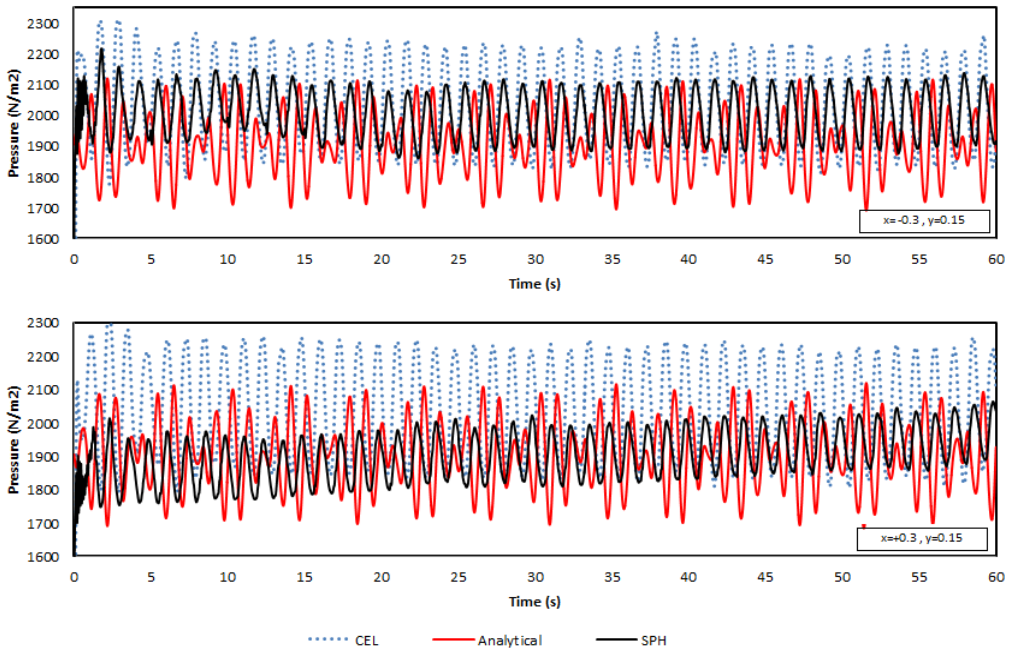

Fig. 3.11. Pressure time histories at two end location of the tank wall obtained by CEL, Analytical and SPH methods with the frequency of 0.8 Hz.

3.4. Discussion

In this section, water sloshing in tank with filling depths 50%H and above are studied experimentally, analytically and numerically. The SPH method and the proposed CEL are applied to simulate water sloshing waves. The solutions are compared with experimental results.

The solution of free surface elevation using the CEL method in general agrees with the experimental results. Nevertheless, the SPH solution of pressure history at a fixed position exhibits severe spurious fluctuation. This indicates that the incompressibility condition is not satisfactorily enforced. The proposed ways to improve fluctuation in the SPH method, i.e. the arc method for free surface particle recognition and incompressibility adjustment of free surface particles, are proved to some extent to be effective to improve particle distribution and help mitigate pressure fluctuation amplitude. The proposed CEL is applied to simulate water sloshing with different excitation conditions. The pressure contour of CEL solution is quite smooth. Compared with SPH results, the CEL solutions agree better with experimental results in terms of time histories of free surface elevation and especially pressure.

Different parameters which affect the sloshing waves are analyzed. It is concluded that a filling depth of approximately 45%-70% of the tank height produces the highest sloshing pressure and free surface elevation. The larger excitation amplitude produces higher free

surface elevation and hydrodynamic pressure. Additionally, for various excitation frequencies, resonant frequency produces the largest free surface elevation and pressure. The conclusions from the research findings are consistent with other published results (Wu et al., 1998; Cho and Lee 2004; Ibrahim, 2005). In addition, the experimental data acquired from a valuable database which could be used to validate numerical models.

3.5. Summary

In this chapter, sloshing waves in rectangular tanks due to harmonic motions are studied experimentally, analytically and numerically.

Sloshing in deep water exhibits nonlinear standing waves. The highest free surface elevation and largest hydrodynamic pressure are observed when resonance occurs. Larger excitation amplitude produces higher free surface elevation and hydrodynamic pressure.

The SPH solution of pressure history in liquid sloshing exhibits severe spurious fluctuation. The proposed two ways to improve pressure fluctuation in SPH method, i.e. the arc method for free surface particle recognition and incompressibility adjustment of free surface particles, are shown effective to improve particle distribution and help suppress pressure fluctuation amplitude.

The pressure contour of CEL solution is smooth even when severe sloshing occurs. Compared with SPH results, the CEL solutions agree much better with the experimental results, particularly in terms of severe distribution and pressure, but it is expensive and time consuming.

References

[1] Ahmadzadeh, M., Saranjam, B., Hoseini Fard, A. and Binesh, A.R.: Numerical simulation of sphere water entry problem using Eulerian-Lagrangian method, J. Applied Mathematical Modelling, article in press, 2013.

[2] Aquelet, N., Souli, M., Gabrys, J.: Olovsson, L. A new ALE formulation for sloshing analysis, J. Struct. Eng. Mech. 16, pp.423–440, 2003.

[3] Aquelet, N., Souli, M., Olovson, L. : Euler Lagrange coupling with damping effects: Application to slamming problems, J. Comput. Methods Appl. Mech. Eng. 195, pp.110–132, 2005.

[4] Belytschko, T., Liu, W.K., Moran, B. : Nonlinear finite elements for continua and structures, Wiley, New York, 2000.

[5] Benson, D.J. : A mixture theory for contact in multimaterial Eulerian formulations, J. Comput. Meth. Appl. Mech. Eng. 140, pp.59–86, 1997.

[6] Chen, Y.H., Hwang, W.S., Ko, C.H. : Sloshing Behaviors of Rectangular and Cylindrical Liquid Tanks Subjected to Harmonic and Seismic Excitations, J. Earthquake Engineering and Structural Dynamics 36, pp.1701– 1717, 2007.

[7] El-Zeiny, A.: Nonlinear Time-Dependent Seismic Response of Unanchored Liquid Storage Tanks, Ph.D. Dissertation, Department of Civil and Environmental Engineering, University of California, Irvine, 1995.

[8] Fischera, F.D., Rammerstorferb, F.G. : A Refined Analysis of Sloshing Effects in Seismically Excited Tanks, Int. J. Press. Vessels Piping 76, pp.693–709, 1999.

[9] Ghosh, S., Kikuchi, N. : An arbitrary Lagrangian-Eulerian finite element method for large deformation analysis of elastic-viscoplastic solid, J. Comput. Meth. Appl. Mech. Engng. 86, pp.127–188, 1991.

[10] Gronenboom, P.H.L., Cartwright, B.K.: Hydrodynamics and fluid-structure interaction by coupling SPH-FE method, J. Hydraul., No. 48, pp.61-73, 2010.

[11] Hatayama, K. : Lessons from the 2003 Tokachi-oki, Japan, earthquake for prediction of long period strong ground motions and slashing damage to oil storage tanks, Springer Science Business Media B.V. J Seismol 12, pp.255-263, 2008.

[12] Hirt, C.W., Amsden, A.A., Cook, J.L.: An arbitrary Lagrangian-Eulerian computing method for all flow speeds, J. Comput. Phys., No. 135(2), pp.203-216, 1997.

[13] Ibrahim, R.A.: Liquid Sloshing Dynamics: Theory and Applications, Cambridge University Press, New York, USA, 2005.

[14] Ozdemir, Z., Souli, M., Fahjan, Y.M. : FSI methods for seismic analysis of sloshing tank problems, J. M´ecanique & Industries, 11, pp.133–147, 2010.

[15] Liu, D., Lin, P.: A numerical study of three-dimensional liquid sloshing in tanks, J. Comput. Phys. 227, pp.3921–3939, 2008.

[16] Longatte, E., Bendjeddou, Z., Souli, M. : Application of Arbitrary Lagrange Euler Formulations to Flow- Induced Vibration problems, J. Press. Vessel Technology 125, pp.411–417, 2003.

[17] Koketsu, K., Hiroe Miyake, H.: A seismological overview of long-period ground motion, Springer Science Business Media B.V. J Seismol 12, pp.133-143, 2008.

[18] Manos, G.C.: Dynamic response of a broad storage tank model under a variety of simulated earthquake motions. Proc. 3rd U.S. Nat. Conf. on Earthquake Engrg., Earthquake Engineering Research Institute, E1 Cerrito, Calif., pp.2131–2142, 1986.

[19] Mitra, S., Upadhyay, P.P., Sinhamahapatra, K.P. : Slosh Dynamics of Inviscid Fluids in Two-Dimensional Tanks of Various Geometry Using Finite Element Method, Int. J. Num. Methods Fluids 56, pp.1625–1651, 2008

[20] Monaghan, J.J.: Smoothed particle hydrodynamics. Reports on progress in physics. No.68, pp. 1703-1759, 2005.

[21] Qiu, G., Henke, S. and Grabe, J. : Application of a coupled Eulerian-Lagrangian approach to geomechanical problems involving large deformations, J. Computers and Geotechnics, Vol. 38, pp. 30-39, 2011.

[22] Rafiee, A., Cummins, S., Rudman, M., Thiagarajan, K. : Comparative study on the accuracy and stability of SPH schemes in simulating energetic free-surface flows, European Journal of Mechanics B/Fluids, Vol.36, pp.1-16, 2012.

[23] Raghunandan, M., and Liel, A.B. : Effect of ground motion duration on Earthquake-induced structural collapse, J. Structural Safety, Vol. 41, pp. 119-133, 2013.

[24] Rezvantalab, S., Azadi, S., Tarriverdilo, Shabani, R. and Sheidaii, M.R. : Pressure distribution on the wall of liquid contained tanks due to near field and far field ground motions, Pro. Sixth International Conference of Seismology and Earthquake Engineering , May 2013, Tehran, Iran.

[25] Souli, M., Ouahsine, A., Lewin, L.: ALE formulation for fluid-structure interaction problems, J. Comput. Methods Appl. Mech. Eng. 190, pp.659–675, 2000.

[26] Souli, M., Zolesio, J.P.: Arbitrary Lagrangian-Eulerian and free surface methods in fluids mechanics, J. Comput. Methods Appl. Mech. Eng. 191, pp.451–466, 2001.

[27] Vakilazadsarabi, A., Miyajima, M., and Murata, M. : Study of sloshing phenomena in water reservoirs and tanks due to long period-long duration ground motions, Proc. of 15th World Conference on Earthquake Engineering, September 2012.

[28] Vakilazadsarabi, A, Miyajima, , Sloshing of Tanks due to Long Period-Long Duration Ground Motions, International Journal of Civil Engineering Research (IJCER), (article in press) , 2014.

[29] Veletsos, A.S, Yang, J.Y. : Earthquake response of liquid storage tanks. Advances in Civil Engineering Through Engineering Mechanics, Proceedings of the Engineering Mechanics Division Specialty Conferences, ASCE, Raleigh, North Carolina, pp.1–24, 1977.

[30] Yang, Q., Jones, V., McCue, L.: Free-surface flow interactions with deformable structures using an SPH-FEM model, Int. J. Ocean Engineering, Vol.55, pp.136-147, 2012.

4. Sloshing phenomena in tanks due to seismic ground motions

4.1. General remarks

As mentioned in the last chapters, to investigate the abnormal water distribution which occurred exactly after the earthquake in water systems, we need to study sloshing phenomena in tanks due to long period-Long duration ground motions. In order to this, two records of ground motions have been chosen that include characteristics of long period-long duration ground motions under different conditions in which four fundamental characteristics are effective in response of reservoirs that are:

- The effect of changing the stiffness of the reservoir material
- The effect of changing the thickness of the reservoir, which in this study, two types of tank wall thickness, 5 and 8 mm have been studied.
- The effect of changes in reservoir geometry, which in present study examined three types of geometry for the reservoir including $Width/Length = 0.66$, $W/L = 0.50$ and $W/L = 0.33$
- The effect of water filling depth in the reservoir, which is include three modes "$H_w/H = 0.50$", "$H_w/H = 0.64$" and "$H_w/H = 0.83$ " has been studied.

For this purpose, in this chapter of the study, the effect of changes in each of the above mentioned characteristics, five outputs of the analysis, is evaluated and compared. These five outputs of the results are as follows:

- Evaluation of the maximum and minimum stresses in the tank wall during the loading time
- Evaluation of the maximum hydrodynamic pressure in the tank during the loading time
- Evaluation of the maximum displacements in the tank wall during the loading time
- Evaluation most critical deformation (distortion) induced along the tank wall height
- Evaluation the height of the water free surface in the two ends of tank wall (in case of the investigation of the effect of changes in reservoir geometry and the effect of water filling in the reservoir)

4.2. Long periods-long duration ground motions

National Institute for Earth science and Disaster prevention (NIED) in Japan organizes the digital strong-motion seismograph (K-net & Kik-net) across the all of Japan. The collected seismic data analyses are available to the public on the internet. The data taken from this institute are modified in this research to remove noise in time history graphs by using zero order methods. Also, Trifunac and Westermo developed a frequency dependent definition of duration where the duration is considered separately in several narrow frequency bands. They define the duration as the sum of time intervals during which the integral $(\int f^2(t)dt)$ where f(t) is the ground acceleration, velocity, or displacement has the steepest slope and gains a significant portion (90%) of its final value. By considering this and time consuming process of numerical analysis, this research is considered just 90 seconds of Tokachi-Oki earthquake and 120 seconds of Tohoku earthquake. Also Shimada and et al. (1988) mentioned that the effects of vertical excitation in sloshing phenomena and it is negligible in engineering terms, so we considered the effect of horizontal excitation in simulation of water reservoir tanks.

4.2.1 Tokachi-Oki (2003)

The 2003 Tokachi-oki earthquake provided the southern coast of Hokkaido, Japan, with one of the most significant examples (Koketsu et al. 2005; Hatayama 2008) of long-period ground motion. This large earthquake in 2003 occurred in the southeast of Hokkaido along the Kuril trench. The city of Tomakomai in Hokkaido suffered serious damage to large oil tanks from long-period ground motions generated by an earthquake more than 250 km away offshore. A very important contribution to this long-period ground motion comes from surface waves stimulated in a basin, either directly or by conversing at the margins, which lead to large amplitudes and long durations of shaking. The direct and converted surface waves also imply the importance of velocity structures, both along the propagation path and within the basin, respectively. Fluid sloshing in damaged oil storage tanks occurred in a period close to the dominant ground motion (7 to 8 s), producing displacements of a few meters and long fluid oscillation, which contributed to the destruction of floating roofs and fire in two tanks. (Koketsu et al. 2007). The acceleration time-history (in three directions) records and velocity response spectrum and acceleration response spectrum are given in figures 4.1-4.5, respectively.

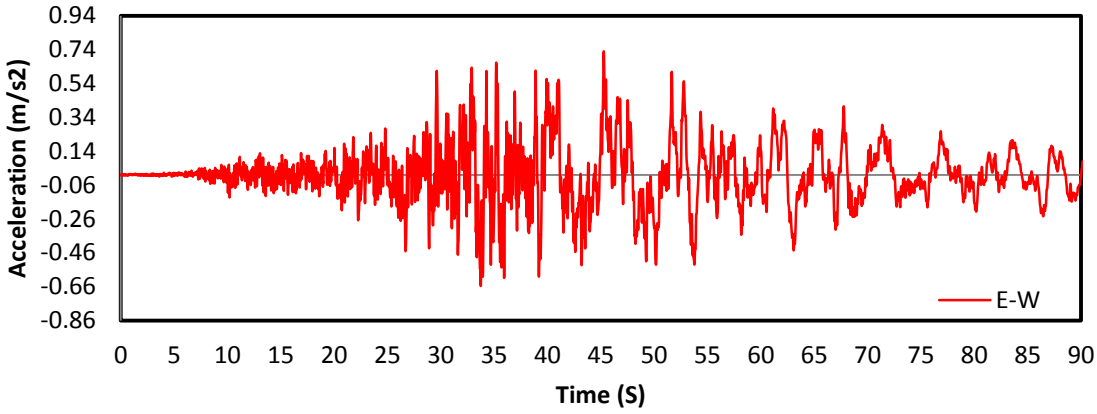

Fig. 4.1.Section of EW acceleration seismograms observed at Tomakomai stationalong a propagation path from the 2003 Tokachi-Okiearthquake (K-NET)

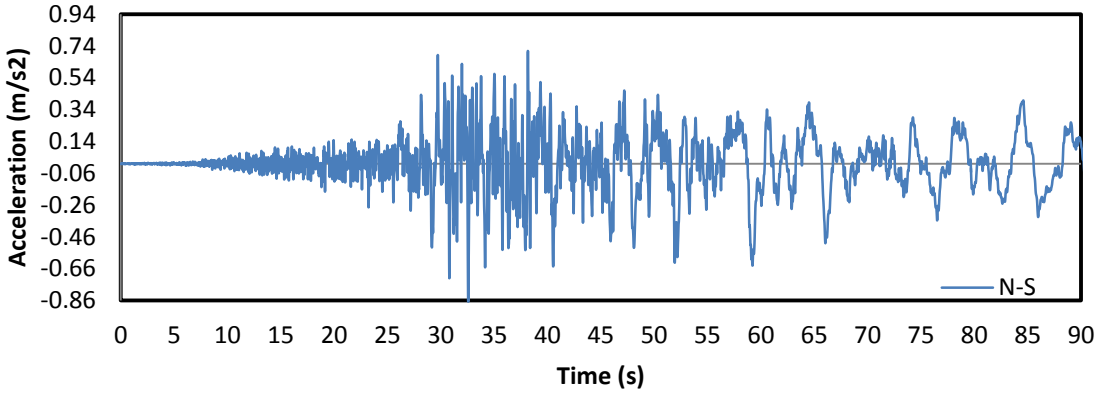

Fig. 4.2.Section of NS acceleration seismograms observed at Tomakomai stationalong a propagation path from the 2003 Tokachi-Okiearthquake (K-NET)

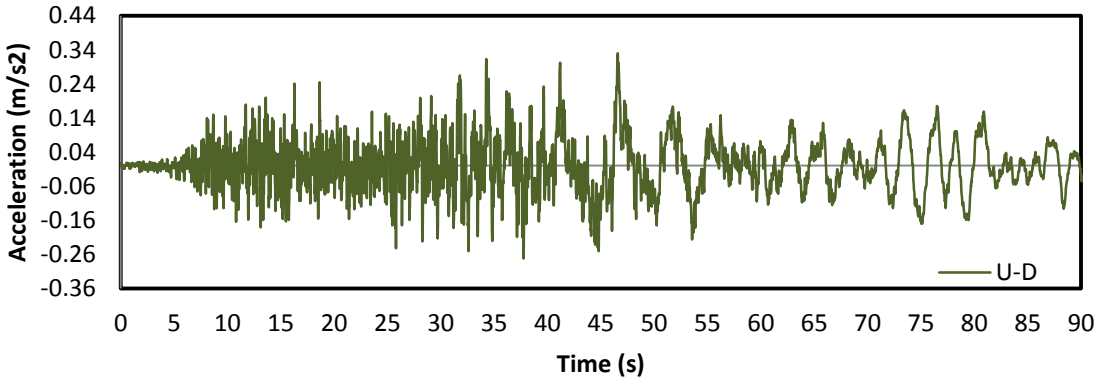

Fig. 4.3.Section of UD acceleration seismograms observed at Tomakomai stationalong a propagation path from the 2003 Tokachi-Okiearthquake (K-NET)

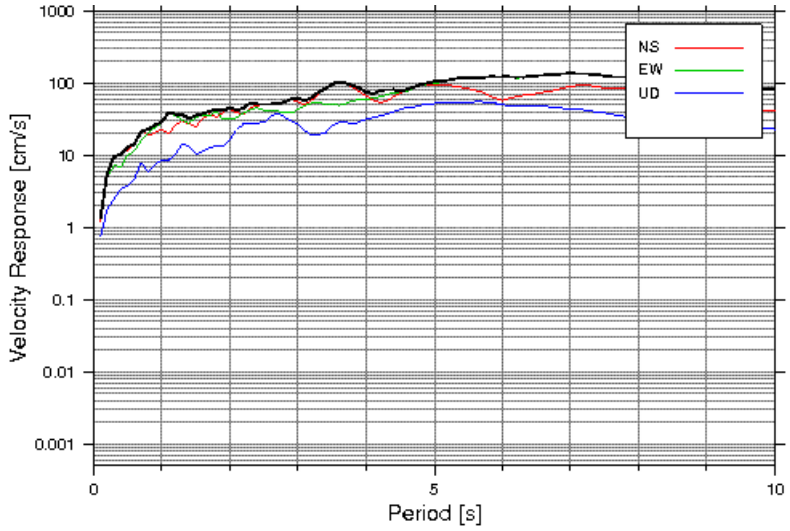

Fig.4.4. Velocity response spectra for 2003 Tokachi-Oki earthquake in all directions (K-NET)

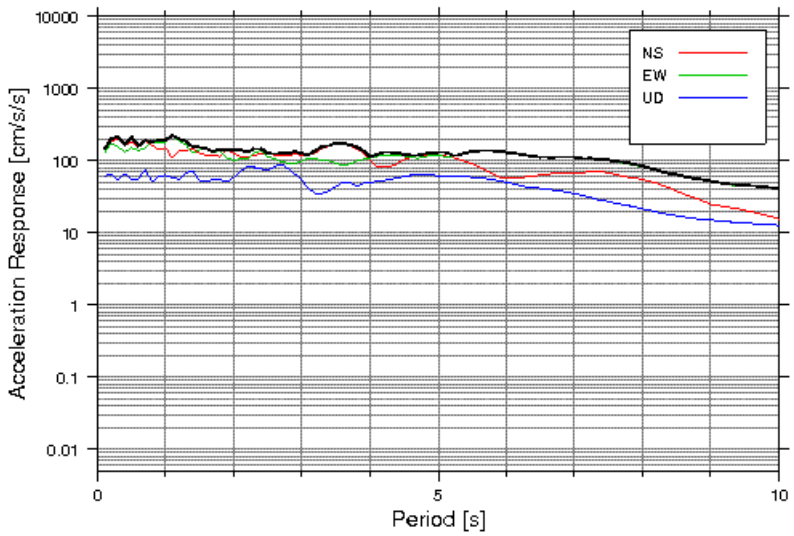

Fig.4.5. Acceleration response spectra for 2003 Tokachi-Oki earthquake in all directions (K-NET)

4.2.2 Tohoku earthquake (2011)

On 11 March 2011, Tohoku Earthquake occurred. After the main shock, several earthquakes occurred. “The main shock was recorded at more than 900 stations of K-net & Kik-net. In velocity spectrum and energy spectrum, the MYG010 wave (Ishinomaki City) showed high responses at more than 1 second periods. The city was among the most seriously affected by the 2011 Tōhoku earthquake and tsunami. Several tsunamis, up to

about 10 meters high traveled inland up to 5 kilometers from the coast. The tsunamis damaged about 80% of the 700 houses in the coastal whaling port of Ayukawa, and the Kadonowaki neighborhood was largely leveled. About 46% of the city was flooded by the tsunami." The acceleration time-history (in three directions) records and velocity response spectrum and acceleration response spectrum are given in figures 1, 2 and 3, respectively.

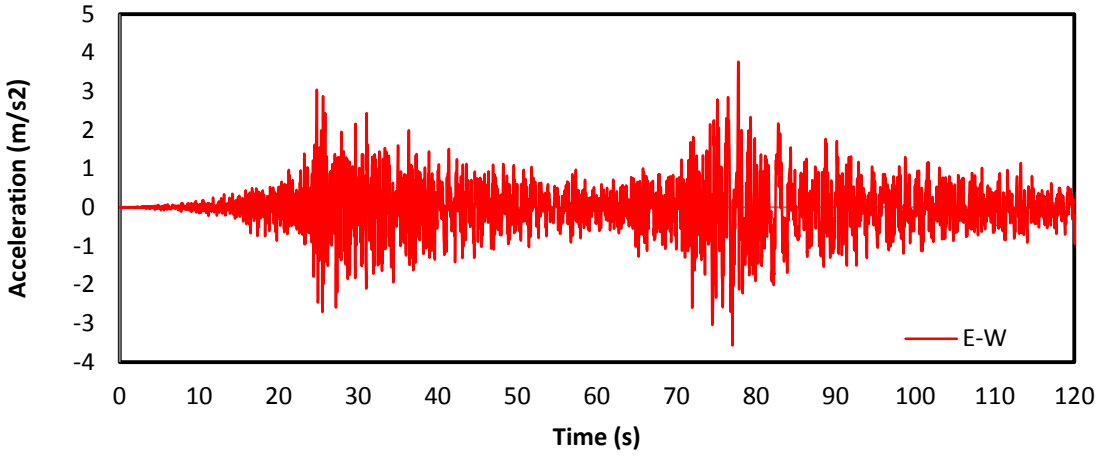

Fig. 4.6.Section of EW acceleration seismograms observed at Tomakomai stationalong a propagation path from the 2003 Tokachi-Okiearthquake (K-NET)

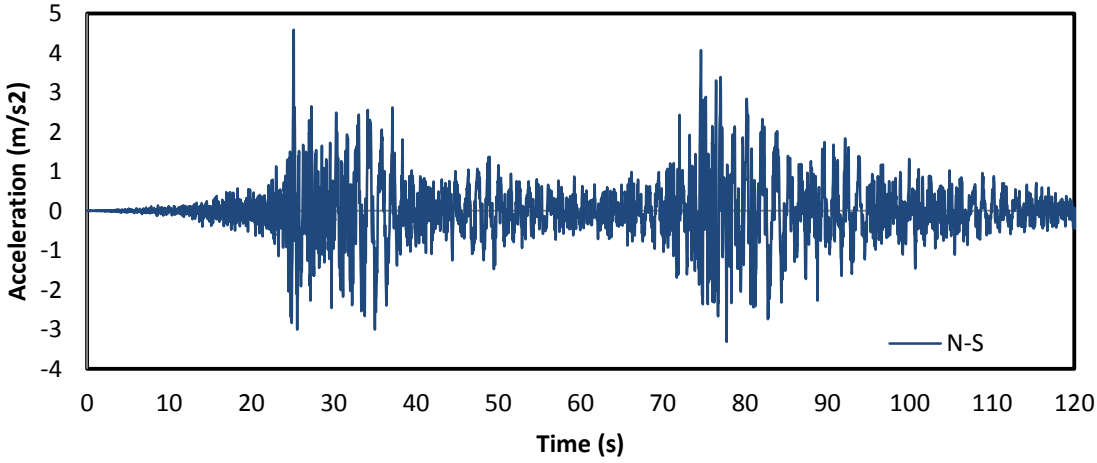

Fig. 4.7.Section of EW acceleration seismograms observed at Tomakomai stationalong a propagation path from the 2003 Tokachi-Okiearthquake (K-NET)

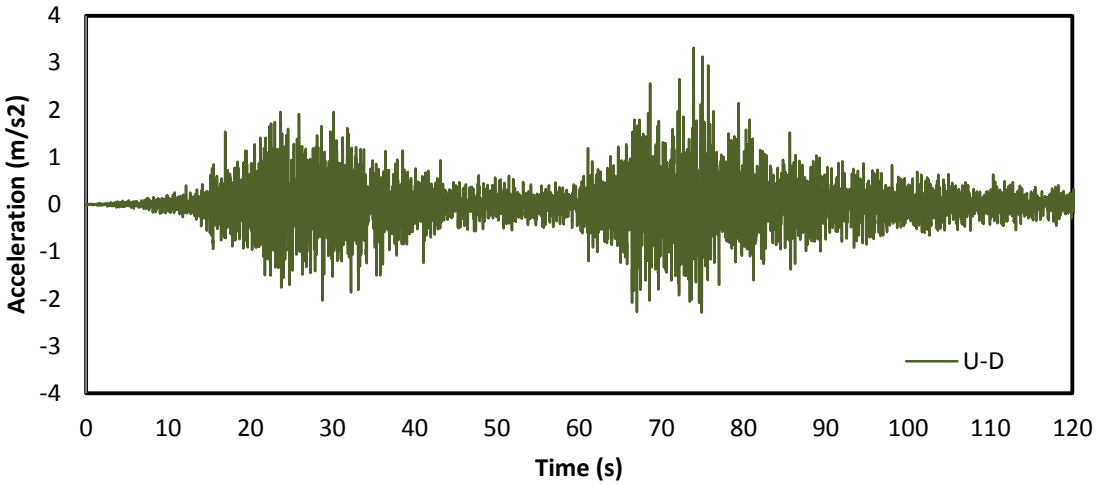

Fig. 4.8.Section of EW acceleration seismograms observed at Tomakomai stationalong a propagation path from the 2003 Tokachi-Okiearthquake (K-NET)

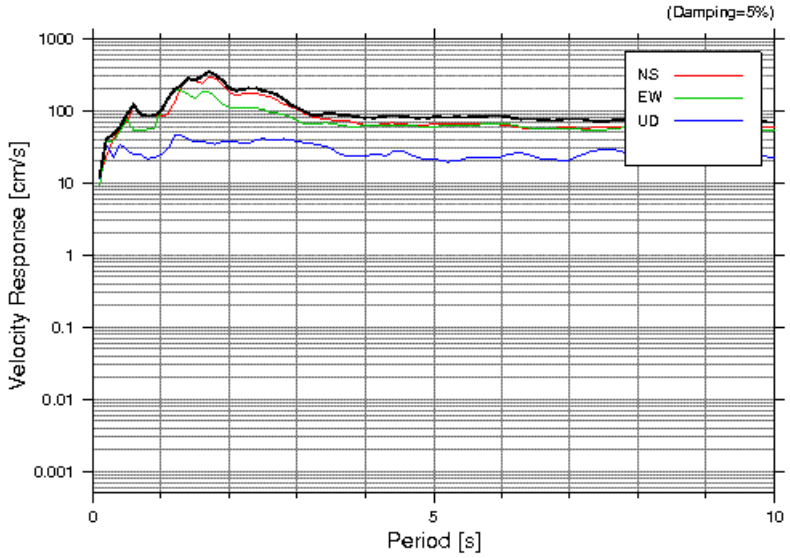

Fig.4.9. Velocity response spectra for 2011 Tohoku earthquake in all directions (K-NET)

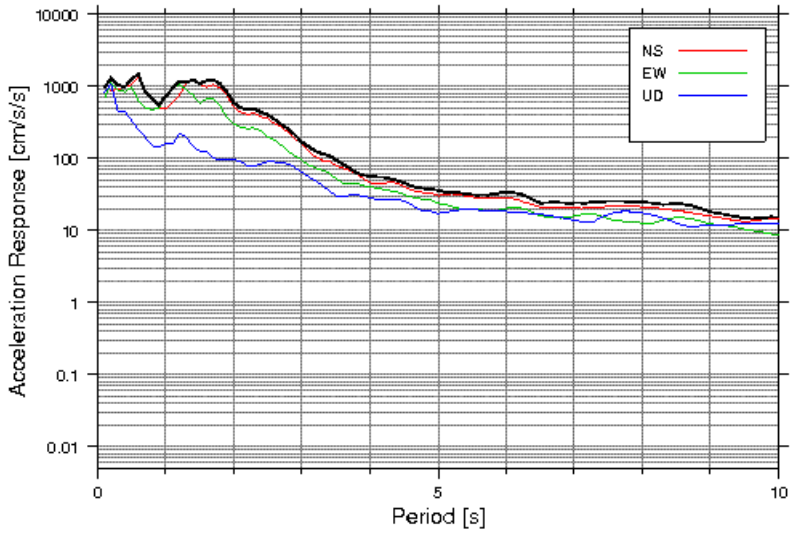

Fig.4.10. Acceleration response spectra for 2011 Tohoku earthquake in all directions (K-NET)

4.3. Modelling of fluid (water) reservoir in terms of seismic loading

To study the sloshing phenomena on reservoir behavior under different conditions, such as "material changes in tank wall", "wall thickness of the tank", "variation of tank height to length of tank ratio", "Changes in the free surface of the fluid inside the tank (filling)", and finally "effect of period and duration of seismic load" due to above conditions, 14 models have been analyzed. According to the Table 3, in analysis No.1, 2, 11 and 12 the reservoirs material has been studied. Also in Analysis No.1, 2, 3 and 4, the thickness of the tank, in both 5 and 8 mm thickness, with the same conditions has been investigated. The comparison of the reservoir geometry, the models No. 3, 4, 5, 6, 7 and 8 are provided in which the tank height equal to 36 cm and length are different. Also the filling of reservoirs in model No. 1, 2, 9, 10, 13 and 14 have been investigated in which the water level is equal to zero, 23 cm and 30 cm which is corresponding to 50, 64, and 83 percent of "Free-Board" surface.

Table.4.1.Definition and Specification of analytical models in this research

Model number	Earthquake Type		Material stiffness (GPa)		Tank thickness (mm)		Width/Length (water level=23cm)			Water filling depth (cm)			Comparison due to model number			
	Tohoku	Tokachi-oki	21.0	30.5	5	8	0.33	0.5	0.66	18	23	30	Material	Thickness	W/L	Water depth
1	*		*		*			*			*		*	*	*	*
2		*	*		*			*			*		*	*	*	*
3	*		*			*		*			*			*		
4		*	*			*		*			*			*		
5	*		*		*		*				*				*	
6		*	*		*		*				*				*	
7	*		*		*				*		*				*	
8		*	*		*				*		*				*	
9	*		*		*			*				*				*
10		*	*		*			*				*				*
11	*			*	*			*			*		*			
12		*		*	*			*			*		*			
13	*		*		*			*		*						*
14		*	*		*			*		*						*

4.4. Dynamic responses of the reservoir wall due to changing the stiffness of the reservoir wall

According to the contents of the previous chapters, in order to evaluate the dynamic response of the tank wall by changes in construction materials, two kinds of materials with a modulus of elasticity of 21GPa and 31.5GPa are used.

4.4.1. Evaluation of the maximum stresses in the tank wall during the loading time

Figures 4.11 and 4.12, respectively, show the maximum stresses induced on the reservoir wall during the loading time due to mentioned Tohoku and Tokachi-Oki earthquakes. For this purpose, all the elements in the tank wall, as a separated part from other parts have been isolated. The stress response of elements during this time period is derived individually, then by using data post-processing capability of the program, the maximum

and minimum stress values are obtained as a text file and by using other software converted to figures.

The graphs show that the values of stresses in the tank wall which is built with a tolerant material generally higher than the values of stresses in the tank wall that is made of low-resistance material; but to provide a numerical value to compare and evaluate the results, trend-line diagram for maximum stress can be used.

The trend-line relationships between changes in the stress response for four models are given in this section, respectively, for tank with at low-resistance metal as (models no.1 and 2):

$$\sigma_{max}(t) = 14825(t) + 2 \times 10^3 \quad (6.1)$$

$$\sigma_{max}(t) = 1090(t) + 1 \times 10^3 \quad (6.2)$$

and for tank with a tolerant metal as (models no.11 and 12):

$$\sigma_{max}(t) = 18062.4\,(t) + \times 10^3 \quad (6.3)$$

$$\sigma_{max}(t) = 1401.6\,(t) + 1 \times 10^3 \quad (6.4)$$

where σ_{max} is the maximum Mises stress (Pa), and t is time (seconds).

These equation dealing that, approximately the values of stresses are 17.1% and 18.4% higher in the elements of the tanks with module of elasticity equal to 31.5GPa, comparing with the tanks with a module of elasticity equal to 21GPa, while this change is achieved by changing the elasticity of wall material by 50%.

The study of the charts shows that the maximum stress in the tank wall with the low tolerant material occurred at 76.4s (no.1) and 55.6s (no.2) from the beginning of loading, and it is equal 25300 Pa and 1980 Pa, respectively, and for high tolerant material occurred in 77.5s (no.11) and 39.1s (no.12) from the beginning of loading, and it is equal 28560 Pa and 2380 Pa, respectively. It means that the maximum stress is 12.88% and 16.58% more deal with increasing the elasticity by 50% by applying Tohoku and Tokachi-Oki earthquakes in the same conditions.

To scrutinize comparisons, figures 4.13 and 4.14, respectively, show the contour of the tank wall stress distribution in the two models of Tokachi earthquake, and at the moment of maximum stress in the wall.

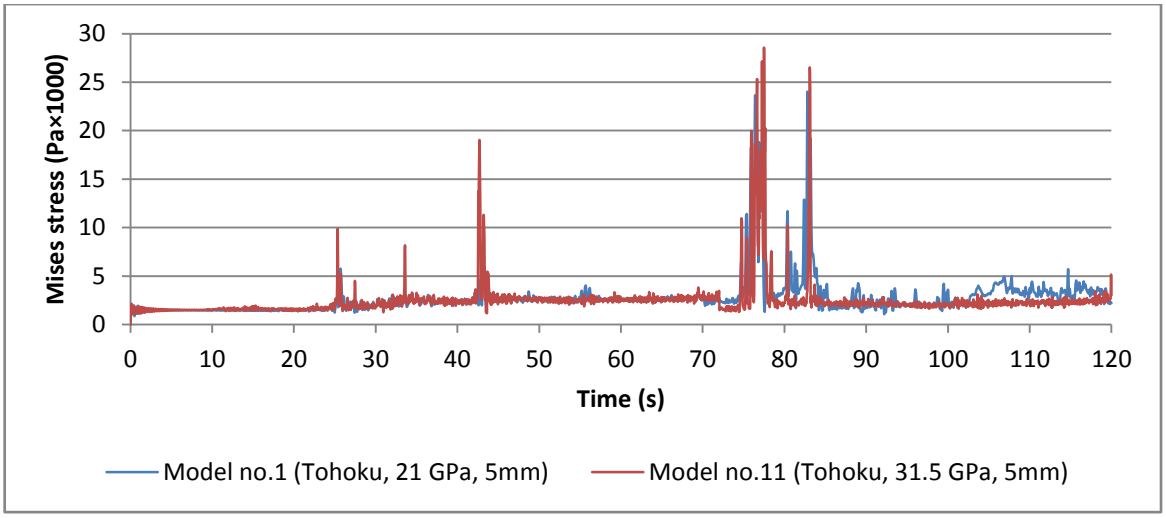

Fig.4.11. The maximum envelope stresses in Tank wall due to Tohoku earthquake

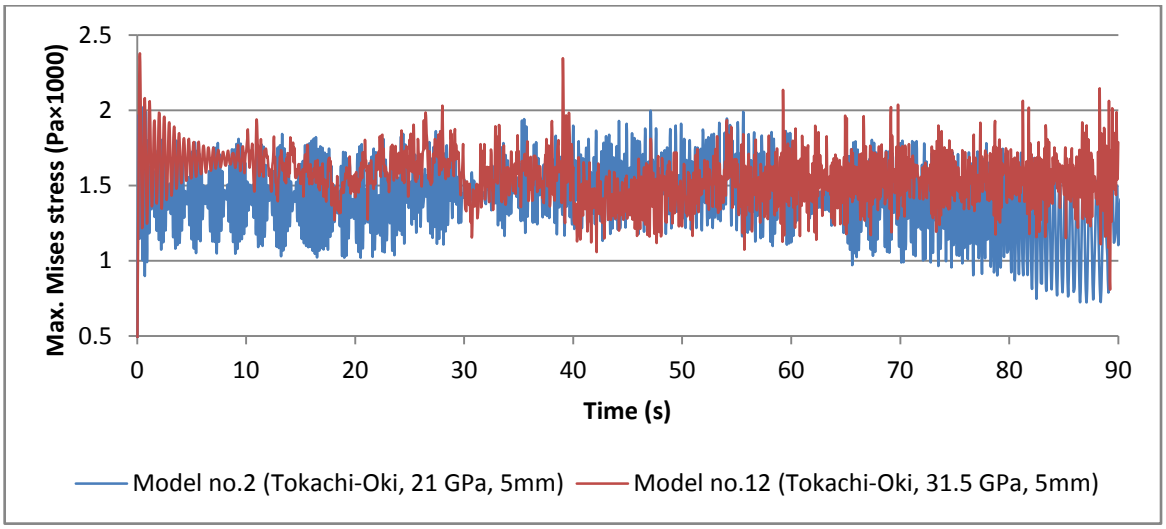

Fig. 4.12. The maximum envelope stresses in Tank wall due to Tokachi-OKi earthquake

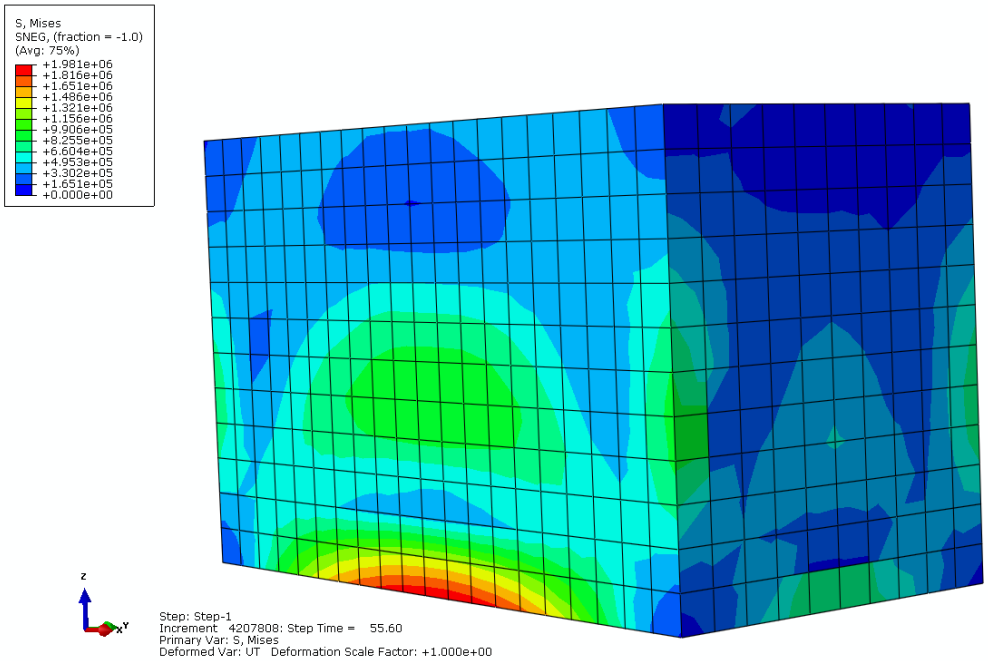

Fig.4.13. Stress distribution in tank no.2 while the maximum stress occurred

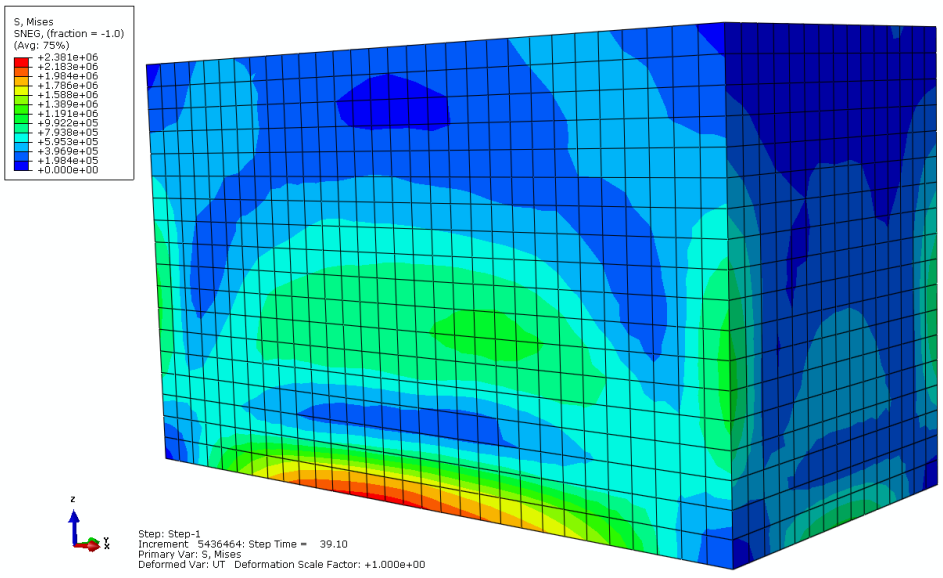

Fig.4.14. Stress distribution in tank no.12 while the maximum stress occurred

4.4.2. Evaluation of the maximum displacements in the tank wall during the loading time

Because the seismic excitation in two perpendicular directions (Y and X) is studied, so it is necessary to investigate the displacements in the two directions of the tank wall during the period of applying load. For this purpose, the maximum displacement created on the walls of the tanks are presented in two directions as U_x and U_y in figures 4.15 and 4.16.

Positive values are due to the movement of the tank in a positive direction from the initial position of the tank (static initial conditions) and negative values due to the movement of the in the negative direction from the initial position of the tank. Because the reservoir has an elevation component in Z direction, so at any particular moment, there is an element of the tank wall which has the maximum displacement (either positive or negative). The time-Maximum envelope displacement diagram is shown in Figure 5 in the x direction and Figure 6 for the y direction considering Tokachi-Oki earthquake. Also same as above mentioned explanation; at same particular time, there is an element of the tank wall which has the minimum displacement (either positive or negative).

Generally observed that during the period of applying seismic load, tanks with less resistance wall material have more displacement in their wall, so considering the input seismic acceleration and dynamic motions induced in a tank wall (which is mainly because of sloshing phenomena), the maximum displacement in either direction is a negative displacement from its initial position, which surely the absolute numerical value is important and the nature of the reservoir wall direction is not important.

Table 1 shows the time and the minimum and maximum displacements in the tank wall in both perpendicular directions which are earthquake motion applied.

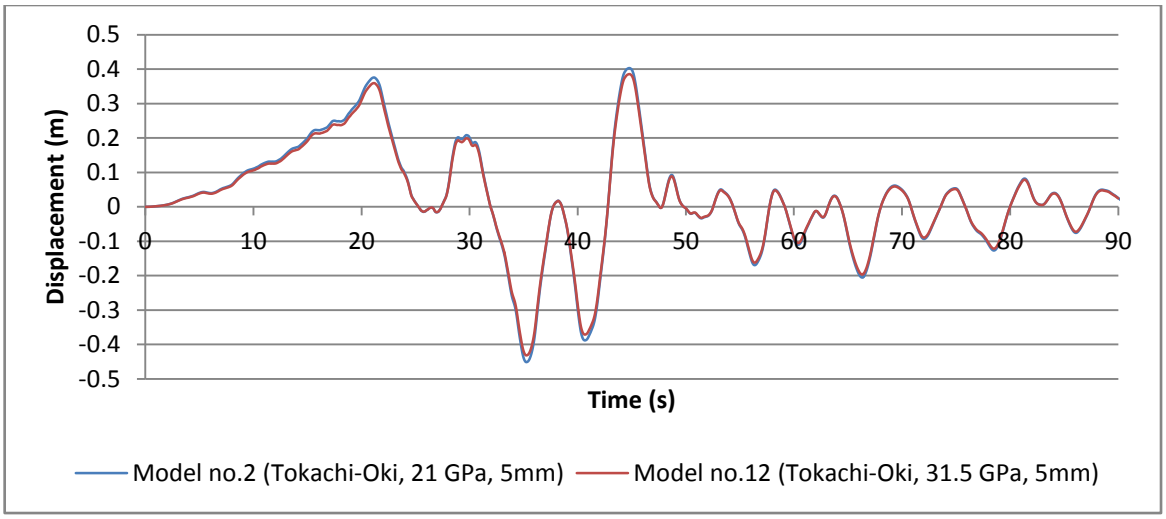

Fig. 4.15. Maximum envelope displacements in tank in x direction during Tokachi-oki earthquake

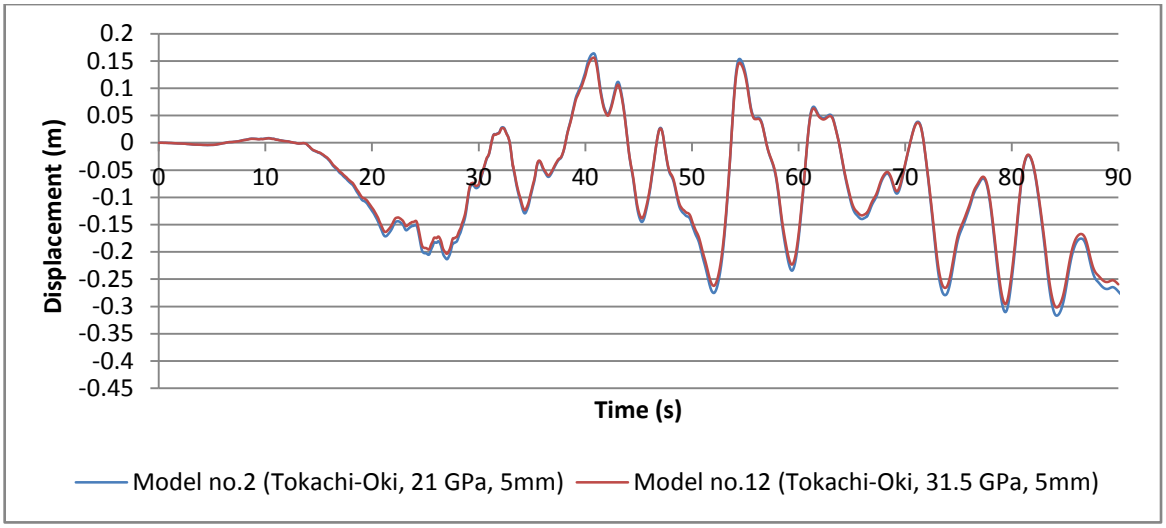

Fig. 4.16. Maximum displacements in tank in Y direction during Tokachi-oki earthquake

Table.4.2. Time and quantities of maximum and minimum displacements in tank wall in two perpendicular directions of applying ground motions

	Model no.	Model properties	Peak MAX		Peak MIN	
			Time (s)	Quantity	Time (s)	Quantity
Ux(cm)	No.2	E=21GPa/t=5mm/L=0.6m/h=0.23m	45.1	39.8	35.5	-51.8
	No.12	E=31.5GPa/t=5mm/L=0.6m/h=0.23m	44.95	38	35.4	-45.1
Uy(cm)	No. 2	E=21GPa/t=5mm/L=0.6m/h=0.23m	40.7	16.2	84.6	-30.8
	No.12	E=31.5GPa/t=5mm/L=0.6m/h=0.23m	40.45	14.3	84.5	-29.7

4.4.3. Evaluation distortion induced along the tank wall height

By examining and comparing the results of maximum strains in the tank wall, we consider the critical time for each of models to extract deformation occurring in the tank wall.

For this purpose, we choose the path along the height of the tank which maximum strains occurred and coordinate values for elements, at critical moments is recorded, individually. The resulting quantity, in fact, shows the drift of the element's position related to the rigid floor. Therefore, by this method the nature of the distortion induced in the tank wall at the critical time can be obtained. By knowing the type and levels of deformation occurring at the height of the tank wall, we can find an appropriate solution to the seismic retrofit of the tank wall.

The importance of this object is that by knowing the deformation and the height of it, we can use an appropriate solution for the seismic retrofit of the tank wall.

Figures 4.17a, 4.17b and 4.18a, 4.18b show the deformations caused by the above-mentioned conditions for models 1, 11 and 2, 12 in both longitudinal and lateral directions. According to table 4.3, the maximum amount of "bulging" and "concavity" of the tank wall and also the height levels for each one is given. It is clear that by using lower strength material in the tank wall, the amount of bulging and concavity in a tank wall is increasing considerably comparing to high strength material.

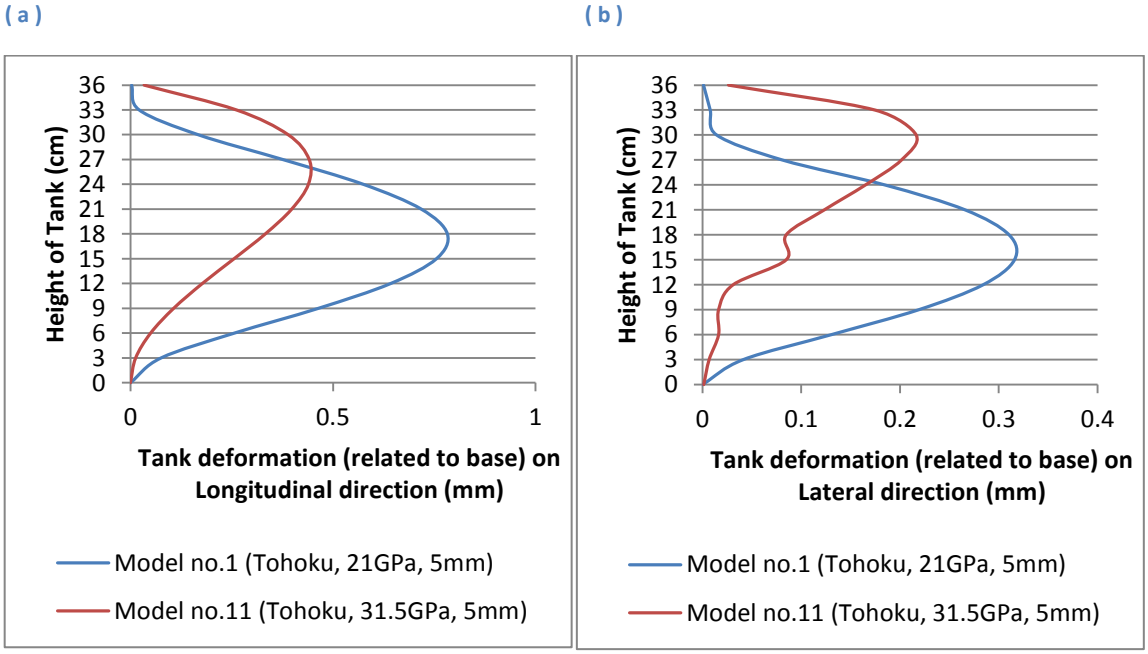

Fig. 4.17. Distortion induced along the tank wall height due to Tohoku earthquake in longitudinal and lateral direction

Table.4.3. Height and quantities of maximum deformation in a tank wall in two perpendicular directions of applying ground motions (Tohoku)

	Model no.	Model properties	Peak MAX	
			Height (cm)	Quantity
Deformation (Y, mm)	No.1	Tohoku/E=21GPa/t=5mm/L=0.6m/h=0.23m	18	0.78
	No.11	Tohoku/E=31.5GPa/t=5mm/L=0.6m/h=0.23m	26	0.439
Deformation (X, mm)	No. 1	Tohoku/E=21GPa/t=5mm/L=0.6m/h=0.23m	16	0.315
	No.11	Tohoku/E=31.5GPa/t=5mm/L=0.6m/h=0.23m	30	0.216

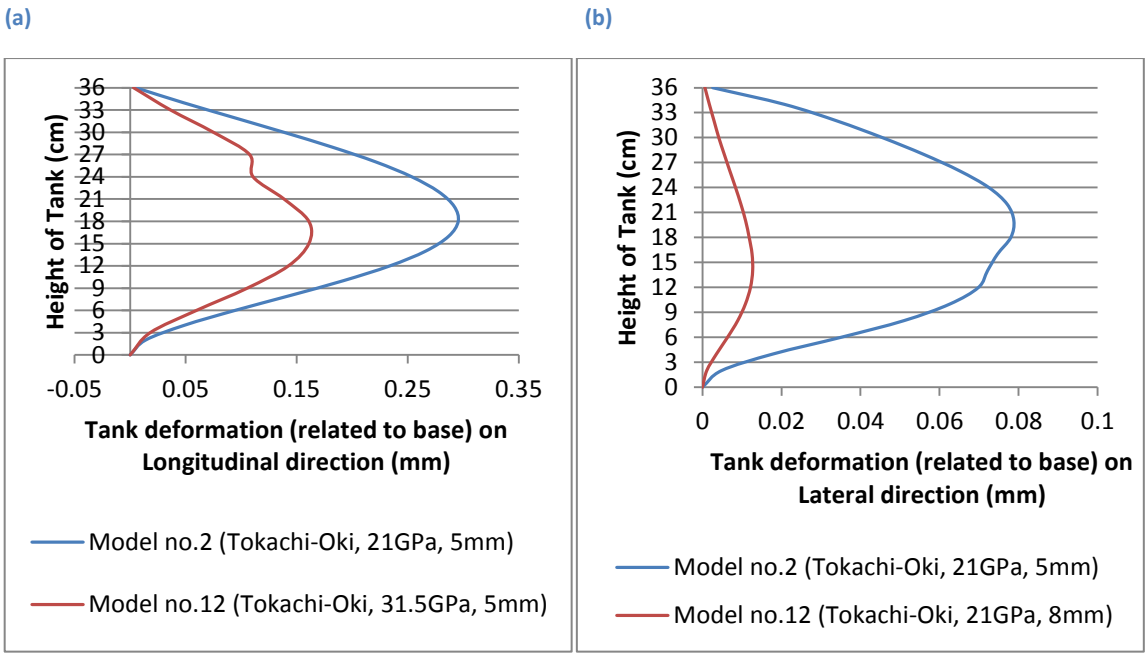

Fig. 4.18. Distortion induced along the tank wall height due to Tohoku earthquake in longitudinal and lateral direction

Table.4.4. Height and quantities of maximum deformation in a tank wall in two perpendicular directions of applying ground motions (Tokachi-Oki)

	Model no.	Model properties	Peak MAX	
			Height (cm)	Quantity
Deformation (Y, mm)	No.2	Tokachi/E=21GPa/t=5mm/L=0.6m/h=0.23m	18	0.29
	No.12	Tokachi /E=31.5GPa/t=5mm/L=0.6m/h=0.23m	16.5	0.16
Deformation (X, mm)	No. 2	Tokachi /E=21GPa/t=5mm/L=0.6m/h=0.23m	20	0.0788
	No.12	Tokachi /E=31. 5GPa/t=5mm/L=0.6m/h=0.23m	15	0.013

4.5. Dynamic responses of tank wall due to changing the thickness of the reservoir wall

According to the contents of last season, the two thick plates with a thickness of 5 mm and a thickness of 8 mm is used to evaluate the dynamic response of the tank wall structures.

4.5.1. Evaluation of the maximum stresses on the tank wall during the loading time

Figures 4.19 and 4.20 show the total maximum stresses (Von–Mises) in the tank wall during the loading period, respectively. The graphs indicate that the values of stresses in the wall of the tank with different thickness, does not greatly differ from each other, this is because of numerical values of thickness are close together. Of course due to the requirement of system stability of structural models, the above thickness values are used.

Because the analysis did not converge due to changing the thickness much higher or much lower than the normal thickness; we cannot use a variety of thicknesses.

Same as the last part, to provide a numerical value to compare and evaluate the results, trend-line diagram for maximum stress can be used.

The trend-line relationships between changes in the stress response for four models are given in this section, respectively, for a tank with a thickness of 5 mm as (models no. 1 and 2):

$$\sigma_{max}(t) = 14825(t) + 2 \times 10^3 \quad (6.5)$$

$$\sigma_{max}(t) = 1090(t) + 1 \times 10^3 \quad (6.6)$$

and for tank with a thickness of 8 mm as (models no.3 and 4):

$$\sigma_{max}(t) = 9345.3\,(t) + 2 \times 10^3 \quad (6.7)$$

$$\sigma_{max}(t) = 826.4\,(t) + 1 \times 10^3 \quad (6.8)$$

which is dealing that, approximately the values of stresses are 11.1% less than in the elements of the second tank, for Tohoku earthquake and 3.42% for Tokachi earthquake comparing with the first tank, while this change is achieved by changing the thickness of the wall by 40%. Which it shows that the thickness of wall is although effective, but the stresses depend on the type and severity of the earthquake. The study of the charts shows that the maximum stress in the tank wall with thicker wall occurred at 77.85s from the beginning of loading, for Tohoku earthquake and it is equal 17000 Pa, and for thin wall thickness occurred at 82.8s from the beginning of loading, and it is equal 23240 Pa, and the maximum stress in the tank wall with thicker wall occurred at 48.9s from the beginning of loading, for Tokachi earthquake and it is equal 2310 Pa, and for thin wall thickness occurred at 47.1s from the beginning of loading, and it is equal 2190 Pa. It means that the maximum stress is just 5 % more deal with increasing the thickness of the wall.

Therefore, for design considerations should be considered that just by increasing wall thickness, we cannot control enough the stress distribution on reservoir structures, and for the optimal design, in addition to increasing of thickness, the other appropriate methods should be used to reduce the risk of damage.

To scrutinize comparisons, figures 4.21 and 4.22, respectively, show the contour of the tank wall stress distribution in the two models; no.3 and no.4, and at the moment of

maximum stress in the wall.

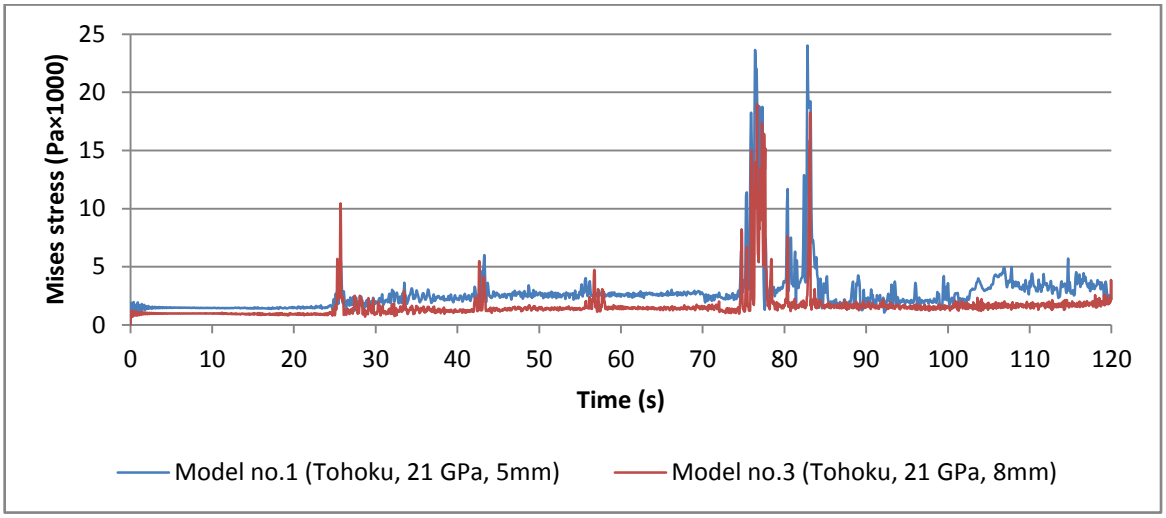

Fig.4.19. The maximum envelope stresses in tank wall due to Tohoku earthquake

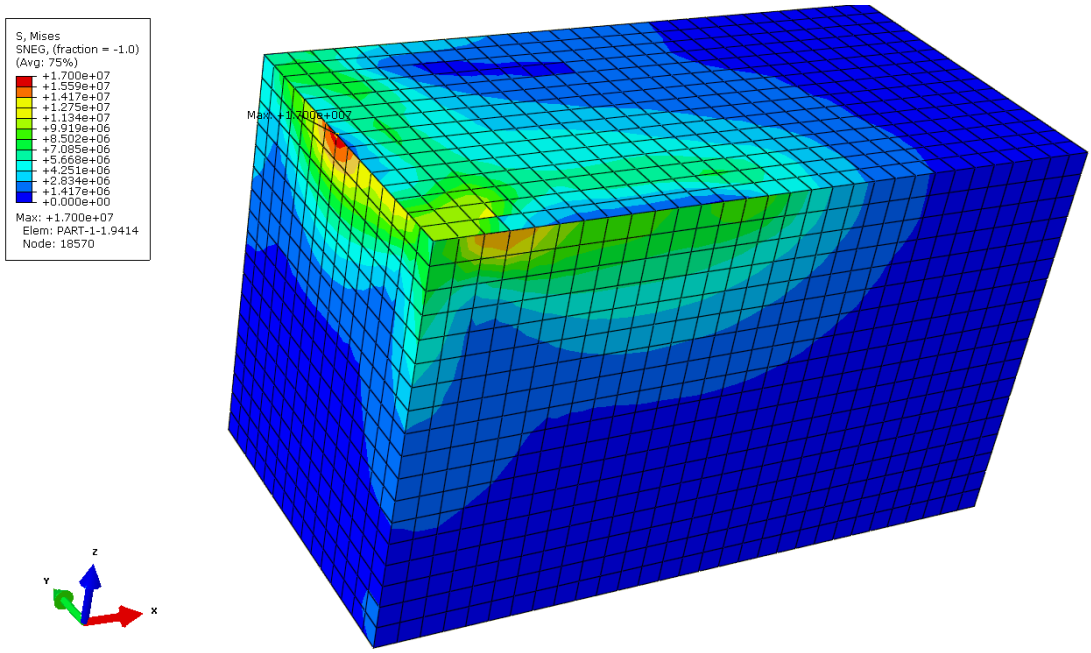

Fig.4.20. Stress distribution in tank no.3 while the maximum stress occurred

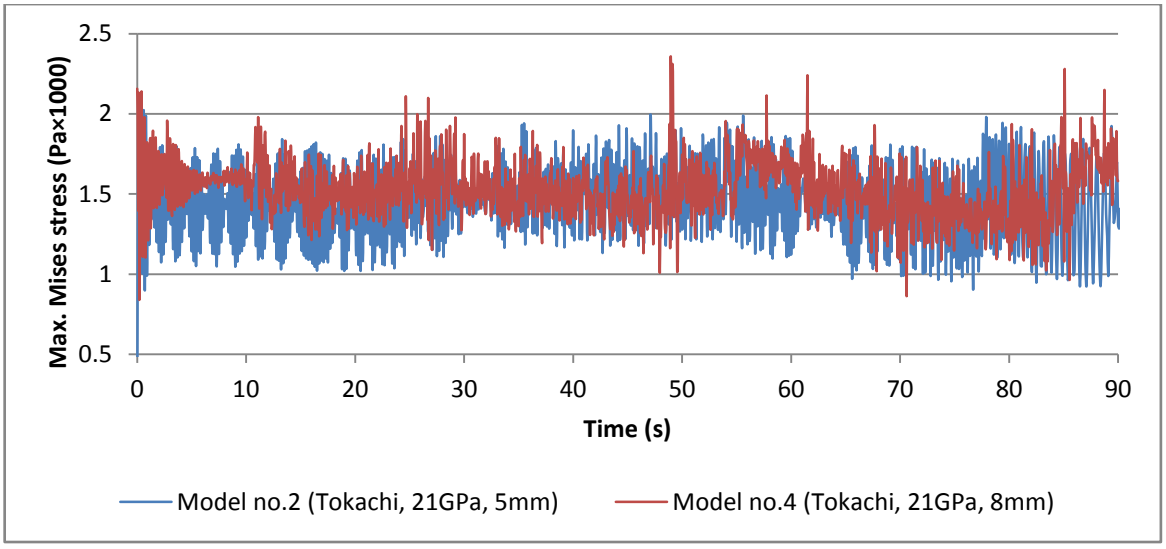

Fig.4.21. The maximum envelope stresses in Tank wall due to Tokachi-Oki earthquake

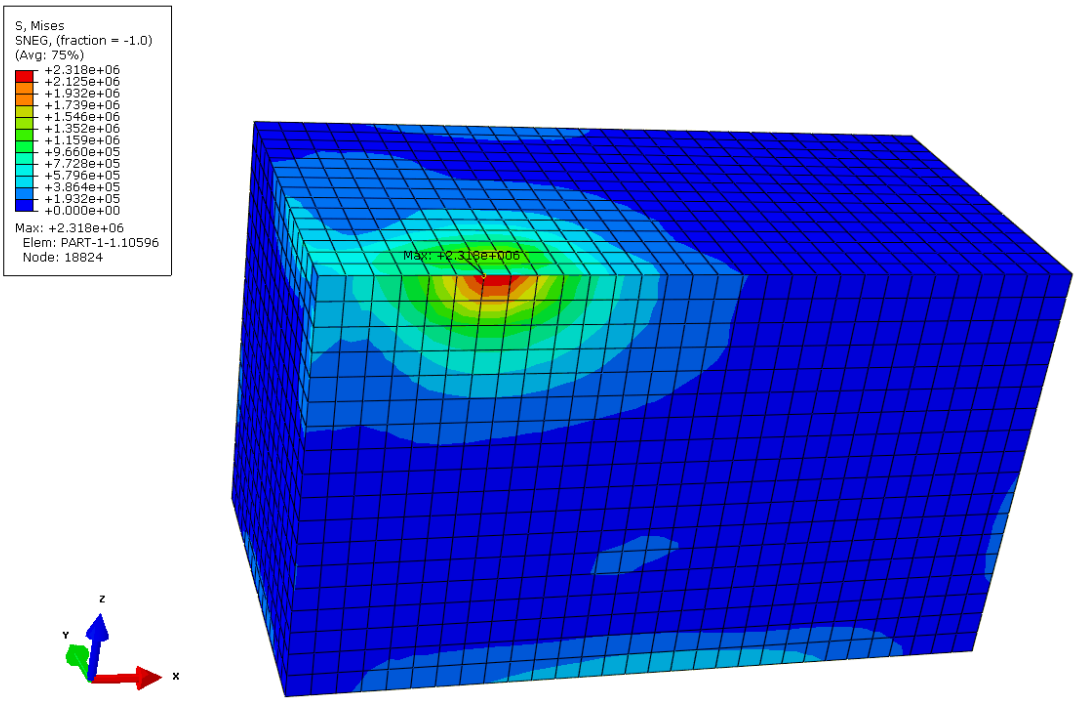

Fig.4.22. Stress distribution in tank no.4 while the maximum stress occurred

4.5.2. Evaluation of the maximum displacements in the tank wall during the loading time

To evaluate the effect of reservoir thickness variations on the displacement of the wall elements, figures 4.23 and 4.24, are presented for both directions which are Tokachi-Oki earthquake acceleration is applied.

Positive values are due to the movement of the in a positive direction from the initial

position of the tank (static initial conditions) and negative values due to the movement of the in the negative direction from the initial position of the tank. Because the reservoir has an elevation component in Z direction, so at any particular moment, there is an element of the tank wall which has the maximum displacement (either positive or negative). The time-displacement diagram is shown in Figure 4.23 in the x direction, and Figure 4.24 for the y direction.

Generally observed that during the period of applying seismic load, tanks with thicker wall have more displacement in their wall, so considering the input seismic acceleration and dynamic motions mainly because of sloshing phenomena, this is partly because of the increasing structural weight and proportionally increasing the dynamic forces caused by system excitation. The maximum displacement in either direction is a negative displacement from its initial position, there is such a case due to the behavior of the earthquake acceleration and dynamic response of the reservoir. Surely the absolute numerical value is important and nature of the reservoir wall direction is not important.

Table.4.5 shows the time and the minimum and maximum displacements in the tank wall in both perpendicular directions which are earthquake motion applied.

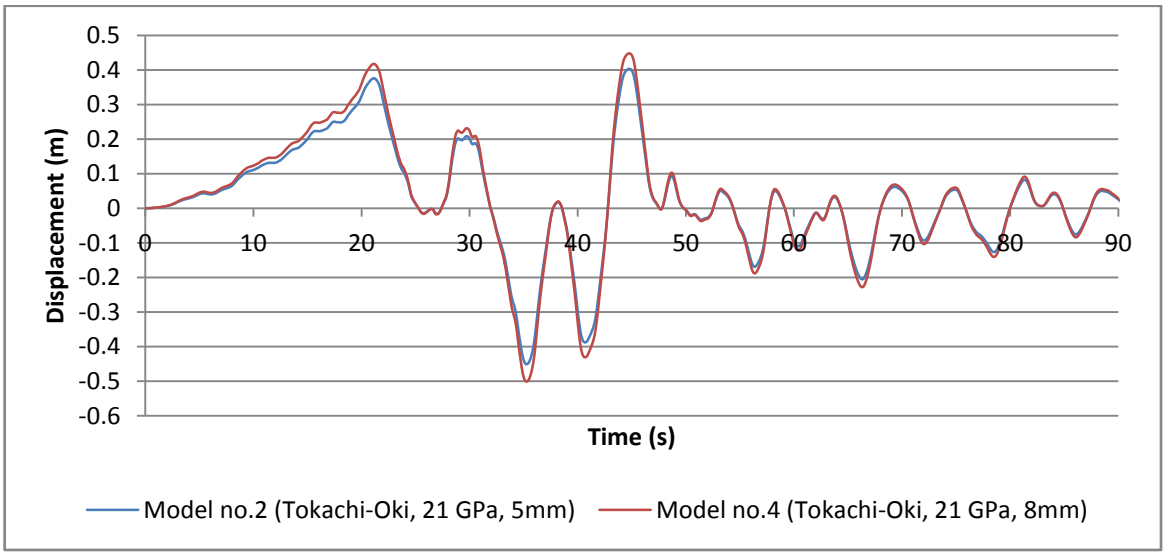

Fig.4.23. Maximum envelope displacements in tank in x direction during Tokachi-Oki earthquake

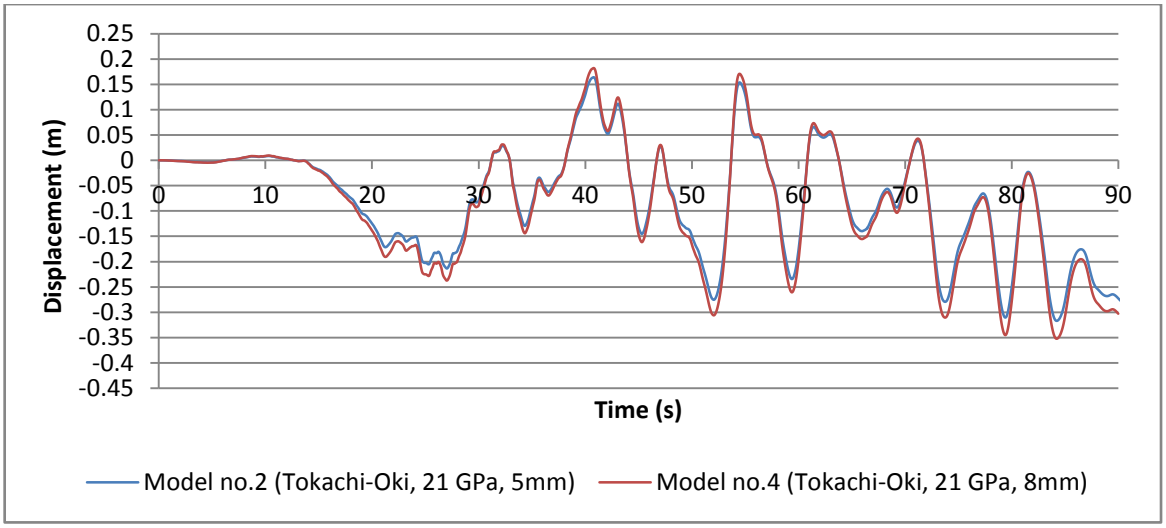

Fig.4.24. Maximum envelope displacements in tank in Y direction during Tokachi-Oki earthquake

Table.4.5. Time and quantities of maximum and minimum displacements in tank wall in two perpendicular directions of applying ground motions

	Model no.	Model properties	Peak MAX		Peak MIN	
			Time (s)	Quantity	Time (s)	Quantity
Ux(cm)	No.2	E=21GPa/t=5mm/L=0.6m/h=0.23m	43.95	41	35.1	-44
	No.4	E=21GPa/t=5mm/L=0.6m/h=0.23m	44.95	38	35.4	-50.5
Uy(cm)	No. 2	E=21GPa/t=8mm/L=0.6m/h=0.23m	40.1	16.4	85	-31.1
	No.4	E=21GPa/t=8mm/L=0.6m/h=0.23m	41	17.2	84.05	-33.5

4.5.3. Evaluation distortion induced along the tank wall height

In order to determine the critical deformation on the tank wall it is necessary to find out the time, direction and position of the element which maximum deformation occurred there (certainly because of tensile forces due to internal fluid hydrostatic pressure, it is as a tensile form). And to do these comparisons, the amount of deformation is calculated at each level of height relative to the baseline level. Figure.24 shows the deformations caused by the above-mentioned Tohoku earthquake for models 1 and 3, on the longitudinal (Fig.4.24a) and lateral side (Fig.4.24b). The maximum amount of bulging and concavity of the tank wall and also the height levels for each one is given in table 4.6. It can be seen that the tanks with thin wall thickness have less distortion than reservoirs with thicker wall thickness in the same condition. So it is considered as a case study, in model No. 3 in a critical state of deformation, just wall bulging was happening. It is noted that the meaning of the above statement is not that there are no local concavities in the thick-walled tanks; but in the most critical distortion situation, deformation of the wall

would be as a bulging, which it is created at the different levels of the total height of the reservoir for.

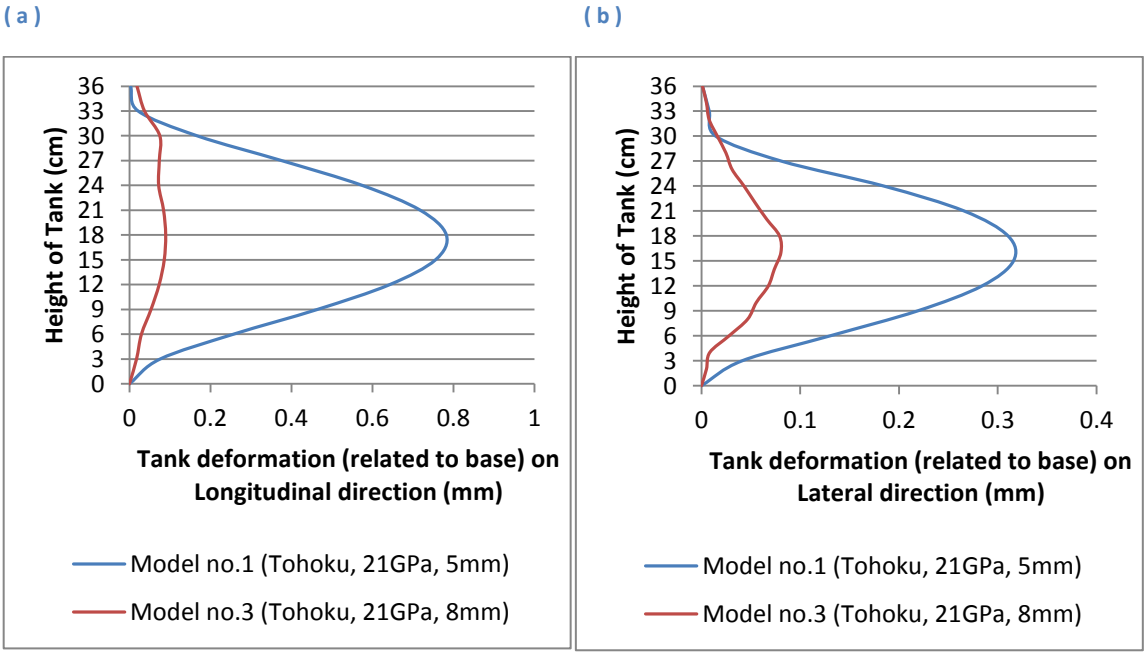

Fig. 4.25. Distortion induced along the tank wall height due to Tohoku earthquake in (a) longitudinal and (b) lateral direction).

Table.4.6. Height and quantities of maximum deformation in a tank wall in two perpendicular directions of applying ground motions (Tohoku)

	Model no.	Model properties	Peak MAX	
			Height (cm)	Quantity
Deformation (Y, mm)	No.1	Tohoku/E=21GPa/t=5mm/L=0.6m/h=0.23m	18	0.78
	No.3	Tohoku/E=21GPa/t=8mm/L=0.6m/h=0.23m	17	0.089
Deformation (X, mm)	No. 1	Tohoku/E=21GPa/t=5mm/L=0.6m/h=0.23m	16	0.315
	No.3	Tohoku/E=21GPa/t=8mm/L=0.6m/h=0.23m	18	0.079

Also, figure.26 shows the deformations caused by Tokachi-Oki earthquake for models no.2 and 4, on the longitudinal (Fig.4.25a) and lateral side (Fig.4.25b). The maximum amount of bulging of the tank wall and also the height levels for each one is given in table 4.6. It can be seen that the tanks with thin wall thickness have less distortion than reservoirs with thicker wall thickness in the same condition.

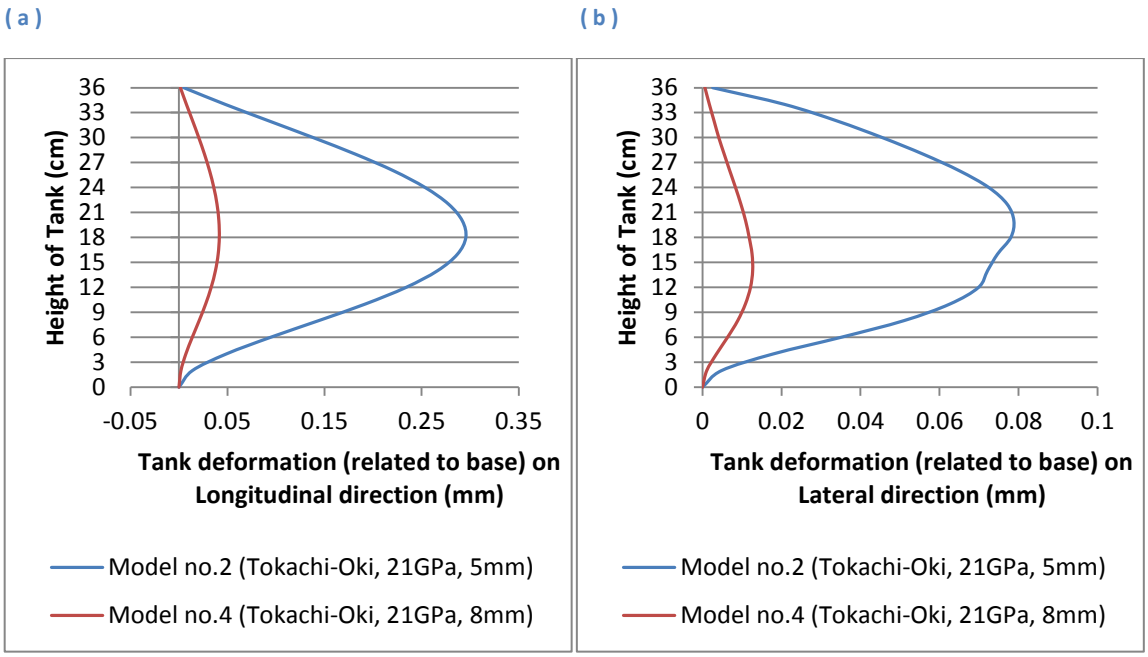

Fig. 4.26. Distortion induced along the tank wall height due to Tokachi-Oki earthquake in (a) longitudinal and (b) lateral direction).

Table.4.7 Height and quantities of maximum deformation in a tank wall in two perpendicular directions of applying ground motions (Tokachi-Oki)

	Model no.	Model properties	Peak MAX	
			Height (cm)	Quantity
Deformation (Y, mm)	No.2	Tokachi/E=21GPa/t=5mm/L=0.6m/h=0.23m	18	0.29
	No.4	Tokachi /E=21GPa/t=8mm/L=0.6m/h=0.23m	16.5	0.041
Deformation (X, mm)	No. 2	Tokachi /E=21GPa/t=5mm/L=0.6m/h=0.23m	20	0.0788
	No.4	Tokachi /E=21GPa/t=8mm/L=0.6m/h=0.23m	14	0.012

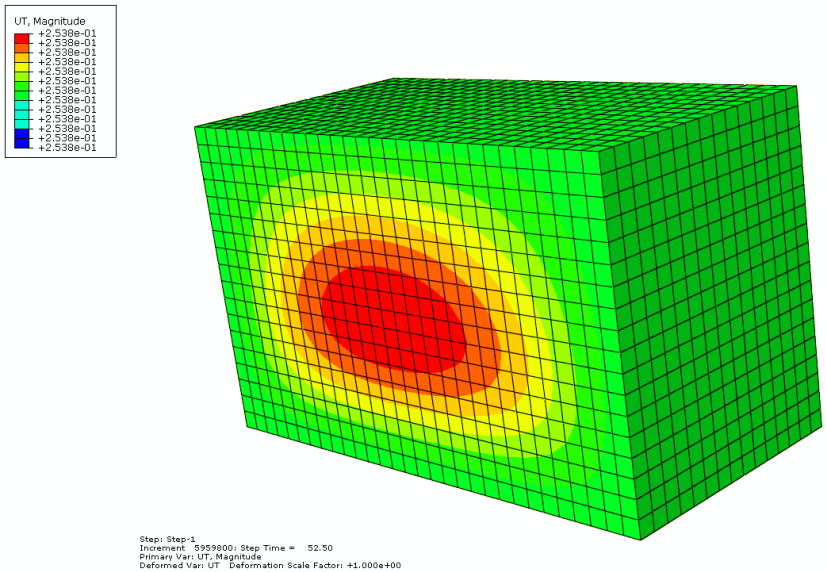

Fig.4.27. Deformation of wall in longitudinal direction due to Tokachi-Oki earthquake at the moment 52.50s.

4.6. The effect of changes in reservoir geometry

As mentioned in previous sections, to investigate the effects of reservoir geometry on the dynamic response of the tank, three different geometry aspect ratios are used, which they are all equal in the reservoir width of 0.30 m and variable length equal to 0.66, 0.5 and 0.33 m were selected and respectively the models no.1, 5, and 7 for Tohoku earthquake and no.2, 6, and 8 for Tokachi-Oki earthquake; in this section of the study were compared.

4.6.1. Evaluation of the maximum stresses in the tank wall during the loading time

Fig.28 and Fig.29 show the total maximum stresses (Von–Mises) in the tank wall during the loading period with different dimensions, respectively for Tohoku and Tokachi earthquakes. The graphs indicate that the values of stresses in wall of tank with different dimensions have the inverse relationship with ratio of $Width/Length$. So that as the W/L ratio decreases, the maximum stress values are increased in the tank wall. Thus, can be seen stresses in the tank wall model no. 5 are more than on the models no. 1 and no.7 for Tohoku earthquake. This could be evaluated that due to the increased hydrostatic forces acting on the inner wall tanks, so that the stress on the tank wall in the model no. 5 increases as the plastic zones appear on the wall. While in the tank wall in model no.7, all the time the material is in the linear range.

Same as the last part, to provide a numerical value to compare and evaluate the results, trend-line diagram for maximum stress can be used.

The trend-line relationship between changes in stress response for three models in this section, respectively, due to Tohoku earthquake for tank no.1 as:

$$\sigma_{max}(t) = 14825(t) + 2 \times 10^3 \quad (6.9)$$

for tank no.5 as:

$$\sigma_{max}(t) = 6866(t) + 3 \times 10^3 \quad (6.10)$$

And for tank no.7 as:

$$\sigma_{max}(t) = 1954.2(t) + 2 \times 10^3 \quad (6.11)$$

The study of the charts shows that 33 % reduction in the ratio of width to the length of the tank (Comparing the ratio of the tank no. 5 to no. 1), is the cause to increase the stresses up to 18 %, and also a 50 % reduction in the ratio of width to the length of the tank (Comparing the ratio of the tank no. 5 to no.7), is the cause to increase the stresses on the wall up to 40.43 %. Accurate results for the maximum stresses are presented in Table 4.8.

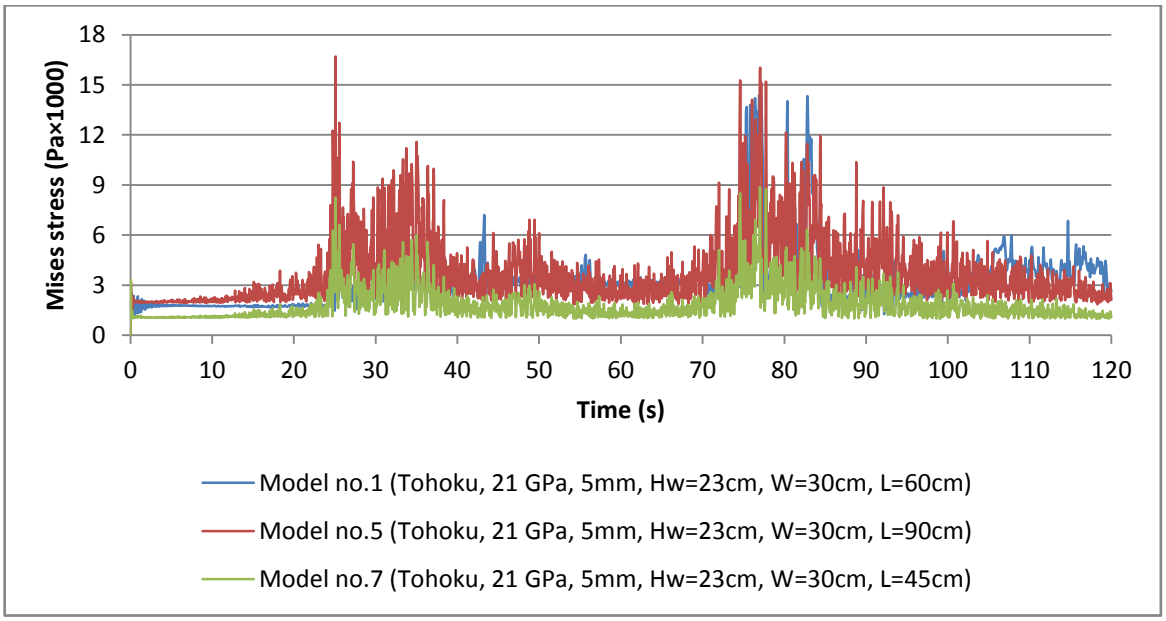

Fig.4.28. The maximum envelope stresses in tank wall due to Tohoku earthquake

Table.4.8. Moment and the amounts of the maximum Mises stress in the tank wall due to Tohoku earthquake

	Model no.		Model properties	Peak MAX	
				Time (s)	Quantity
Stress (Pa× 1000)	W/L=0.6	No.1	E=21GPa/t=5mm/L=0.6m/h=0.23m	82.8	14
	W/L=0.4	No.5	E=21GPa/t=5mm/L=0.90m/h=0.23m	25.1	16.7
	W/L=0.8	No.7	E=21GPa/t=5mm/L=0.45m/h=0.23m	77	8.9

The trend-line relationship between changes in stress response for three models in this section, respectively, due to Tokachi-Oki earthquake for tank no.2 as:

$$\sigma_{max}(t) = 2645.7(t) + 1 \times 10^3 \quad (6.12)$$

for tank no.6 as:

$$\sigma_{max}(t) = 2856.5(t) + 2 \times 10^3 \quad (6.13)$$

And for tank no.8 as:

$$\sigma_{max}(t) = 183.59(t) + 1 \times 10^3 \quad (6.14)$$

The study of the charts shows that 33 % reduction in the ratio of height to the length of the tank (Comparing the ratio of the tank no. 6 to no. 2), is the cause to increase the stresses up to 28 %, and also a 50 % reduction in the ratio of width to the length of the tank (Comparing the ratio of the tank no. 6 to no.8), is the cause to increase the stresses

on the wall up to 38.43 %. Accurate results for the maximum stresses are presented in Table 4.9.

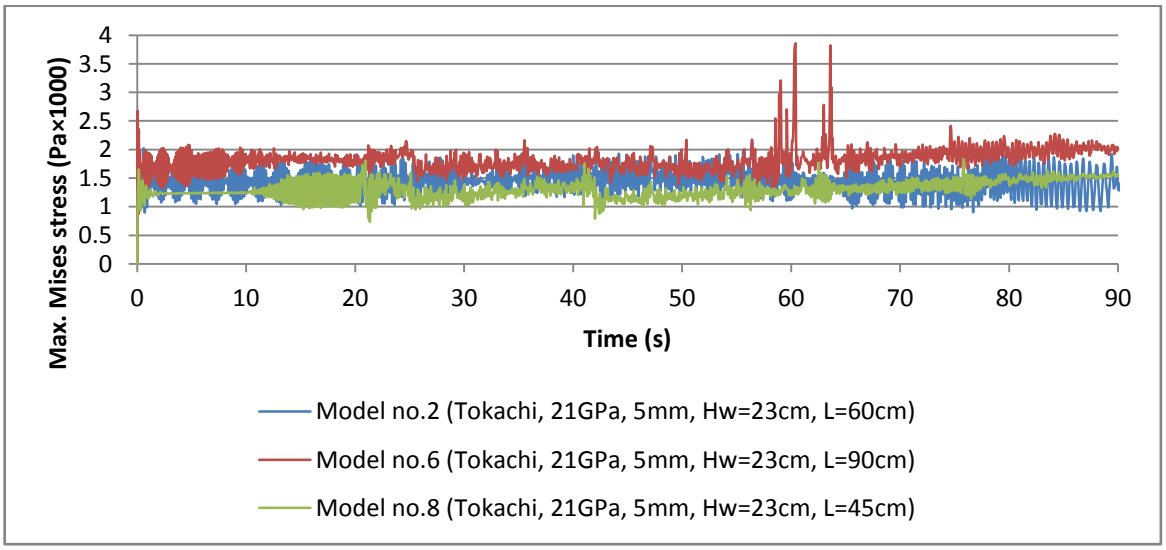

Fig.4.29. The maximum envelope stresses in tank wall due to Tohoku earthquake

Table.4.9. Moment and the amounts of the maximum Mises stress in the tank wall due to Tokachi-Oki earthquake

	Model no.		Model properties	Peak MAX	
				Time (s)	Quantity
Stress (Pa ×1000)	H/L=0.6	No.1	E=21GPa/t=5mm/L=0.6m/W=30m	59.45	2
	H/L=0.4	No.5	E=21GPa/t=5mm/L=0.90m/W=0. 30m	60.35	3.72
	H/L=0.8	No.7	E=21GPa/t=5mm/L=0.45m/W=0.30m	60.3	1.65

To scrutinize comparisons, Fig.4.30, shows the contour of the tank wall stress distribution in the model no. 6, at 60.25 while the maximum stress occurs in the wall.

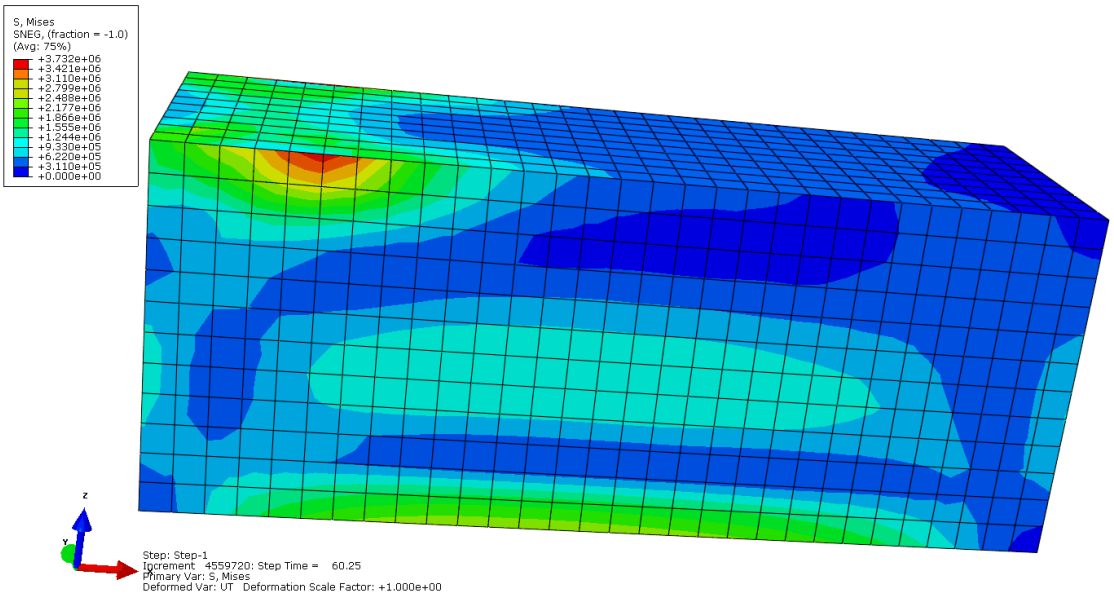

Fig.4.30. Maximum Mises stress in Tank no.6 due to Tokachi-Oki earthquake at the moment of 60.25s.

4.6.2. Evaluation of the maximum displacements in the tank wall during the loading time

In order to investigate the effect of tank geometry, the maximum envelope displacements of the wall elements, in Fig.4.31 and Fig.4.32, for each direction of applying earthquake acceleration are presented, which positive and negative values, represent the movement direction of the tank from its static initial conditions. In general, by comparison of mentioned graphs can be seen that by decreasing the ratio of height to length of the tank, the amount of displacement of the structure (wall) in the x direction, increases. This procedure is based on the input earthquake acceleration in the direction (Y) for the displacement in the negative direction (-Y) is true, but by the movement in the direction (+ Y) for a ratio of 0.4, in comparison with others has the maximum positive displacement; However, it can be due to the nature of input acceleration which is applied in the direction (Y). However, generally, by decreasing the ratio of the height to length, the displacement increases in the tank wall. Because the weight of the tank and fluid increases and therefore the more dynamic forces during an earthquake is applied and cause further displacement in the tank. Table 4.10 shows the maximum displacement created in the tank wall with different geometric dimensions in two directions of applying earthquake acceleration (Y and X).

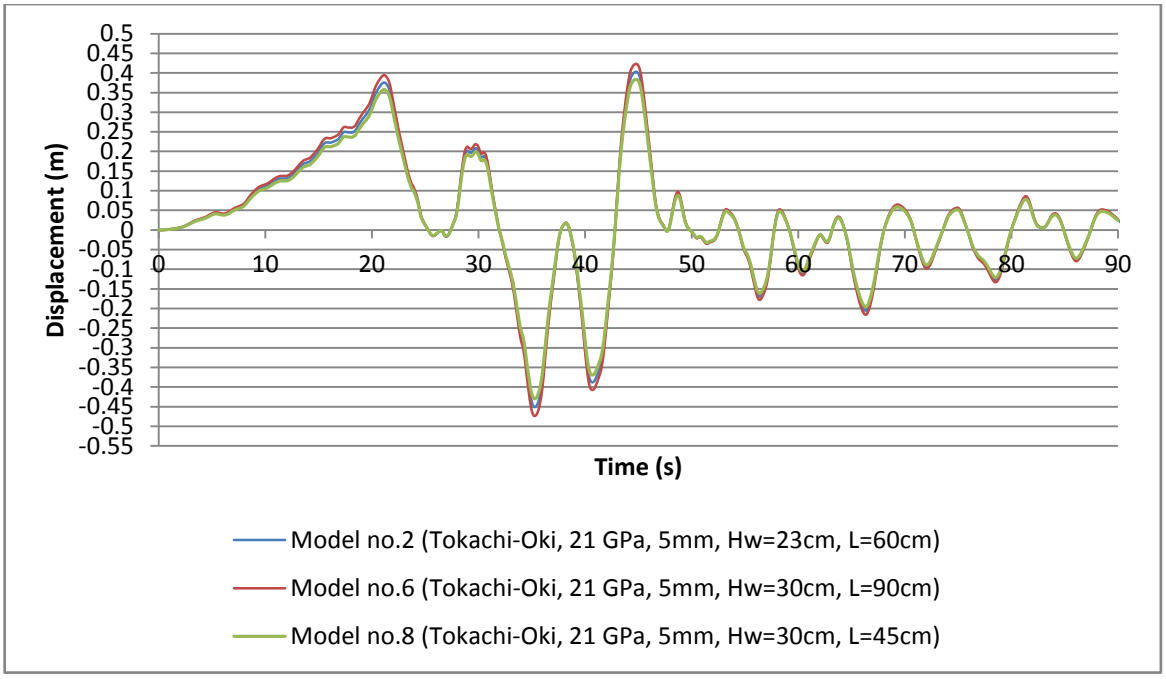

Fig. 4.31 Maximum envelope displacements in tank in x direction during Tokachi-Oki earthquake

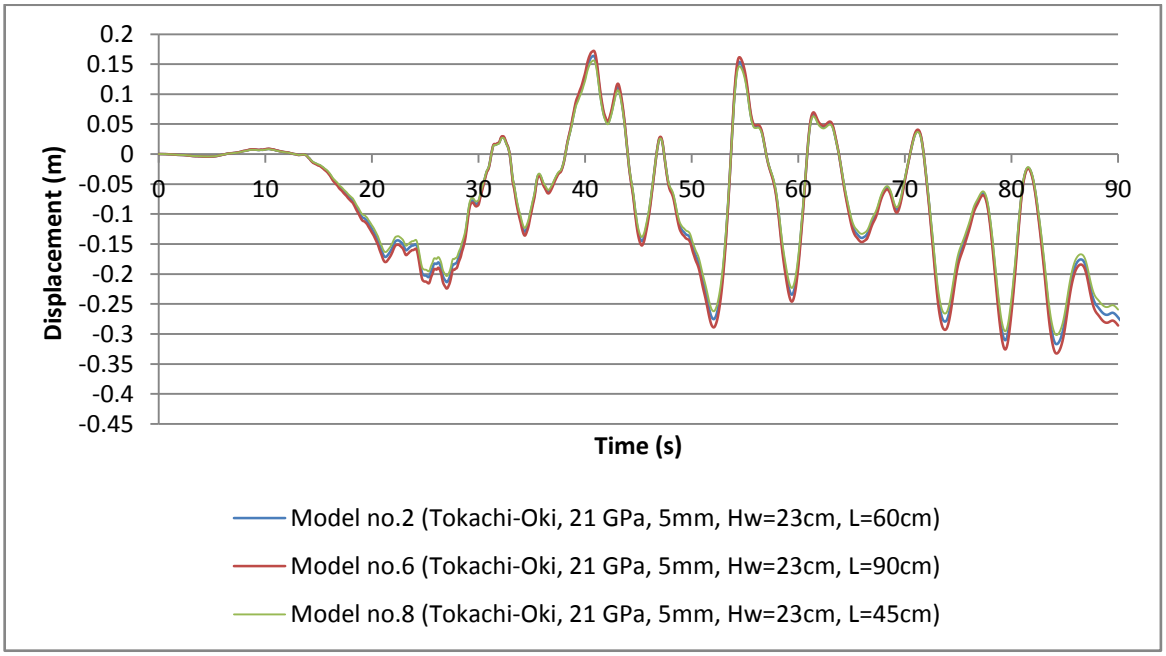

Fig. 4.32. Maximum envelope displacements in tank in Y direction during Tokachi-Oki earthquake

Table.4.10. Time and quantities of maximum and minimum displacements in tank wall in two perpendicular directions of applying ground motions

	Model no.	Model properties	Peak MAX		Peak MIN	
			Time (s)	Quantity	Time (s)	Quantity
Ux(cm)	No.2	E=21GPa/t=5mm/L=0.6m/h=0.23m	44.75	40.6	35.5	-45.4
	No.6	E=21GPa/t=5mm/L=0.9m/h=0.23m	45.05	38.3	35.05	-46.6
	No.8	E=21GPa/t=5mm/L=0.45m/h=0.23m	44.05	36.7	35	-43.1
Uy(cm)	No. 2	E=21GPa/t=5mm/L=0.6m/h=0.23m	40.45	15.8	83.75	-30.7
	No.4	E=21GPa/t=5mm/L=0.9m/h=0.23m	40.35	16.2	84.05	-32.7
	No.8	E=21GPa/t=5mm/L=0.45m/h=0.23m	40.35	15.4	83.95	-29.4

4.6.3. Evaluation distortion along the height of tank wall

In order to determine the critical deformation of the tank wall with different geometric dimensions, same as previous parts, it is necessary to find out the time, direction and location of the element which maximum deformation occurred there. And to do these comparisons, the amount of deformation is calculated at each level of height relative to the baseline level. Figure 4.33 shows the deformations caused by the above-mentioned conditions for models 1, 5 and 7 due to Tohoku earthquake. The maximum amount of bulging and concavity of the tank wall and also the height levels for each one is given in table 4.11. It represents that in tanks by a lower ratio of height to length, the maximum distortion can be seen in the tank wall, which is because of increasing hydrostatic forces and proportionally increasing hydrodynamic forces due to seismic excitation conditions. Also by evaluation height levels related to the maximum distortion in water tanks, range up to 40% from the floor level, is recommended as a critical range of seismic strengthening due to sloshing.

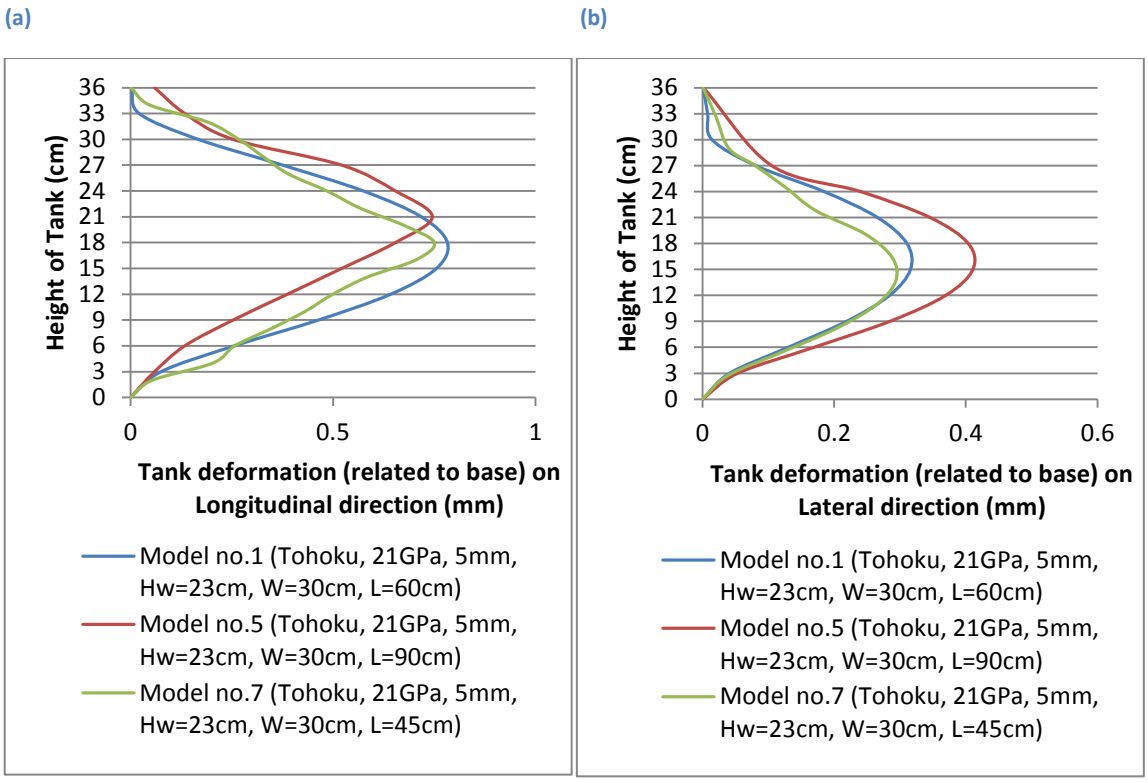

Fig. 4.33. Distortion induced along the tank wall height due to Tohoku earthquake in longitudinal (a) and lateral (b) direction (effect of changing tank geometry).

Table.4.11. Height and quantities of maximum deformation in a tank wall in two perpendicular directions of applying ground motions (Tohoku)

	Model no.		Model properties	Peak MAX	
				Height (cm)	Quantity
Deformation (Y, mm)	H/L=0.6	No.1	E=21GPa/t=5mm/L=0.6m/h=0.23m	17.2	0.78
	H/L=0.4	No.5	E=21GPa/t=5mm/L=0.90m/h=0.23m	21	0.744
	H/L=0.8	No.7	E=21GPa/t=5mm/L=0.45m/h=0.23m	18	0.75
Deformation (X, mm)	H/L=0.6	No.1	E=21GPa/t=5mm/L=0.6m/h=0.23m	16.2	0.32
	H/L=0.4	No.5	E=21GPa/t=5mm/L=0.90m/h=0.23m	16	0.42
	H/L=0.8	No.7	E=21GPa/t=5mm/L=0.45m/h=0.23m	14.6	0.29

Also, Fig. 4.34 shows the deformations caused by the above-mentioned conditions for models 2, 6 and 8 due to Tohoku earthquake. The maximum amount of bulging and concavity of the tank wall and also the height levels for each one is given in table 4.12. It represents that in tanks by lower ratio of height to length, the maximum distortion can be seen in the tank wall, which is because of increasing hydrostatic forces and proportionally increasing hydrodynamic forces due to seismic excitation conditions.

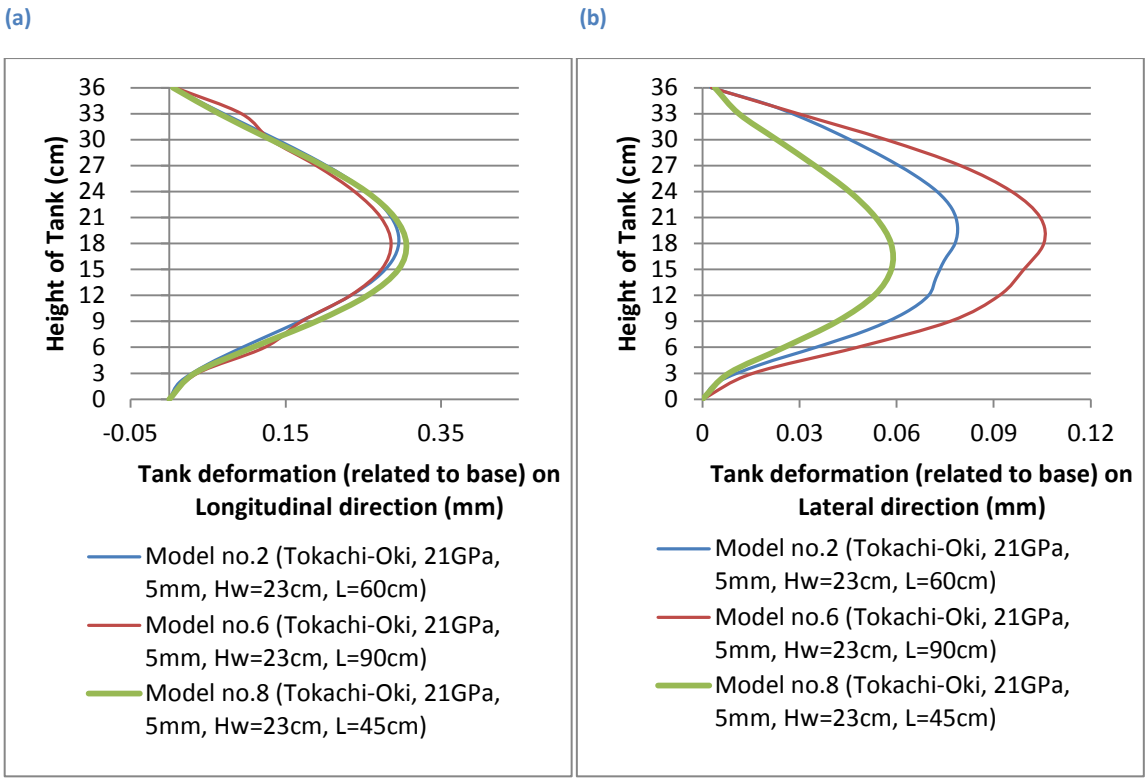

Fig. 4.34. Distortion induced along the tank wall height due to Tokachi-Oki earthquake in longitudinal (a) and lateral (b) direction (effect of changing tank geometry).

Table.4.12. Height and quantities of maximum deformation in a tank wall in two perpendicular directions of applying ground motions (Tokachi-Oki)

	Model no.		Model properties	Peak MAX	
				Height (cm)	Quantity
Deformation (Y, mm)	H/L=0.6	No.2	E=21GPa/t=5mm/L=0.6m/h=0.23m	18.1	0.295
	H/L=0.4	No.6	E=21GPa/t=5mm/L=0.90m/h=0.23m	17.6	0.29
	H/L=0.8	No.8	E=21GPa/t=5mm/L=0.45m/h=0.23m	18	0.305
Deformation (X, mm)	H/L=0.6	No.2	E=21GPa/t=5mm/L=0.6m/h=0.23m	20	0.079
	H/L=0.4	No.6	E=21GPa/t=5mm/L=0.90m/h=0.23m	21	0.1
	H/L=0.8	No.8	E=21GPa/t=5mm/L=0.45m/h=0.23m	15.9	0.06

4.6.4. Evaluation of the maximum hydrodynamic pressure in the tank during the loading time

Figures 4.35 and 4.36, respectively, show the maximum water hydrodynamic pressure in the reservoir during the loading time due to mentioned Tohoku and Tokachi-Oki earthquakes. For this purpose, all the Eulerian elements in the tank, as a separated part from other parts have been isolated. The pressure response of elements during this time period is derived individually, and then by using data post-processing capability of the program, the maximum envelope pressure values are obtained as a text file and by using

other software converted to figures.

The graphs show that the values of hydrodynamic pressure in the tank no.7 which the height to length ratio is equal to 0.8, generally less than the values of pressure in the tanks that height to length ratio are equal to 0.6 and 0.4; but to provide a numerical value to compare and evaluate the results, trend-line diagram for maximum stress can be used.

The trend-line relationships between changes in hydrodynamic pressure for three models are given in this section, respectively, for different geometry aspect ratios (models no.1, no.5, and 7) due to Tohoku earthquake:

$$\sigma_{max}(t) = 589.07(t) + 92.950 \quad (6.15)$$

$$\sigma_{max}(t) = 35.95(t) + 123.596 \quad (6.16)$$

$$\sigma_{max}(t) = 279.58(t) + 65.149 \quad (6.17)$$

The study of the charts shows that 33 % reduction in the ratio of height to the length of the tank (Comparing the ratio of the tank no. 5 to no. 1), is the cause to increase the stresses up to 11.1 %, and also a 50 % reduction in the ratio of height to the length of the tank (Comparing the ratio of the tank no. 5 to no.7), is the cause to increase the stresses on the wall up to 73.6 %. Accurate results for the maximum stresses are presented in Table 4.13.

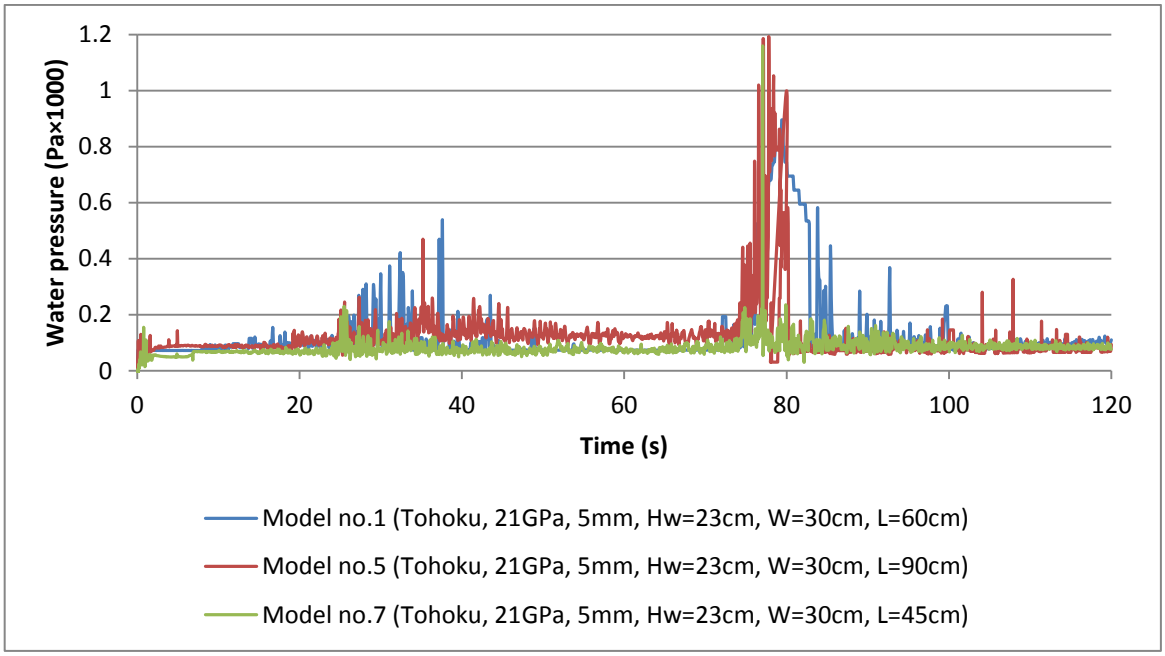

Fig.4.35. The maximum envelope hydrodynamic pressure in tank due to Tohoku earthquake

Table.4.13. Time and quantities of maximum hydrodynamic pressure in a tank due to Tohoku earthquake

	Model no.		Model properties	Peak MAX	
				Time (s)	Quantity
Hydrodynamic pressure (Pa× 1000)	H/L=0.6	No.1	E=21GPa/t=5mm/L=0.6m/h=0.23m	79.8	1.12
	H/L=0.4	No.5	E=21GPa/t=5mm/L=0.90m/h=0.23m	78.5	1.19
	H/L=0.8	No.7	E=21GPa/t=5mm/L=0.45m/h=0.23m	77.05	1.09

The trend-line relationship between changes in hydrodynamic response for three models in this section, respectively, due to Tokachi-Oki earthquake for tank no. 2 as:

$$\sigma_{max}(t) = 1023\,(t) - 10.877 \tag{6.18}$$

for tank no.6 as:

$$\sigma_{max}(t) = 85.15\,(t) + 25.908 \tag{6.19}$$

and for tank no.8 as:

$$\sigma_{max}(t) = -119.67\,(t) + 13.109 \tag{6.20}$$

Which is dealing that 33 % reduction in the ratio of height to the length of the tank (Comparing the ratio of the tank no. 6 to no. 2), is the cause to increase the pressure up to 35.2 %, and also a 50 % reduction in the ratio of height to the length of the tank (Comparing the ratio of the tank no. 6 to no. 8), is the cause to increase the stresses on the wall up to 84.6 %. Accurate results for the maximum stresses are presented in Table 4.14.

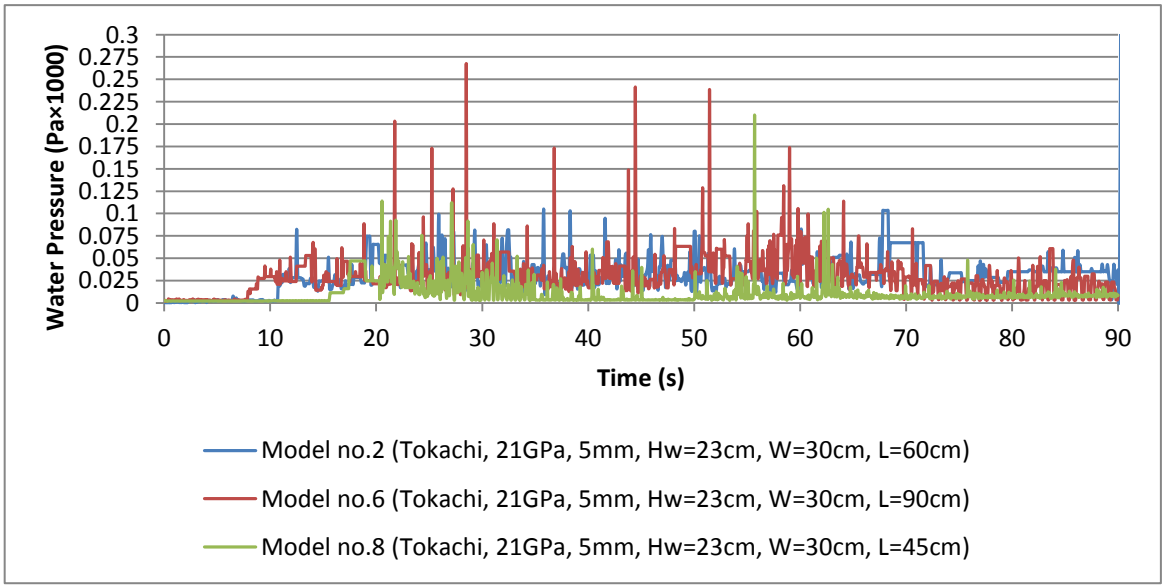

Fig.4.36. The maximum envelope hydrodynamic pressure in tank due to Tokachi-Oki earthquake

Table.4.14. Time and quantities of maximum hydrodynamic pressure in a tank due to Tokachi-Oki earthquake

	Model no.		Model properties	Peak MAX	
				Time (s)	Quantity
Hydrodynamic pressure (Pa× 1000)	H/L=0.6	No.2	E=21GPa/t=5mm/L=0.6m/h=0.23m	35.8	0.125
	H/L=0.4	No.6	E=21GPa/t=5m/L=0.90m/h=0.23m	28.5	0.267
	H/L=0.8	No.8	E=21GPa/t=5mm/L=0.45m/h=0.23m	55.7	0.21

4.6.5. Evaluation of water free surface elevation

Liquid sloshing inside the scaled 3D rectangular tank model induced by two recorded earthquake excitation is evaluated with presenting numerical methods with different geometry ratios and the results compared together.

Fig. 4.37 shows the time history response of the free surface elevation of the Tohoku earthquake under consideration, compared with geometry ratios of 0.4, 0.6 and 0.8 (models no. 7, no.1, and no.5), where the elevation is measured at the right end of the tank. It is clear that the elevation is a function of acceleration time-history, and in tank no.5 is greater than tanks no.1 and no.7 considerably. Table 4.15 represents the maximum values of water surface elevation in tanks no. 1, no.5 and no.7.

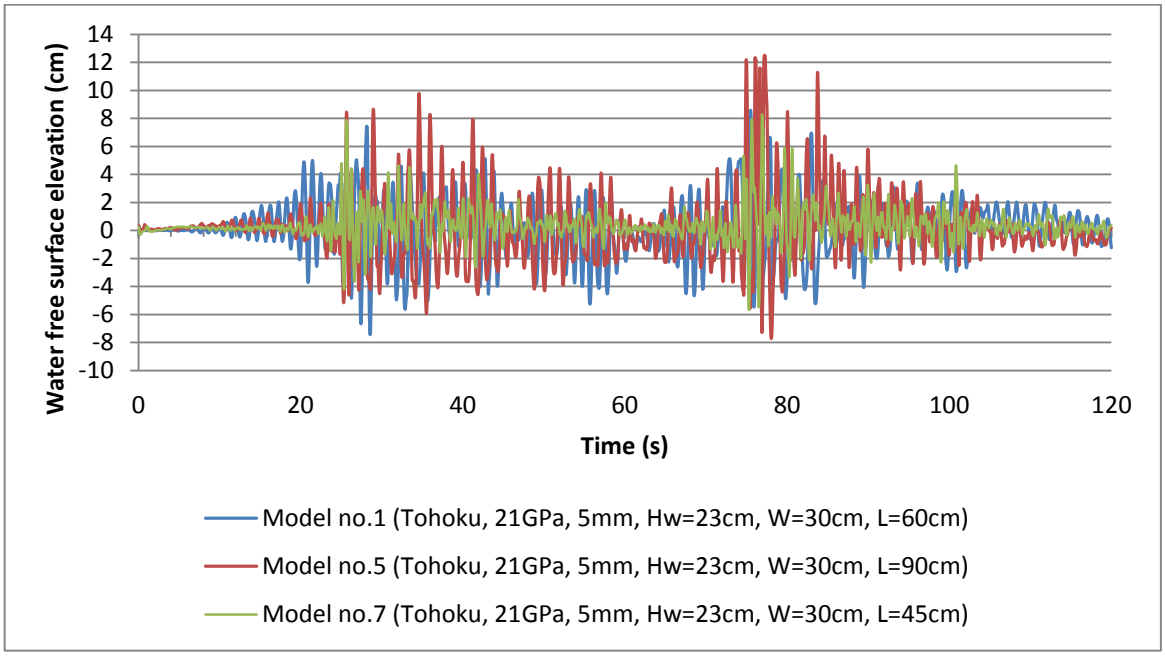

Fig.4.37. Water free surface average elevation at right hand side of the tank due to Tohoku earthquake

Table.4.15. Time and quantities of maximum hydrodynamic pressure in a tank due to Tohoku earthquake

	Model no.		Model properties	Peak MAX	
				Time (s)	Quantity
Free surface elevation (cm)	H/L=0.6	No.1	E=21GPa/t=5mm/L=0.6m/h=0.23m	79.8	13
	H/L=0.4	No.5	E=21GPa/t=5mm/L=0.90m/h=0.23m	78.5	9.8
	H/L=0.8	No.7	E=21GPa/t=5mm/L=0.45m/h=0.23m	79.05	8.5

Also, Fig. 4.38 shows the time history response of the free surface elevation of the Tokachi-Oki earthquake under consideration, compared with geometry ratios of 0.4, 0.6 and 0.8 (models no. 8, no.2, and no.6), where the elevation is measured at the right end of the tank. It is clear that the elevation is a function of acceleration time-history, and in tank no.6 is greater than tanks no.2 and no.8 considerably. Table 4.16 represents the maximum values of water surface elevation in tanks no. 2, no.6 and no.8.

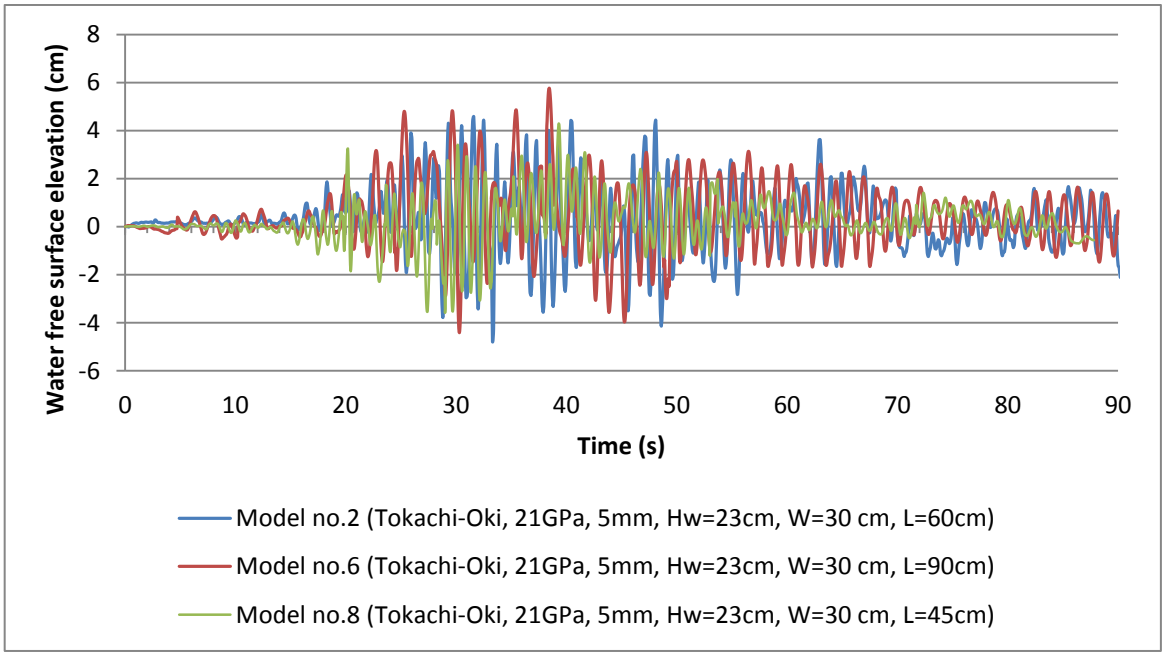

Fig.4.38. Water free surface average elevation at right hand side of the tank due to Tokachi-Oki earthquake

Table.4.16. Time and quantities of maximum hydrodynamic pressure in a tank due to Tohoku earthquake

	Model no.		Model properties	Peak MAX	
				Time (s)	Quantity
Free surface elevation (cm)	H/L=0.6	No.1	E=21GPa/t=5mm/L=0.6m/h=0.23m	79.8	13
	H/L=0.4	No.5	E=21GPa/t=5mm/L=0.90m/h=0.23m	78.5	9.8
	H/L=0.8	No.7	E=21GPa/t=5mm/L=0.45m/h=0.23m	79.05	8.5

4.7. Effect of water filling depth in the reservoir on dynamic responses of the reservoir wall

In the last part of this research the effect of water filling depth in the reservoir on dynamic responses of the reservoir wall is evaluated. For this purpose, the models with the same geometry, materials and boundary conditions and different water filling depths which are including three models "$h/H = 0.83$" , "$h/H = 0.64$" and "$h/H = 0.50$" are simulated.

4.7.1 Evaluation of the maximum stresses in the tank wall during the loading time

Fig.4.39 and Fig.4.42 show the total maximum (Von–Mises) in the tank wall during the loading period with different water depth, respectively. The graphs indicate that the between the values of stresses in the wall of the tank with different water depths there is a significant difference, because obviously in the most time steps of loading, there will be elements of the wall that the maximum stress occurs in the wall and their stress values are close to the yield strength of tank materials. The initial difference between the stresses mostly because of hydrostatic pressure, but while PGA increases, because of sloshing and slamming phenomena, the stress increase suddenly in tanks; especially in tanks with a filling depth ratio of 50% and 63%. Same as the last parts, to provide a numerical value to compare and evaluate the results, trend-line diagram for maximum stress can be used.

The trend-line relationship between changes in stress response for three models in this section, respectively, due to Tohoku earthquake for tank no.1 as:

$$\sigma_{\max}(\mathrm{t}) = 14825(\mathrm{t}) + 2 \times 10^3 \tag{6.21}$$

for tank no.9 as:

$$\sigma_{\max}(\mathrm{t}) = 322.01(\mathrm{t}) + 3 \times 10^3 \tag{6.22}$$

And for tank no.13 as:

$$\sigma_{max}(t) = 12322(t) + 769.411 \tag{6.23}$$

The study of the charts shows that 33 % reduction in the ratio of water filling depth of the tank (Comparing the ratio of the tank no. 9 to no. 1), is the cause to decrease the stresses up to 11 %, and also a 50 % reduction in the ratio of height to the length of the tank (Comparing the ratio of the tank no. 9 to no.13), is the cause to decrease the stresses on the wall up to 54.7 %. Accurate results for the maximum stresses are presented in Table 4.17.

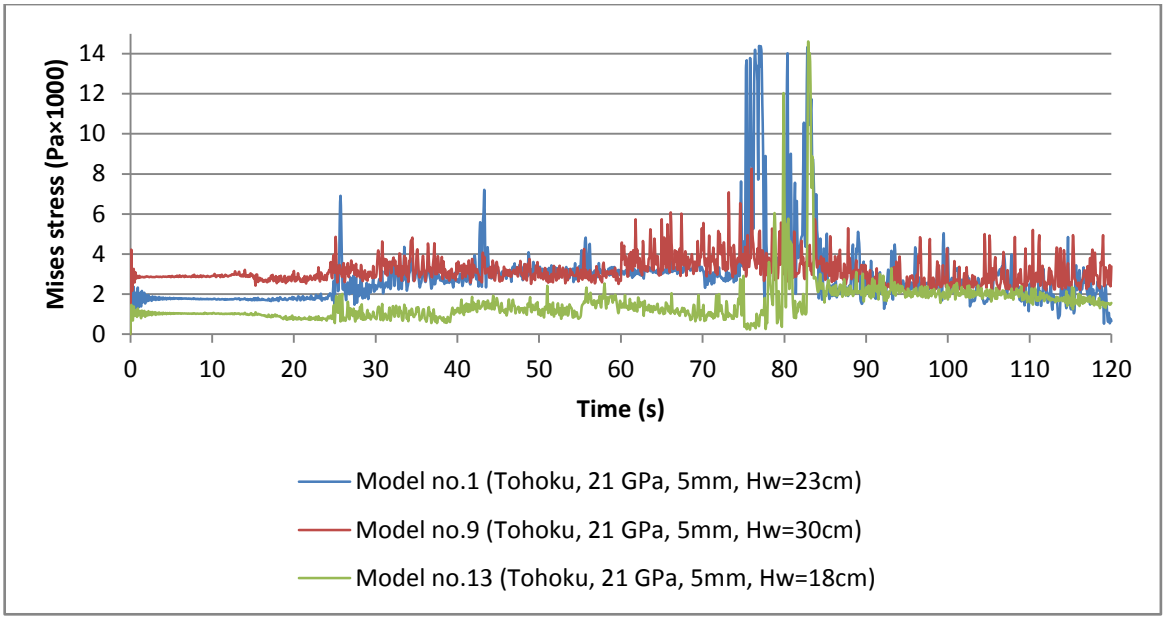

Fig.4.39. The maximum envelope stresses in tank wall due to Tohoku earthquake

Table.4.17. Moment and the amounts of the maximum Mises stress in the tank wall due to Tohoku earthquake

	Model no.		Model properties	Peak MAX	
				Time (s)	Quantity
Mises Stress (Pa×1000)	h/H=0.64	No.1	E=21GPa/t=5mm/L=0.6m/h=0.23m	75.8	14.2
	h/H=0.83	No.9	E=21GPa/t=5m/L=0.60m/h=0.30m	78.3	8.2
	h/H=0.5	No.13	E=21GPa/t=5mm/L=0.6m/h=0.18m	82.9	14.4

The trend-line relationship between changes in stress response for three models in this section, respectively, due to Tokachi-Oki earthquake for tank no.2 as:

$$\sigma_{max}(t) = 1883.59(t) + 1 \times 10^3 \quad (6.24)$$

for tank no.10 as:

$$\sigma_{max}(t) = 5317.5(t) + 2 \times 10^3 \quad (6.25)$$

And for tank no.14 as:

$$\sigma_{max}(t) = -4562(t) + 895.713 \quad (6.26)$$

The study of the charts shows that 33 % reduction in the ratio of water filling depth of the tank (Comparing the ratio of the tank no. 10 to no. 2), is the cause to decrease the stresses up to 18 %, and also a 50 % reduction in the ratio of height to the length of the tank (Comparing the ratio of the tank no. 10 to no.14), is the cause to decrease the stresses on the wall up to 63.5 %. Accurate results for the maximum stresses are presented in Table

4.18.

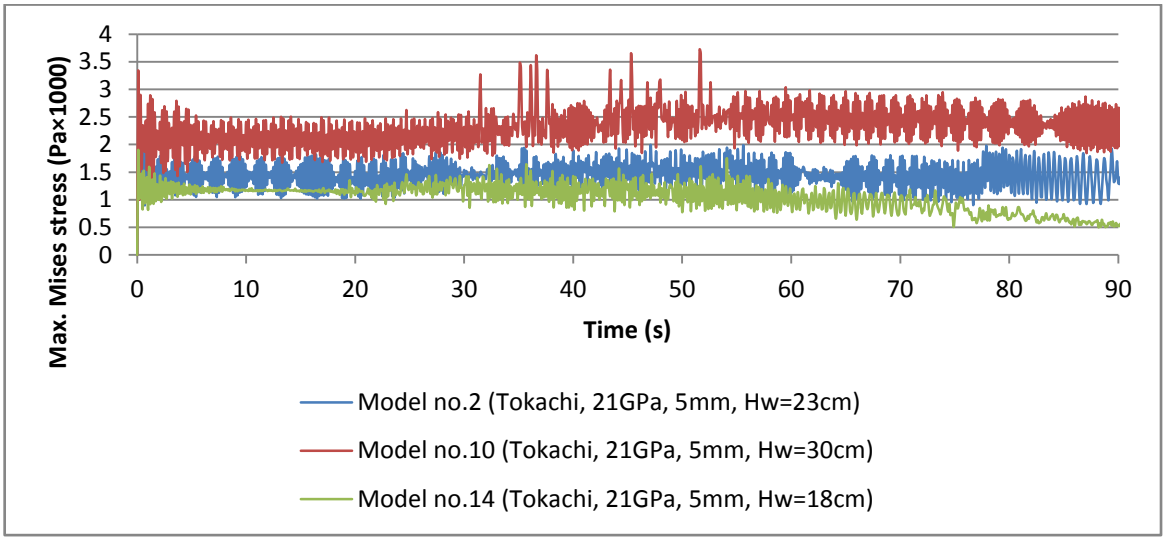

Fig.4.40. The maximum envelope stresses in tank wall due to Tohoku earthquake

Table.4.18. Moment and the amounts of the maximum Mises stress in the tank wall due to Tohoku earthquake

	Model no.		Model properties	Peak MAX	
				Time (s)	Quantity
Mises Stress (Pa×1000)	h/H=0.64	No.1	E=21GPa/t=5mm/L=0.6m/h=0.23m	53.1	1.98
	h/H=0.83	No.9	E=21GPa/t=5mm/L=0.60m/h=0.30m	52.6	3.8
	h/H=0.5	No.13	E=21GPa/t=5mm/L=0.60m/h=0.18m	54.1	1.26

To do scrutinize comparisons, figures 4.41 and 4.42, respectively, show the contour of the tank wall stress distribution in the models no.10 and no.14 (at the moment of 52.6s and 54.1s, respectively).

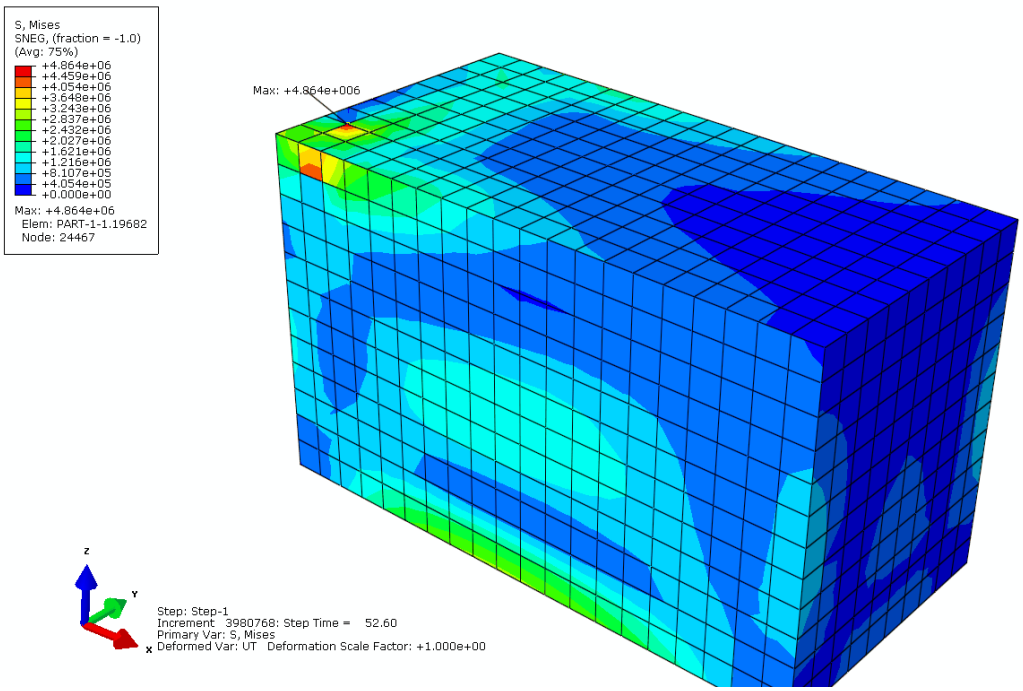

Fig.4.41. Maximum Mises stress in Tank no.13 due to Tokachi-Oki earthquake at the moment of 52.6s.

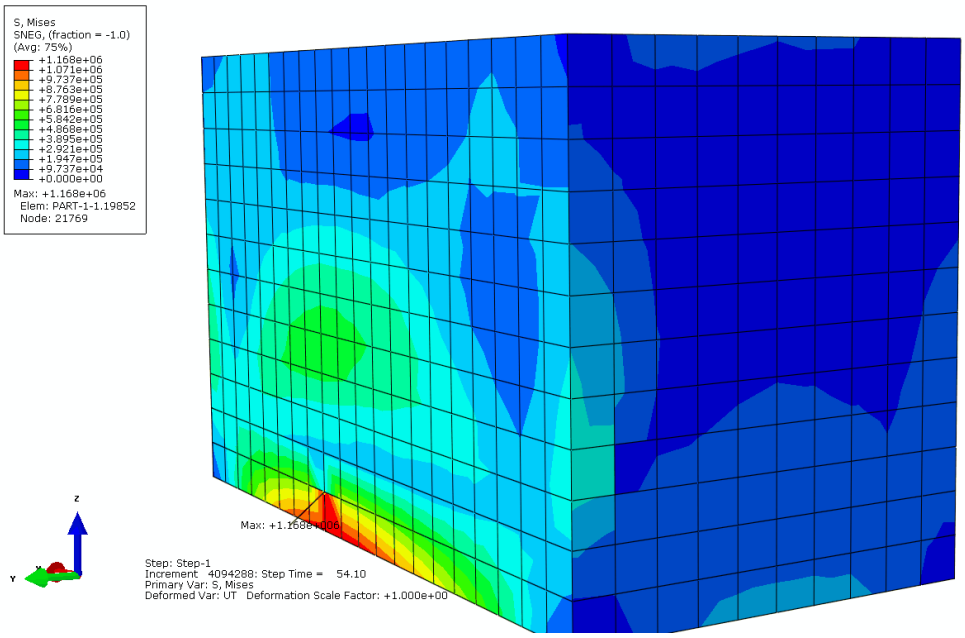

Fig.4.42. Maximum Mises stress in Tank no.13 due to Tokachi-Oki earthquake at the moment of 54.1.

4.7.2. Evaluation of the maximum displacements in the tank wall during the loading time

In order to investigate the effect of water filling depth, the displacements of the wall elements for each direction of applying earthquake acceleration are presented. Fig.4.43 and Fig.4.44, respectively, show the maximum displacement of the tank wall elements in the direction of (Y and X), which positive and negative values, represent the movement direction of the tank from its static initial conditions.

In general, by comparison of mentioned graphs can be seen that the tanks with different filling depth, have different responses (wall displacement) relative to their static initial conditions, by comparing the tank wall displacement in either direction (+ Y and + X), half-filled tank has a maximum displacement. However, generally, the maximum displacements in each specified direction are affected by conditions and applied input acceleration. Table 4.19 shows the maximum and minimum displacement created in the tank wall with a different water filling depth in two directions of applying earthquake acceleration (Y and X).

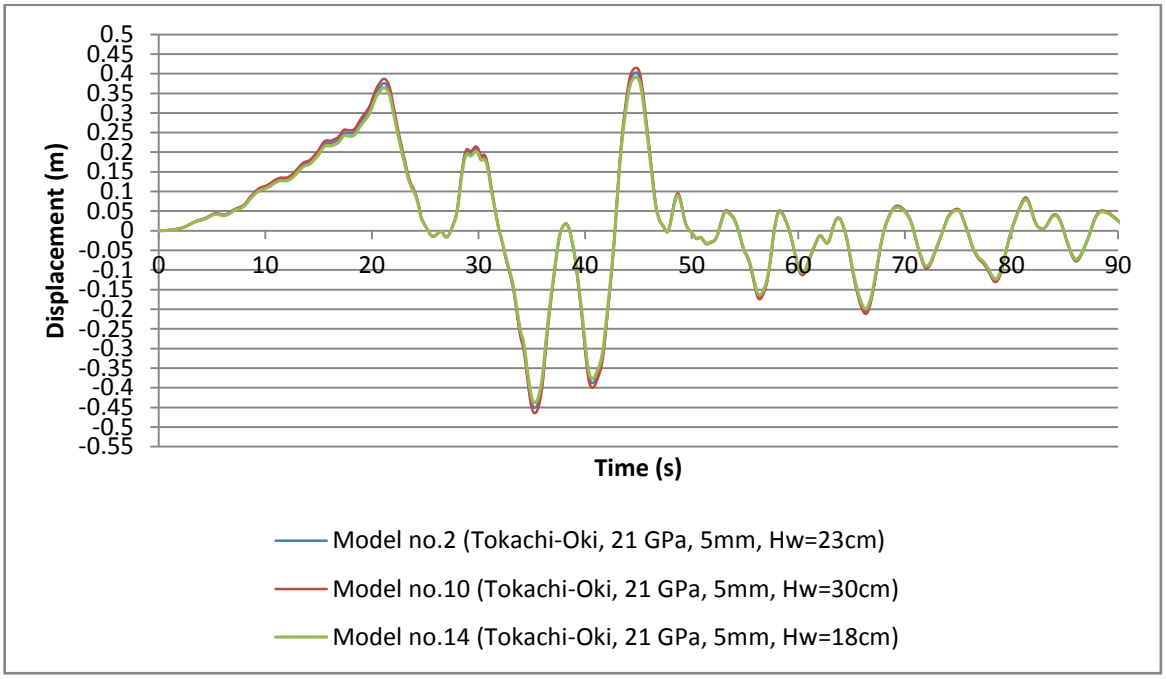

Fig.4.43. Maximum envelope displacements in tank in x direction during Tokachi-Oki earthquake

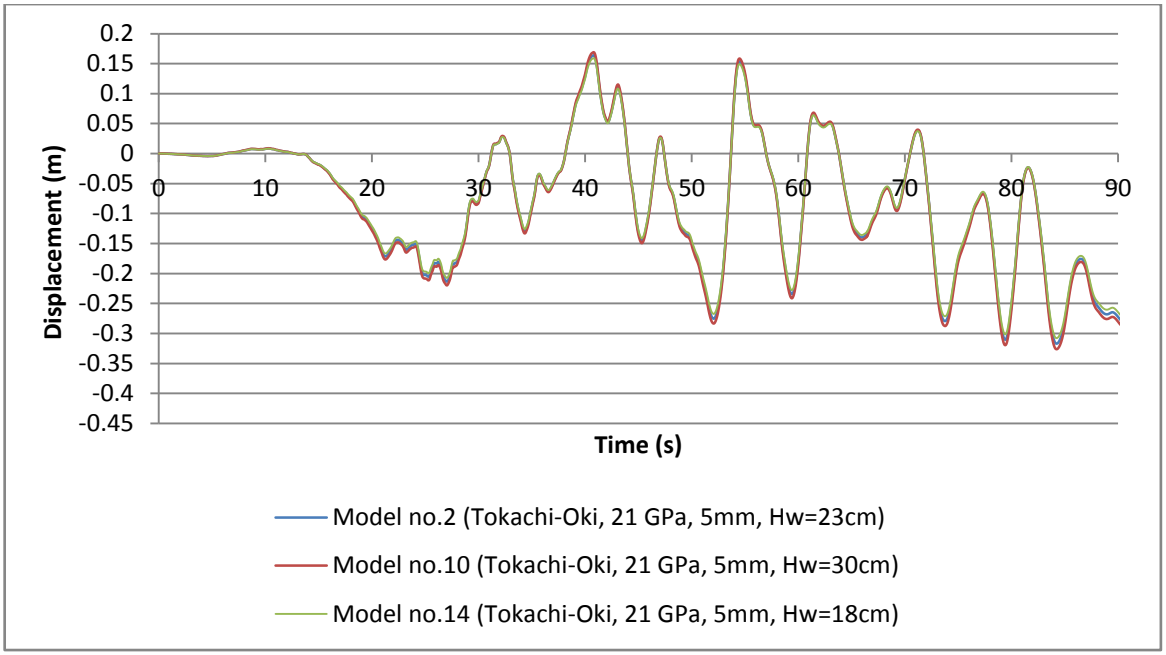

Fig.4.44. Maximum envelope displacements in tank in x direction during Tokachi-Oki earthquake

Table.4.19. Time and quantities of maximum and minimum displacements in tanks wall in two perpendicular directions of applying ground motions

	Model no.	Model properties	Peak MAX		Peak MIN	
			Time (s)	Quantity	Time (s)	Quantity
Ux(cm)	No.2	E=21GPa/t=5mm/L=0.6m/h=0.23m	44.95	41.8	35.1	-45
	No.10	E=21GPa/t=5mm/L=0.6m/h=0.30m	44.95	41.2	35.4	-46.8
	No.14	E=21GPa/t=5mm/L=0.6m/h=0.18m	44.85	40.7	35	-43.6
Uy(cm)	No. 2	E=21GPa/t=5mm/L=0.6m/h=0.23m	40.7	16.5	85	-31.4
	No.10	E=21GPa/t=5mm/L=0.6m/h=0.30m	41	17.2	84.85	-32.8
	No.14	E=21GPa/t=5mm/L=0.6m/h=0.18m	41	16.2	85.05	-30.9

4.7.3. Evaluation distortion along the height of tank wall

In order to determine the critical deformation in the tank wall, the time, location and direction of the critical element of the wall are chosen, and to do a comparison, the amount of deformation for every elevation relative to baseline levels will be examined.

By examining and comparing the graphs presented in the previous section, the maximum displacements induced in the tank wall, we consider the critical time for each of models to extract deformation occurring in the tank wall.

For this purpose, we choose the path along the height of the tank which maximum displacement occurred and coordinate values for elements, at critical moments is recorded, individually. Fig.4.45 and Fig.4.46 show the deformations caused by the above-mentioned conditions for models no.1, no.9 and no.13 due to Tohoku earthquake and

models no.2, no.10 and no.14 due to Tokachi-Oki earthquake. The maximum amount of bulging of the tank wall and also the height levels for each one is given. It is clear that tanks, no. 9 and no. 10 with filling depth ratio of 83% have more distortion relative to other tanks. This issue, with quantities stated in the previous section correspond to the maximum displacement of the wall is compatible, because in positive and negative directions of motion and maximum values (absolute value) of seismic displacements in the direction in half full tanks were more than others. More distortions in wall of half-filled tank relative to full filled tank can be to attributed with lower elevation of the fluid in the half filled tank which provides more freedom of movement for the wall elements (especially at high accelerations). Because the wall of a fully filled tank has more support surface, especially when moves opposite the direction of motion of fluid motion (sloshing wave), which causes less deformation relative to semi half-filled tanks.

On the other hand the weight of half-filled tank, due to its fluid, more than empty reservoir and in excitation conditions more dynamic forces are generated which induce more stresses and strains. About the height levels associated with wall distortions, it can be seen that in tanks at approximately near to the free surface level of the tank height need special attention for seismic retrofitting.

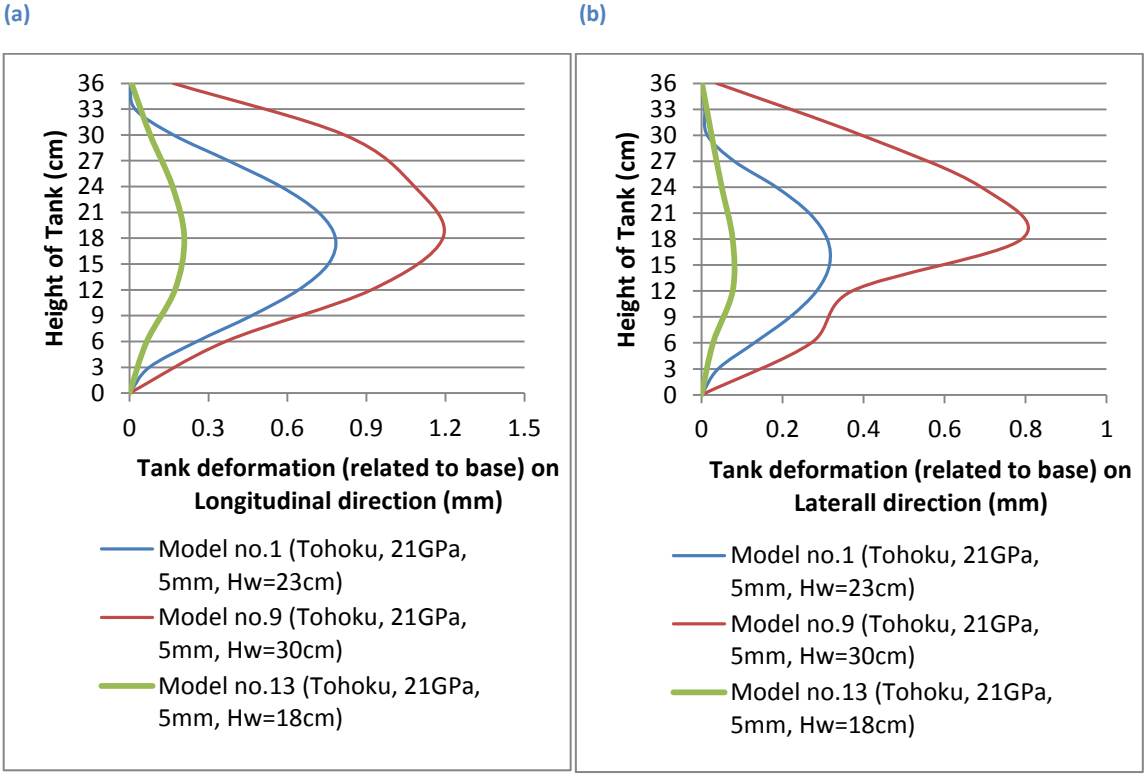

Fig. 4.45. Distortion induced along the tank wall height due to Tohoku earthquake in (a) longitudinal and (b) lateral direction

The maximum amount of bulging and concavity of the tank wall and also the height levels for each one is given in table 4.20 and table 4.21, respectively due to Tohoku and Tokachi-Oki earthquakes.

Table.4.20. Height and quantities of maximum deformation in a tank wall in two perpendicular directions of applying ground motions (Tohoku)

	Model no.		Model properties	Peak MAX	
				Height (cm)	Quantity
Deformation (Y, mm)	H/L=0.6	No.1	E=21GPa/t=5mm/L=0.6m/h=0.23m	19.2	0.78
	H/L=0.4	No.9	E=21GPa/t=5mm/L=0.60m/h=0.30m	20.2	1.21
	H/L=0.8	No.13	E=21GPa/t=5mm/L=0.60m/h=0.18m	17.8	0.21
Deformation (X, mm)	H/L=0.6	No.1	E=21GPa/t=5mm/L=0.6m/h=0.23m	17.1	0.81
	H/L=0.4	No.9	E=21GPa/t=5mm/L=0.60/h=0.30m	20.2	0.33
	H/L=0.8	No.13	E=21GPa/t=5mm/L=0.60m/h=0.18m	15.5	0.079

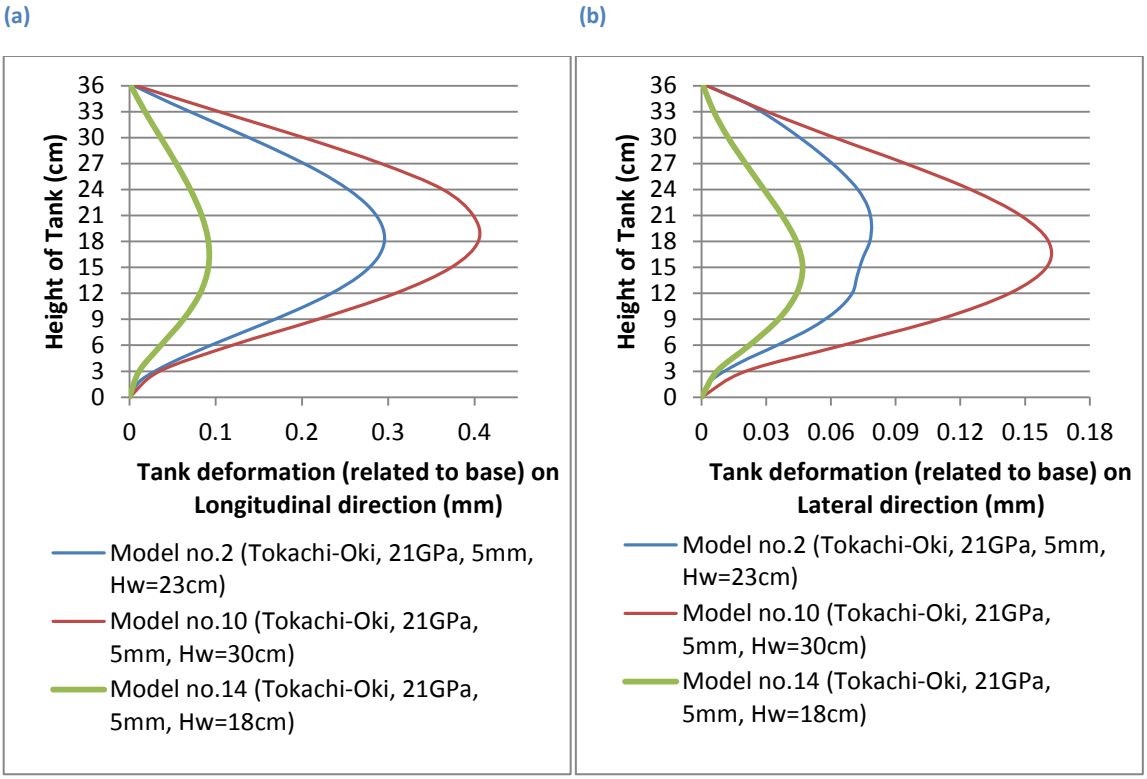

Fig. 4.46. Distortion induced along the tank wall height due to Tokachi-Oki earthquake in (a) longitudinal and (b) lateral direction

Table.4.21. Height and quantities of maximum deformation in a tank wall in two perpendicular directions of applying ground motions (Tokachi-Oki)

	Model no.		Model properties	Peak MAX	
				Height (cm)	Quantity
Deformation (Y, mm)	H/L=0.6	No.2	E=21GPa/t=5mm/L=0.6m/h=0.23m	18	0.295
	H/L=0.4	No.10	E=21GPa/t=5mm/L=0.60m/h=0.30m	20	0.42
	H/L=0.8	No.14	E=21GPa/t=5mm/L=0.60m/h=0.18m	17.5	0.95
Deformation (X, mm)	H/L=0.6	No.2	E=21GPa/t=5mm/L=0.6m/h=0.23m	20	0.079
	H/L=0.4	No.10	E=21GPa/t=5mm/L=0.60m/h=0.30m	16.5	0.16
	H/L=0.8	No.14	E=21GPa/t=5mm/L=0.60m/h=0.18m	15	0.047

4.7.4. Evaluation of the maximum hydrodynamic pressure in the tank during the loading time

Figures 4.49 and 4.50, respectively, show the maximum water hydrodynamic pressure in the reservoir during the loading time due to mentioned Tohoku and Tokachi-Oki earthquakes. For this purpose, all the Eulerian elements in the tank, as a separated part from other parts have been isolated. The pressure response of elements during this time period is derived individually, and then by using data post-processing capability of the program, the maximum envelope pressure values are obtained as a text file and by using other software converted to figures.

The graphs show that the values of hydrodynamic pressure in the tank no.1 which the water filling ratio is equal to 0.63, generally more than the values of pressure in the tanks that height to length ratio are equal to 0.83 and 0.5; but to provide a numerical value to compare and evaluate the results, trend-line diagram for maximum pressure can be used.

The trend-line relationships between changes in hydrodynamic pressure for three models are given in this section, respectively, for different filling depth ratios (models no.1, no.9, and no.13) due to Tohoku earthquake:

$$\sigma_{max}(t) = 589.07(t) + 92.950 \quad (6.27)$$

$$\sigma_{max}(t) = 33.95(t) + 61.139 \quad (6.28)$$

$$\sigma_{max}(t) = 450(t) + 63.153 \quad (6.29)$$

The study of the charts shows that 25 % reduction in the ratio of water filling depth of the

tank (Comparing the ratio of the tank no. 9 to no. 1), is the cause to increase the pressure up to 58 %, and also a 39.7 % reduction in the ratio of water filling depth of the tank (Comparing the ratio of the tank no. 9 to no.13), is the cause to increase the hydrodynamic pressure up to 11 %. Accurate results for the maximum stresses are presented in Table 4.22.

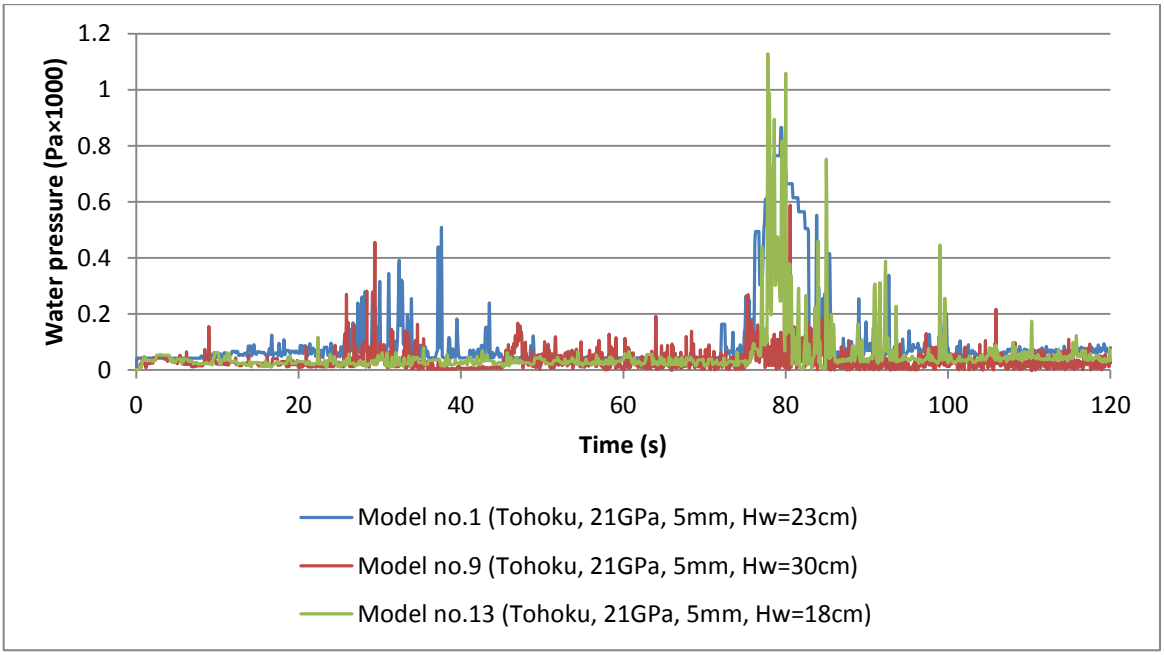

Fig.4.47. The maximum envelope hydrodynamic pressure in tank due to Tohoku earthquake

Table.4.22. Time and quantities of maximum hydrodynamic pressure in a tank due to Tohoku earthquake

	Model no.		Model properties	Peak MAX	
				Time (s)	Quantity
Hydrodynamic pressure (Pa×1000)	h/H=0.63	No.1	E=21GPa/t=5mm/L=0.60m/h=0.23m	79.8	0.88
	h/H=0.83	No.9	E=21GPa/t=5mm/L=0.60m/h=0.30m	78.5	0.58
	h/H=0.5	No.13	E=21GPa/t=5mm/L=0.60m/h=0.18mm	79.05	1.1

The trend-line relationship between changes in hydrodynamic response for three models in this section, respectively, due to Tokachi-Oki earthquake for tank no. 2 as:

$$\sigma_{max}(t) = 1023\,(t) - 10.877 \tag{6.30}$$

for tank no.6 as:

$$\sigma_{max}(t) = 85.15\,(t) + 25.908 \tag{6.31}$$

and for tank no.8 as:

$$\sigma_{max}(t) = -119.67\,(t) + 13.109 \tag{6.32}$$

Which is dealing that 25% reduction in the ratio of water filling depth of the tank (Comparing the ratio of the tank no. 10 to no. 2), is the cause to increase the pressure up to 64.3 %, and also a 39.7 % reduction in the ratio of water filling depth of the tank (Comparing the ratio of the tank no. 10 to no. 14), is the cause to increase the stresses on the wall up to 44.6 %. Accurate results for the maximum stresses are presented in Table 4.23

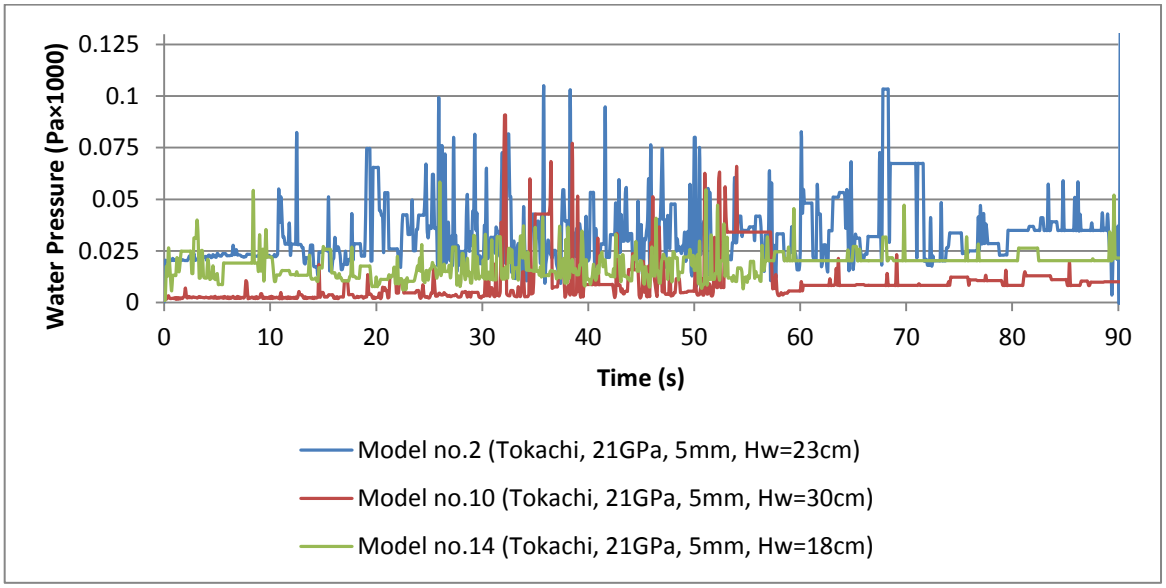

Fig.4.48. The maximum envelope hydrodynamic pressure in tank due to Tokachi-Oki earthquake

Table.4.23. Time and quantities of maximum hydrodynamic pressure in a tank due to Tokachi-Oki earthquake

	Model no.		Model properties	Peak MAX	
				Time (s)	Quantity
Hydrodynamic pressure (Pa×1000)	h/H=0.63	No.2	E=21GPa/t=5mm/L=0.60m/h=0.23m	35.8	0.108
	h/H=0.83	No.10	E=21GPa/t=5mm/L=0.60m/h=0.30m	32.1	0.09
	h/H=0.5	No.14	E=21GPa/t=5mm/L=0.60m/h=0.18m	26	0.06

4.7.5. Water free surface elevation

Liquid sloshing inside the scaled 3D rectangular tank model induced by two recorded earthquake excitation is evaluated with presenting numerical methods with different geometry ratios and the results compared together.

Fig. 4.49 shows the time history response of the free surface elevation of the Tohoku earthquake under consideration, compared filling depth ratios of 0.5, 0.63 and 0.83 (models no. 7, no.1, and no.5), where the elevation is measured at the right end of the

tank. It is clear that the elevation is a function of acceleration time-history, and in tank no.13 is greater than tanks no.1 and no.9 considerably. Table 4.24 represents the maximum values of water surface elevation in tanks no. 1, no.9 and no.13.

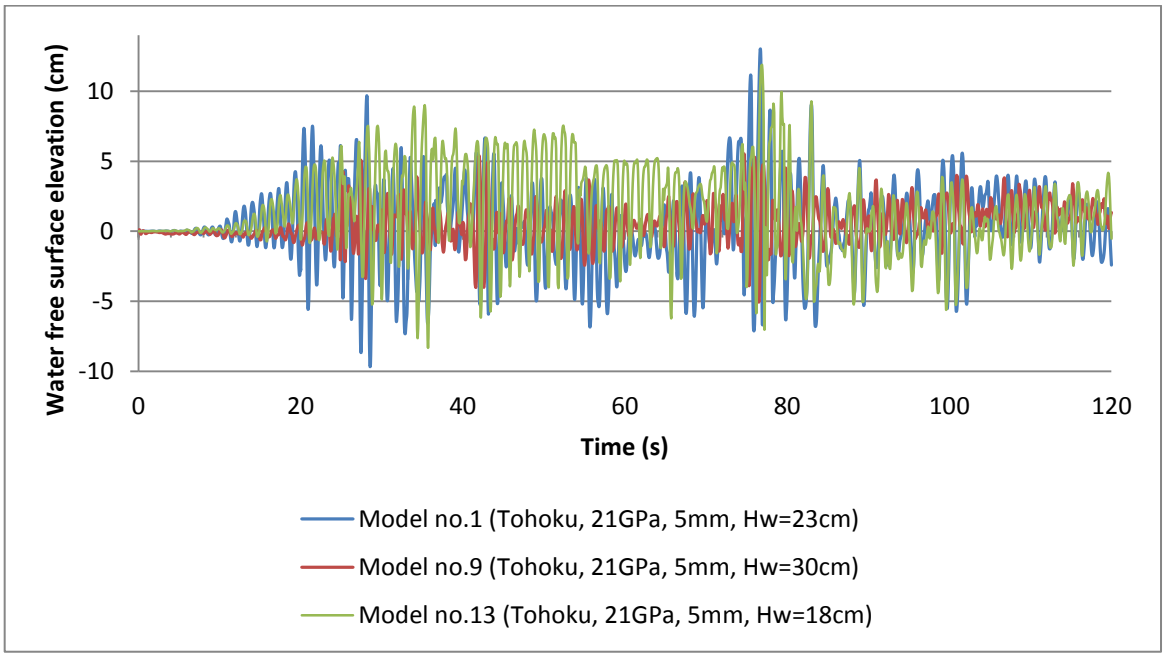

Fig.4.49. Water free surface average elevation at right hand side of the tank due to Tohoku earthquake

Table.4.24. Time and quantities of maximum hydrodynamic pressure in a tank due to Tohoku earthquake

	Model no.		Model properties	Peak MAX	
				Time (s)	Quantity
Free surface elevation (cm)	h/H=0.64	No.2	E=21GPa/t=5mm/L=0.6m/h=0.23m	79.8	13
	h/H=0.83	No.10	E=21GPa/t=5mm/L=0.6m/h=0.30m	78.5	5.7
	h/H=0.5	No.14	E=21GPa/t=5mm/L=0.6m/h=0.18m	79.05	12.5

Also, Fig. 4.50 shows the time history response of the free surface elevation of the Tokachi-Oki earthquake under consideration, compared with geometry ratios of 0.5, 0.63 and 0.83 (models no. 14, no.2, and no.10), where the elevation is measured at the right end of the tank. It is clear that the elevation is a function of acceleration time-history, and in tank no.6 is greater than tanks no.2 and no.8 considerably. Table 4.25 represents the maximum values of water surface elevation in tanks no. 2, no.6 and no.8.

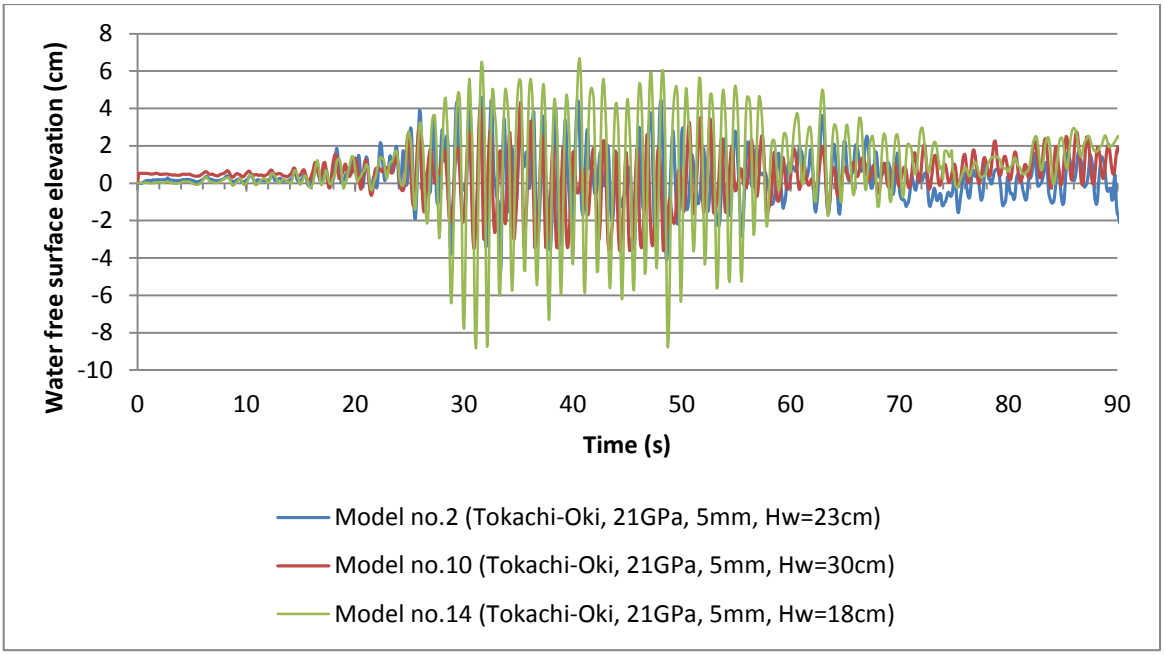

Fig.4.50. Water free surface average elevation at right hand side of the tank due to Tokachi-Oki earthquake

Table.4.25. Time and quantities of maximum hydrodynamic pressure in a tank due to Tokachi-Oki earthquake

	Model no.		Model properties	Peak MAX	
				Time (s)	Quantity
Free surface elevation (cm)	h/H=0.64	No.2	E=21GPa/t=5mm/L=0.6m/h=0.23m	31.5	5.8
	h/H=0.83	No.10	E=21GPa/t=5mm/L=0.6m/h=0.30m	34.9	4.3
	h/H=0.5	No.14	E=21GPa/t=5mm/L=0.6m/h=0.18m	40.5	6.7

Summary

In this chapter, water sloshing in in different condition is studied numerically. The CEL and the SPH methods are applied to simulate water sloshing waves. The numerical solutions are used to find the below parameters:

- The effect of changing the stiffness of the reservoir material
- The effect of changing the thickness of the reservoir, which in this study, two types of tank wall thickness, 5 and 8 mm have been studied.
- The effect of changes in reservoir geometry, which in present study examined three types of geometry for the reservoir including $Height/Length = 0.8$, $H/L = 0.60$ and $H/L = 0.4$.

- The effect of water filling depth in the reservoir, which is included three modes "$h/H = 0.50$", "$h/H = 0.64$" and "$h/H = 0.83$ " has been studied.

To investigate the above mentioned parameters, five outputs of the analysis, is evaluated and compared. These five outputs of the results are as follows:

- Evaluation of the maximum and minimum stresses in the tank wall during the loading time
- Evaluation of the maximum hydrodynamic pressure in the tank wall during the loading time
- Evaluation of the maximum displacements in the tank wall during the loading time
- Evaluation most critical deformation (distortion) induced along the tank wall height
- Evaluation the height of the water free surface in the two ends of tank wall (in case of the investigation of the effect of changes in reservoir geometry and the effect of water filling in the reservoir)

It is concluded that a filling depth of approximately 45%-70% of the tank height produces the highest sloshing pressure and free surface elevation. The larger excitation amplitude produces higher free surface elevation and hydrodynamic pressure. The conclusions from the research findings are consistent with other published results (Wu et al., 1998; Cho and Lee 2004; Ibrahim, 2005).

5. Summary, conclusions, and recommendations for future works

5.1. Summary

The main focus of the current study was to evaluate the effect of sloshing phenomena on the performance of a rectangular ground supported water reservoir tanks under long period-long duration seismic excitations using a rigorous and efficient numerical techniques.

As a result of major advances in computer science and the development of rigorous numerical codes, academic and industrial interest in the use of finite element techniques as a tool to investigate the fluid-structure interaction problems has greatly increased in recent years. Using these techniques, more precise and realistic results are generally obtainable. In this research study, the fluid-structure coupling formulations were solved using finite element techniques. Various kinds of analysis were carried out using the Coupled Eulerian-Lagrangian (CEL) finite element analysis and Smoothed Particle Hydrodynamics (SPH) analysis methods. Throughout this study, the effects of important factors on dynamic behavior of such structures were addressed. The examined parameters were sloshing of liquid free surface, tank wall flexibility, tank wall thickness, ground acceleration, tank geometry aspect ratio, and water filling depth ratio.

The accuracy of the proposed numerical model was verified by comparing the obtained results with other analytical and experimental results available in the literature. According to the methodology commonly used in current design standards, the dynamic response of partially filled liquid tanks is calculated using simplified mechanical models.

The seismic behavior of water tanks was further studied by carrying out a comprehensive parametric study on liquid-filled tanks using the finite element technique. Through this parametric study, a broad range of tank capacities and geometries typically found in use today was covered. This parametric study led to the generation of different distribution graphs for tanks having different geometrical properties. It was also indicated that the proposed graphs could be employed simply in design applications for liquid filled tanks.

For this purpose, the effect of changes in each of the above mentioned characteristics, five outputs of the analysis, is evaluated and compared. These five outputs of the results are as follows:

- Evaluation of the maximum and minimum stresses in the tank wall during the loading time

- Evaluation of the maximum hydrodynamic pressure in the tank during the loading time
- Evaluation of the maximum displacements in the tank wall during the loading time
- Evaluation most critical deformation (distortion) induced along the tank wall height
- Evaluation the height of the water free surface in the two ends of tank wall (in case of the investigation of the effect of changes in reservoir geometry and the effect of water filling in the reservoir)

5.2.Conclusions

Based on the results of this research study, the following conclusions are made regarding the dynamic behavior of ground-supported containers:

1. The proposed FE procedure can be accurately employed in dynamic analysis of liquid containers. Using this method, all aspects in fluid-structure interaction problems can be considered, including wall flexibility, sloshing motion and damping properties of fluid domain, in a three dimensional space.

2. Including the wall flexibility result in a significant increase in the dynamic response of reservoir. Furthermore, the sloshing height of the liquid inside the tanks is not significantly affected by the wall flexibility.

3. Standards and design codes are not capable of appropriately accounting for the effects of wall flexibility and base fixity. That is, it gives the same hydrodynamic pressure values for rigid and flexible tanks as well as for fixed tanks. As a result, design codes estimations could be too conservative in the case of rigid tanks.

4. The values of stresses in the tank wall which is built with a tolerant material generally higher than the values of stresses in the tank wall that is made of low-resistance material.

5- Generally observed that during the period of applying seismic load, tanks with less resistance wall material have more displacement in their wall, so considering the input seismic acceleration and dynamic motions induced in a tank wall which is mainly because of sloshing phenomena.

6- It is clear that by using lower strength material in the tank wall, the amount of bulging and concavity in a tank wall is increasing considerably comparing to high strength material.

7- The values of stresses in the wall of the tank with different thickness, does not greatly differ from each other, this is because of numerical values of thickness are close together.

8- Therefore, for design considerations should be considered that just by increasing wall thickness, we cannot control enough the stress distribution on reservoir structures, and for the optimal design, in addition to increasing of thickness, the other appropriate methods should be used to reduce the risk of damage.

9- Tanks with thicker wall have more displacement in their wall, so considering the input seismic acceleration and dynamic motions mainly because of sloshing phenomena; this is partly because of the increasing structural weight and proportionally increasing the dynamic forces caused by system excitation.

10- It can be seen that the tanks with thin wall thickness have less distortion than reservoirs with thicker wall thickness in the same condition.

11- As the $Width/Length$ ratio decreases, the maximum stress values are increased in the tank wall. This could be evaluated that due to the increased hydrostatic forces acting on the inner wall, so that the stress on the tank wall increases as the plastic zones appear on the wall.

12-In general can be seen that by decreasing the ratio of height to length of the tank, the amount of displacement of the structure (wall) in the x direction, increases. This procedure is based on the input earthquake acceleration in the direction (Y) for the displacement in the negative direction (-Y) is true, but by the movement in the direction (+ Y) for a ratio of 0.4, in comparison with others has the maximum positive displacement; However, it can be due to the nature of input acceleration which is applied in the direction (Y). However, generally, by decreasing the ratio of the height to length, the displacement increases in the tank wall. Because the weight of the tank and fluid increases and therefore the more dynamic forces during an earthquake is applied and cause further displacement in the tank.

13- In tanks by a lower ratio of height to length, the maximum distortion can be seen in the tank wall, which is because of increasing hydrostatic forces and proportionally increasing hydrodynamic forces due to seismic excitation conditions.

14- The values of hydrodynamic pressure in the tank with height to length ratio is equal to 0.8, generally less than the values of pressure in the tanks that height to length ratio are equal to 0.6 and 0.4.

15- It is clear that the water free surface elevation is a function of acceleration time-history, and in a tank with a geometrical ratio of 0.8 is greater than tanks with geometry

ratios of 0.4 and 0.6 considerably.

16- Between the values of stresses in the wall of the tank with different water depths there is a significant difference, because obviously in the most time steps of loading, there will be elements of the wall that the maximum stress occurs in the wall and their stress values are close to the yield strength of tank materials. The initial difference between the stresses mostly because of hydrostatic pressure, but while PGA increases, because of sloshing and slamming phenomena, the stress increase suddenly in tanks; especially in tanks with a filling depth ratio of 50% and 63%.

17- In general, by comparison of mentioned graphs can be seen that the tanks with different filling depth, have different responses (wall displacement) relative to their static initial conditions, by comparing the tank wall displacement in either direction (+ Y and + X), half-filled tank has a maximum displacement. However, generally, the maximum displacements in each specified direction are affected by conditions and applied input acceleration.

18- It is clear that tanks with a filling depth ratio of 83% have more distortion relative to other tanks. This issue corresponds to the maximum displacement of the wall is compatible, because in positive and negative directions of motion and maximum values (absolute value) of seismic displacements in the direction in half full tanks were more than others. More distortions in wall of half-filled tank relative to full filled tank can be to attributed with lower elevation of the fluid in the half filled tank which provides more freedom of movement for the wall elements (especially at high accelerations). Because the wall of a fully filled tank has more support surface, especially when moves opposite the direction of motion of fluid motion (sloshing wave), which causes less deformation relative to semi half-filled tanks.

19- About the water height levels associated with wall distortions, it can be seen that in tanks at approximately near to the free surface level of the tank height need special attention for seismic retrofitting.

The results match quite well with results found in the literature. Moreover, a large amount of oscillation is present in the pressure results, and sometimes the pressure reaches a very high value in a single element, which is probably caused by a numerical instability. Large negative values of the pressure occur, because a shockwave is propagated through the fluid, which is not seen in literature.

Although in this research because of some limitations the small scale size tanks have been chosen to do the analysis, but also based on similarity theory between physical model and

real-world prototype, the results can be extend to large scale models including mechanical, Froude and Reynolds similarities. Inspectional analysis, dimensional analysis, calibration and scale series are available to obtain model-prototype similarity, to quantify scale effects, to investigate how they affect the parameters and to establish limiting criteria where they can be neglected.

The study provides new alternatives and practical approach for solving these highly nonlinear sloshing problems. Considering long period-long duration motions, it seems that the SPH method is more practical because CEL method is expensive and the more time is going on the analysis, the accuracy of this method is reduced. Although the analyses just have done in rectangular tanks, but it is easy to extend to another shape of liquid tanks. The numerical methods used in this study, have obvious advantages over other methods in handling violent fluid-structure interaction and wave breaking on the free fluid surface. The severity of sloshing and its dynamic pressure loads depends on the tank geometry, the depth of the liquid, the amplitude and the nature of the tank motions. They also depend on the frequency of excitation over a range of frequencies closed to the natural frequency of the fluid. In terms of analytical procedures for modeling of sloshing, although, earlier studies had focused on sloshing waves based on the regular excitation. Since the generation of liquid sloshing is explained by resonance between liquids in the tank and ground motions, it is critical, in predicting damages of tanks, to evaluate ground motions in the long period range, including the natural period of liquid sloshing of a storage tank and water reservoirs.

Nevertheless, because of using large dimension tanks in the industry, it requires an enormous amount of computational analysis to do Eulerian-Lagrangian and smoothed particle hydrodynamic analysis. Further improvements should be made based on real long period-long duration ground motions and doing experimental analysis using 6 degrees of freedom shaking table in the future.

5.3. Recommendations for future studies

Based on this research study, some suggestions for further research on dynamic behavior of cylindrical ground-supported and conical elevated water tanks can be made as follows:

1. More case studies with varying tank capacity, liquid depth, tank aspect ratio, and ground excitation properties can be carried out through a careful selection of a wide range of liquid storage tanks in order to verify the effects of these parameters on the dynamic response of such structures.

2. The dynamic response of liquid-filled tanks under vertical ground accelerations can be investigated using the proposed numerical procedure.

3. The effect of the deformable foundation of dynamic behavior of liquid containing structures can be investigated by simulating the soil-structure interaction (SSI) effect in a rigorous numerical model. Moreover, the effect of different support conditions such as unanchored connections can be further studied.

4. It is suggested that the nonlinear behavior of steel and reinforced concrete materials be included in numerical modeling of the tanks.

5. In addition, due to the facility constraint of the shake-table in the water sloshing experiments, only unidirectional regular excitation signal was used. Multi-degree of freedom movements of the tank can be applied in future study. Furthermore, more complicated or irregular external excitation signals may be investigated. Different tank shape other than rectangular tank should be studied in the future to better model the real tank geometry.

APPENDIX A: LAMINA FLUID THEORY

A.1. Housner's method

The lamina fluid theory was used as the basis by Housner (1957; 1963) to calculate the hydrodynamic pressure components in rectangular and cylindrical liquid containers. He separated the hydrodynamic pressures into impulsive and convective parts and proposed practical formulations for predicting the dynamic behavior of each part separately. In the proposed analysis, the fluid was assumed to be incompressible and the fluid displacements were considered to be small. The tank was assumed to be rigid and subjected to horizontal acceleration.

A.1.1. Impulsive pressure

Figure A.1 (a) shows a liquid tank having vertical walls and horizontal floor. The tank is symmetrical with respect to the x-y and z-y planes. As the tank undergoes an acceleration $\ddot{u}_0$ in the horizontal x direction, acceleration components $\ddot{u}$, $\ddot{v}$, and $\ddot{w}$ will be generated in the fluid domain in x, y, and z directions, respectively. It is assumed that $\ddot{w}$ is either zero or very small that it can be neglected. As a result of this assumption, the fluid domain can be assumed as a series of lamina of *dz* thickness which are separated by thin vertical membranes. This will force the fluid to vibrate in the x-y plane only. Therefore, for simplification, it can be considered that the hydrodynamic pressures are generated in a lamina of fluid.

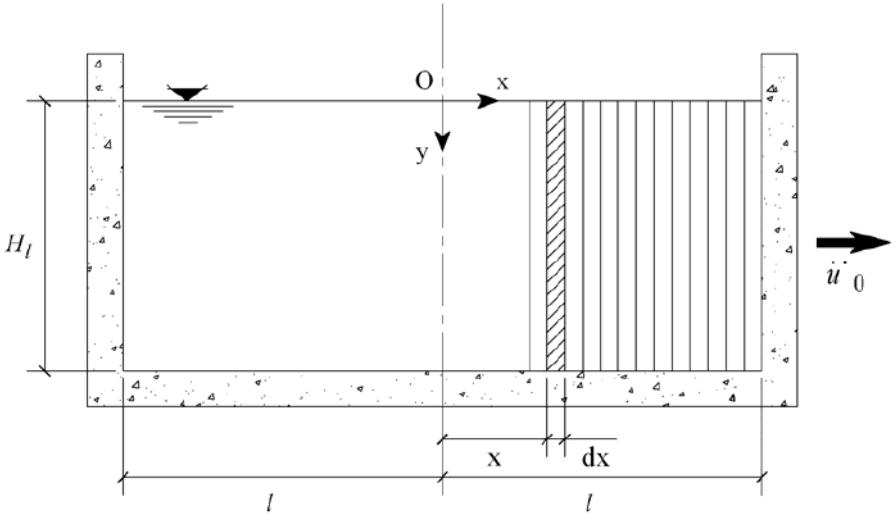

(a)

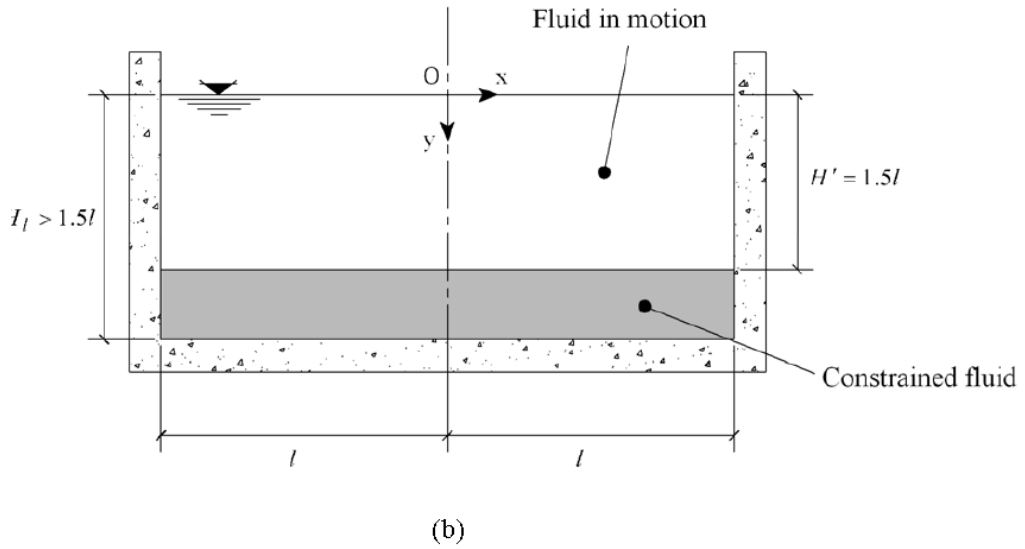

Fig.A.1 Generalized symmetrical tank model; (a) x-y view,
(b) Slender tank special case with $H_l > 1.5l$

A lamina of fluid of unit thickness in the x-y plane is shown in Figure A.1 (a). As a result of the horizontal vibration of the tank, a horizontal and a vertical component of acceleration will be imported to the contained fluid. As a reasonable assumption, the horizontal component of fluid velocity $\dot{u}$ can be considered independent of the y coordinate. Physically, this is equivalent to assuming that the fluid is constrained by thin, massless, vertical membranes, which can move freely along x direction. As shown in the figure, the original distance between the membranes is assumed to be *dx*. As the tank experiences base excitation, the membranes together with the fluid will be accelerated. The fluid will also be squeezed in vertical direction with respect to the membranes. Using the mass balance criterion on the lamina shown in Figure A.2, one can obtain the relation between the horizontal and vertical velocity components, $\dot{u}$ and $\dot{v}$, as follows:

$$\dot{v}dx + \dot{u}(H_l - y) = \left(\dot{u} + \frac{\partial \dot{u}}{\partial x}dx\right)(H_l - y) \qquad \text{or} \qquad \text{(A-1)}$$

$$\dot{v} = (H_l - y)\frac{\partial \dot{u}}{\partial x}$$

Differentiating with respect to time results in:

$$\ddot{v} = (H_l - y)\frac{\partial \ddot{u}}{\partial x} \qquad \text{(A-2)}$$

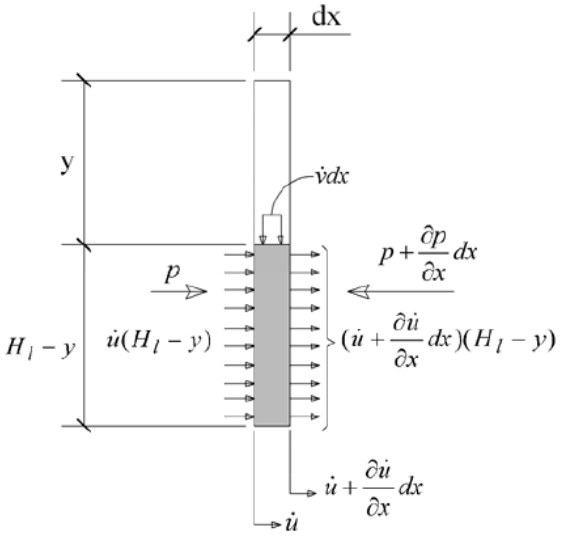

Fig.A.2 Fluid element under consideration

Applying Newton's law to a differential fluid element shown in Figure A.3, one can obtain the equation of motion in the vertical direction:

$$-\frac{\partial \mathrm{p}}{\partial \mathrm{y}}\mathrm{dxdy} = \mathrm{p_l dxdy}\frac{\mathrm{d\dot{v}}}{\mathrm{dt}} \tag{A-3}$$

$$\frac{\partial p}{\partial y} = -p_l \frac{d\dot{v}}{dt} = -p_l\left(\frac{\partial \dot{v}}{\partial t} + \frac{\partial \dot{v}}{\partial x}\frac{dx}{dt} + \frac{\partial \dot{v}}{\partial y}\frac{dy}{dt}\right)$$

where, p is the hydrodynamic impulsive pressure, and p_l is liquid density; $\frac{dx}{dt}$ and $\frac{dy}{dt}$ represent $\dot{u}$ and $\dot{v}$, respectively. As mentioned before the fluid displacements were assumed to be small. As a result, the derivatives of the velocities with respect to x and y are also considered to be small and may be omitted from Eq. A-3 resulting in:

$$\frac{\partial \mathrm{p}}{\partial \mathrm{y}} = -\mathrm{p_l}\frac{\partial \mathrm{\dot{v}}}{\partial \mathrm{t}} \tag{A-4}$$

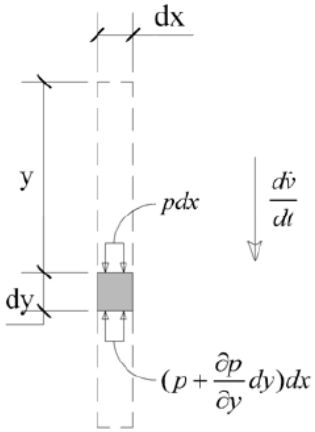

Fig.A.3 Differential fluid element

The total horizontal impulsive force acting on one membrane is obtained by the following integration:

$$P = \int_0^{H_l} p\,dy \tag{A-5}$$

Substituting Eq. A-2 into Eq. A-4, integrating from zero to y, and taking into consideration that $p \overset{y=0}{\rightarrow} 0$ and $\ddot{u} \neq \ddot{u}(y)$, the impulsive pressure is determined as follows:

$$p = -p_l \frac{\partial \ddot{u}}{\partial x} \int_0^y (H_l - \bar{y})d\bar{y} = -p_l H_l^2 \left[\frac{y}{H_l} - \frac{1}{2}\left(\frac{y}{H_l}\right)^2\right] \frac{\partial \ddot{u}}{\partial x} \tag{A-6}$$

Impulsive force can be obtained by substituting Eq. A-6 into Eq. A-5,

$$P = -p_l H_l^2 \frac{\partial \ddot{u}}{\partial x} \int_0^{H_l} \left[\frac{y}{H_l} - \frac{1}{2}\left(\frac{y}{H_l}\right)^2\right] dy = -\frac{1}{3} p_l H_l^3 \frac{\partial \ddot{u}}{\partial x} \tag{A-7}$$

By applying the Newton's rule to the fluid element shown in Figure A.2, one can obtain the equation of motion in the x direction. It is important to note that all higher order terms arising from the time derivative of u · are ignored in obtaining this equation,

$$\frac{\partial P}{\partial x} = -\rho_l H_l \ddot{u} \tag{A-8}$$

Substituting the impulsive force (P) from Eq. A-7 into Eq. A-8,

$$\frac{\partial^2 \ddot{u}}{\partial x^2} - \frac{3}{H_l^2} \ddot{u} = 0 \tag{A-9}$$

It should be noted that $\ddot{u}$ Is considered as a dependent variable which is only a function of x. As a result, Eq. A-9 may be considered as a total differential equation with its solution given as:

$$\ddot{u} = C_1 cosh\sqrt{3}\frac{x}{H_l} + C_2 sinh\sqrt{3}\frac{x}{H_l} \tag{A-10}$$

Eq. A-6 together with Eq. A-10 will be used to determine the impulsive fluid pressure. However, care should be taken that these equations are only applicable when the surface is horizontal. Nevertheless, considering the small displacements of fluid, the equations can still be used even when the fluid surface has been excited into oscillations.

For slender tanks, better results for impulsive pressure distribution may be obtained by applying the equations A-6 and A-7 to the upper part of the fluid domain and considering the lower portion of the fluid as a constrained fluid (see Figure A.1(b)). As a result, it can

be assumed that the upper and lower portions of the fluid domain are separated from each other by means of a fixed rigid membrane located at $= H'$. The equation of motion for the constrained portion of fluid in the horizontal direction is obtained by applying the Newton's law to a differential element as before. Assuming a tank wall acceleration of $\ddot{u}_0$, we have:

$$\frac{\partial p}{\partial x} = -\rho_l \ddot{u}_0 \tag{A-11}$$

Integrating Eq. A-11 and considering that because of symmetry $\xrightarrow{x=0} 0$, we have:

$$\mathrm{p} = -\rho_l \ddot{u}_0 x \tag{A-12}$$

A.1.2. Convective pressure

When the tank walls undergo seismic accelerations, the fluid surface is excited into motion and as a result of this motion, hydrodynamic convective pressures will be produced on the wall and floor of the tank. In order to determine the convective pressures associated with the first mode of fluid vibration, it is assumed that the fluid domain is restrained by horizontal, rigid membranes which are free to rotate as depicted in Figure A.4. Again, u̇ , v̇ , and ẇ denote fluid velocity components in x, y, and z directions. The following two assumptions are made in deriving the equations:

(1) All fluid particles in the element shown in Figures A.4 and A.5 travel with uniform $\dot{u}$.

(2) All fluid particles in the same element travel with uniform $\dot{v}$.

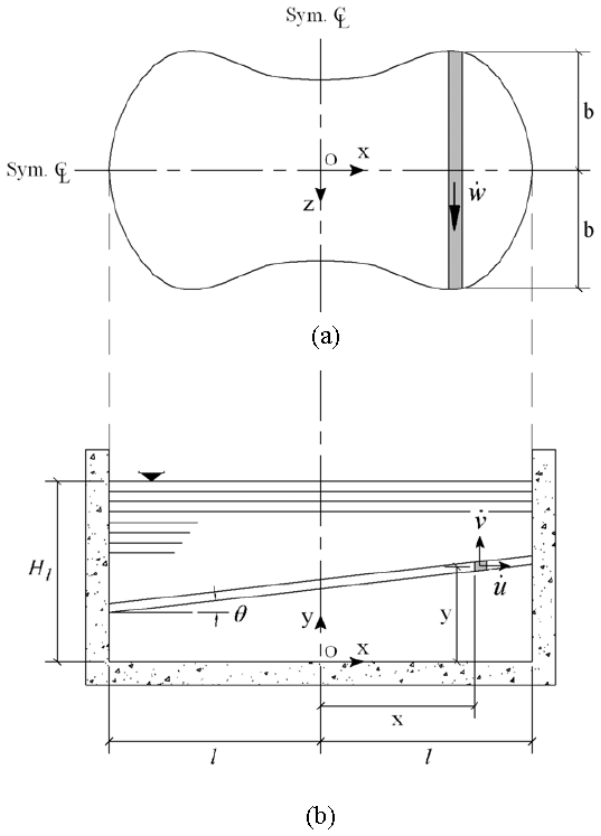

Fig.A.4 Generalized symmetrical tank model; (a)tank plan, (b) tank section

Applying the mass balance criterion on the fluid element shown in Figure A.5 results in the following equation:

$$-2\frac{\partial}{\partial \mathrm{x}}(\dot{\mathrm{u}}\mathrm{b})\mathrm{dxdy} - 2\mathrm{b}\frac{\partial \dot{\mathrm{v}}}{\partial \mathrm{y}}\mathrm{dxdy} = 0 \quad or \tag{A-13}$$

$$\frac{\partial}{\partial x}(\dot{u}b) = -b\frac{\partial \dot{v}}{\partial y}$$

Assumption (2) described above will lead to the following equation:

$$\dot{\mathrm{v}} = \mathrm{x}\dot{\theta} \tag{A-14}$$

where, θ is the derivative of angle of oscillation (θ).

Eq. A-14 is valid only if θ is small enough. The equation of continuity can be obtained by applying the mass balance criterion to a differential element having dimensions *dx, dy,* and *dz,* hence:

$$-\frac{\partial \dot{\mathrm{u}}}{\partial \mathrm{x}}\mathrm{dxdydz} - \frac{\partial \dot{\mathrm{v}}}{\partial \mathrm{y}}\mathrm{dxdydz} - \frac{\partial \dot{\mathrm{w}}}{\partial \mathrm{z}}\mathrm{dxdydz} = 0 \quad \text{or} \tag{A-15}$$

$$\frac{\partial \dot{w}}{\partial z} = -(\frac{\partial \dot{u}}{\partial x} + \frac{\partial \dot{v}}{\partial y})$$

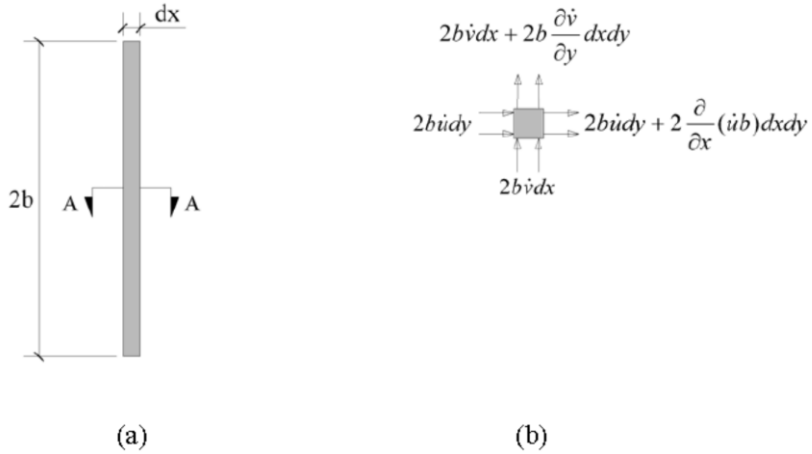

Fig.A.5 Fluid element free body diagram; (a) Plan, (b) Section A-A

It is important to note that θ is a function of y and t but not of x. As a result, at a particular time, the membrane rotation is only a function of its vertical location. The following boundary conditions exist in the considered model:

$$\dot{u} = 0 \; at \; x = \pm l \tag{A-16}$$

$$\dot{w} = 0 \; at \; x = 0 \tag{A-17}$$

$$\theta = 0 \; at \; y = 0 \tag{A-18}$$

$$\theta = \theta_H \; at \; y = H_l \tag{A-19}$$

Similar to the procedure explained in the previous section, the appropriate equations of motion can be determined for the tank under consideration. Substituting the obtained variables in appropriate equations and taking the required integrations, the following equations for velocity components $\dot{u}$ and $\dot{w}$ are resulted:

$$\dot{u} = -\frac{1}{b}\frac{\partial \dot{\theta}}{\partial y}\int_{-l}^{x} b(\bar{x})\bar{x}d\bar{x} \tag{A-20}$$

$$\dot{u} = -z\frac{b\prime}{b^2}\frac{\partial \dot{\theta}}{\partial y}\int_{-l}^{x} b(\bar{x})\bar{x}d\bar{x} \tag{A-21}$$

where, $b' = db/dx$.

In the next step, the total kinetic energy and potential energy are determined and used in

Hamilton's principle. The total kinetic energy is defined as the integral over the volume of the kinetic energy of the fluid elements. The potential energy is calculated by summing the energy contributions from each fluid element located in the disturbed surface due to its average displacement from the equilibrium condition. Applying the Hamilton's principle and taking the required integrations and derivatives, the following equations are derived:

$$\theta_H = \theta_{Hm} \frac{sinh\sqrt{\frac{I}{K}}y}{sinh\sqrt{\frac{I}{K}}H_l} \tag{A-22}$$

in which, θ_{Hm} is the maximum angular amplitude of fluid motion at the free surface and is defined in the flowing equation:

$$\theta_H = \theta_{Hm}\, sin\, \omega t \tag{A-23}$$

Variables I and K are defined as follows:

$$I = \int_{-l}^{l}\int_{-b}^{b} x^2 dxdz \tag{A-24}$$

$$K = 2\int_{-l}^{l}\frac{1}{b}\left[\int_{-l}^{x} b(\bar{x})\bar{x}d\bar{x}\right]^2\left(1+\frac{b\prime^2}{3}\right)dx \tag{A-25}$$

ω is the natural frequency of the fundamental mode of free surface vibration and is defined as follows:

$$\omega^2 = g\sqrt{\frac{I}{K}}tanh\sqrt{\frac{I}{K}}H_l \tag{A-26}$$

Neglecting the higher order terms, the equations of motion can be written as:

$$\frac{\partial p}{\partial x} = -\rho_l \ddot{u} \quad and \tag{A-27}$$

$$\frac{\partial p}{\partial z} = -\rho_l \ddot{w} \tag{A-28}$$

where, p represents the hydrodynamic convective pressure. It is worth noting that in deriving the fluid pressure formulations, only the fluid motion along the x direction is considered, even though the membranes also experience accelerations along the vertical direction. Using Eqs. A-20 and A-21 in Eqs. A-27 and A-28, the pressure differential can be written as:

$$dp = -\rho_l \ddot{u}dx = \rho_l \frac{\partial\ddot{\theta}}{\partial y}\frac{B}{b}dx \tag{A-29}$$

where,

$$B = \int_{-l}^{x} b(\bar{x})\bar{x}d\bar{x} \qquad \textit{(A-30)}$$

Integrating Eq. A-29, with the condition that $(0, \mathrm{y}, 0) = 0$, because of symmetry, we have:

$$p = \rho_l \frac{\partial \ddot{\theta}}{\partial y}\left[\int_0^x \frac{B(\bar{x})}{b\bar{x}} d\bar{x}\right] \qquad \textit{(A-31)}$$

In the above equation, p is the dynamic convective pressure. Having obtained pressure, one can determine the resulting forces and moments on the wall and the floor of the tank simply. The obtained equations can then be applied to any container of specified shape having two-fold symmetry such as rectangular and cylindrical tanks.

APPENDIX B: TEXT COMMAND FILES OF THE TANK'S PARAMETRIC MODEL

B.1. Input file for the tank's parametric model using CEL method

```
*HEADING
Unit Kg,m,sec
*parameter
#
#geometric parameters (can be modified)
#
L = 0.6
W = 0.3
T = 0.005
HT = 0.36
HT2=0.40
L2=0.64
W2=0.34
HW =0.3
MX=32
MZW=18
MYW=17
MXT=5
MYT=3
MZT=4
MZFULL=13
PERCENTEND=0.5
##
##dependent parameters (do not modify)
##
N2=1+MX
N3=(MX+1)*MYW+1
N4=N3+MX
N5=N4*MZW+1
N6=N5+MX
N7=N5+(MX+1)*MYW
N8=N7+MX
MXP1=MX+1
N4P1=N4+1
N4P2=N4+2
N4PN2P2=N4+N2+2
N4PN2P1=N4+N2+1
N2P2=N2+2
N2P1=N2+1
N2M1=N2-1
E4=MX*MYW
NT1=N8+1
NT2=NT1+MXT
NT3=NT1+(MXT+1)*MYT
NT4=NT3+MXT
NT5=(MYT+1)*(MXT+1)*MZT+NT1
NT6=NT5+MXT
NT7=NT5+(MXT+1)*MYT
NT8=NT7+MXT
```

```
MXTP1=MXT+1
NDOR=(MXT+1)*(MYT+1)
ES1=MX*MZW*MYW+1
NT1P1=NT1+1
NT1P2=NT1+2
NT2P1=NT2+1
NT2P2=NT2+2
NT2PNDOR=NT2+NDOR
NT2NDORMXT1=NT2PNDOR+MXT+1
NT2PMXTP1=NT2+MXT+1
ES2=ES1+MXT*MYT
ES3=ES2+MYT*MZT
NT5P1=NT5+1
NT6P2=NT6+2
NT6P1=NT6+1
ES4=ES3+MXT*MYT
NT4PMXTP2=NT4+MXT+2
NT4P1=NT4+1
ES5=ES4+MYT*MZT
NT4P2=NT4+2
NT4P1=NT4+1
ES6=ES5+MXT*MZT
NT3P1=NT3+1
NT3PNDORP1=NT3+NDOR+1
NT3PNDOR=NT3+NDOR
E5=MX*MYW*(MZW-1)
E7=MX*MYW*MZW
THICKNESS=T
WATERCO=HW
WATERPRESS=HW*(-9810)
EFULL=MX*MYW*MZFULL
EFULLP1=EFULL+1
EFULLE=EFULL+MX*MYW
PER_WATER=PERCENTEND
#
#end of parameter list
#
*****************************************************************
*********WATER NODE DEFINITION
*NODE
1,0,<W>,0
<N2>,<L>,<W>,0
<N3>,0,0,0
<N4>,<L>,0,0
<N5>,0,<W>,<HT>
<N6>,<L>,<W>,<HT>
<N7>,0,0,<HT>
<N8>,<L>,0,<HT>
*NGEN,NSET=A1
1,<N3>,<MXP1>
*NGEN,NSET=A2
<N5>,<N7>,<MXP1>
*NGEN,NSET=B1
<N2>,<N4>,<MXP1>
*NGEN,NSET=B2
<N6>,<N8>,<MXP1>
```

```
*NFILL,NSET=A
A1,A2,<MZW>,<N4>
*NFILL,NSET=B
B1,B2,<MZW>,<N4>
*NFILL,NSET=WATER_NODE,BIAS=1
A,B,<MX>,1
**************************************************************
*********WATER ELEMENT DEFINITION
*ELEMENT,TYPE=EC3D8R
1,1,2,<N4P2>,<N4P1>,<N2P1>,<N2P2>,<N4PN2P2>,<N4PN2P1>
*ELGEN,ELSET=WATER_ELEMENT
1,<MX>,1,1,<MYW>,<N2>,<N2M1>,<MZW>,<N4>,<E4>
**************************************************************
*********SHELL NODE DEFINITION
*NODE
<NT1>,0,<W>,0
<NT2>,<L>,<W>,0
<NT3>,0,0,0
<NT4>,<L>,0,0
<NT5>,0,<W>,<HT>
<NT6>,<L>,<W>,<HT>
<NT7>,0,0,<HT>
<NT8>,<L>,0,<HT>
*NGEN,NSET=AT1
<NT1>,<NT3>,<MXTP1>
*NGEN,NSET=AT2
<NT5>,<NT7>,<MXTP1>
*NGEN,NSET=BT1
<NT2>,<NT4>,<MXTP1>
*NGEN,NSET=BT2
<NT6>,<NT8>,<MXTP1>
*NFILL,NSET=AT
AT1,AT2,<MZT>,<NDOR>
*NFILL,NSET=BT
BT1,BT2,<MZT>,<NDOR>
*NFILL,NSET=SHELL_NODE,BIAS=1
AT,BT,<MXT>,1
**************************************************************
*********SHELL ELEMENT DEFINITION
*ELEMENT,TYPE=S4R
<ES1>,<NT1>,<NT1P1>,<NT2P2>,<NT2P1>
*ELGEN,ELSET=SHELL_ELEMENT_1
<ES1>,<MXT>,1,1,<MYT>,<MXTP1>,<MXT>
*ELEMENT,TYPE=S4R
<ES2>,<NT2>,<NT2PNDOR>,<NT2NDORMXT1>,<NT2PMXTP1>
*ELGEN,ELSET=SHELL_ELEMENT_2
<ES2>,<MZT>,<NDOR>,1,<MYT>,<MXTP1>,<MZT>
*ELEMENT,TYPE=S4R
<ES3>,<NT6P1>,<NT6P2>,<NT5P1>,<NT5>
*ELGEN,ELSET=SHELL_ELEMENT_3
<ES3>,<MXT>,1,1,<MYT>,<MXTP1>,<MXT>
*ELEMENT,TYPE=S4R
<ES4>,<NT1>,<NT2P1>,<NT4PMXTP2>,<NT4P1>
*ELGEN,ELSET=SHELL_ELEMENT_4
<ES4>,<MZT>,<NDOR>,1,<MYT>,<MXTP1>,<MZT>
*ELEMENT,TYPE=S4R
```

```
<ES5>,<NT4P1>,<NT4P2>,<NT1P1>,<NT1>
*ELGEN,ELSET=SHELL_ELEMENT_5
<ES5>,<MXT>,1,1,<MZT>,<NDOR>,<MXT>
*ELEMENT,TYPE=S4R
<ES6>,<NT3>,<NT3P1>,<NT3PNDORP1>,<NT3PNDOR>
*ELGEN,ELSET=SHELL_ELEMENT_6
<ES6>,<MXT>,1,1,<MZT>,<NDOR>,<MXT>
*ELSET,ELSET=SHELL_ELEMENT
SHELL_ELEMENT_1,SHELL_ELEMENT_2,SHELL_ELEMENT_3,SHELL_ELEMENT_4,S
HELL_ELEMENT_5,SHELL_ELEMENT_6
**************************************************************
*********MATERIAL DEFINITION
*SHELL SECTION, ELSET=SHELL_ELEMENT, MATERIAL=STEEL,offset=SNEG
<THICKNESS>
*MATERIAL,NAME=STEEL
*DENSITY
 7846,
*ELASTIC
21000000000, 0.3
*ELSET,ELSET=WATER_FULL,GENERATE
1,<EFULL>,1
*ELSET,ELSET=WATER_FULL-E,GENERATE
<EFULLP1>,<EFULLE>,1
*ELSET,ELSET=WATER_LEVEL
WATER_FULL,WATER_FULL-E
*Eulerian Section, ELSET=WATER_ELEMENT
WATER, WATER-1
*Surface, type=EULERIAN MATERIAL, name=WATERSURF
WATER-1
*SURFACE,TYPE=ELEMENT, NAME=SHELLSURF
SHELL_ELEMENT,SNEG
***K=300,K/G=1.E+6, (Actual K of water = 300000)
*MATERIAL, NAME=WATER
*VISCOSITY
1.0E-3,
*DENSITY
983.2,
*EOS, TYPE=USUP
45.85,0.,0.
**************************************************************
*********BOUNDARY DEFINITION
*NSET,NSET=EDGES,GENERATE
<NT1>,<NT4>,1
*BOUNDARY
EDGES,3,6,0.0
*INITIAL CONDITIONS, TYPE=STRESS, GEOSTATIC
WATER_LEVEL,0.,<WATERCO>,<WATERPRESS>,0,1.,1.,
*NSET,NSET=VZERO3,GEN
1,<N4>,1
<N5>,<N8>,1
*BOUNDARY, TYPE=VELOCITY
VZERO3, 3, 3
*surfaceinteraction, name=rough
*friction,rough
*Initial Conditions, type=VOLUME FRACTION
WATER_FULL, WATER-1, 1
```

```
WATER_FULL-E, WATER-1, <PER_WATER>
**********************************************************************
*********LOADING DEFINITION
*INCLUDE, INPUT=AMP-TO-100.inp
**********************************************************************
*********TIME OUT DEFINITION
*Filter, name=smooth, type=butterworth
2000,4
*Mass adjust, Target DT=7.528e-07
SHELL_ELEMENT, current
**********************************************************************
*********STEP DEFINITION
*STEP
*DYNAMIC, EXPLICIT
,55
*Bulk Viscosity
0.06, 1.2
*Fixed Mass Scaling, elset=SHELL_ELEMENT, dt=7.528e-07,
type=below min
**
*contact, op=NEW
*contactinclusions,ALL EXTERIOR
*CONTACT PROPERTY ASSIGNMENT
,,rough
*EULERIAN MESH
MOTION,ELSET=WATER_ELEMENT,SURFACE=SHELLSURF,OP=NEW,ASPECT RATIO
MAX=1,BUFFER=INITIAL
2,2,1,0,0,1
,,,,,
,,
*DLOAD
WATER_ELEMENT, GRAV, 9.81, 0., 0.,-1.
*BOUNDARY,TYPE=ACCELERATION,AMPLITUDE=AMP-X
EDGES,1,1,1.
*BOUNDARY,TYPE=ACCELERATION,AMPLITUDE=AMP-Y
EDGES,2,2,1.
**********************************************************************
*********OUTPUT DEFINITION
*NSET, NSET=ALL_N
SHELL_NODE,WATER_NODE
*ELSET, ELSET=ALL_E
SHELL_ELEMENT,WATER_ELEMENT
*OUTPUT, FIELD, TIME MARKS=YES, NUMBER INTERVAL=550
*ELEMENT OUTPUT, ELSET=SHELL_ELEMENT
P,S,MISESMAX,SP,PRESS
*NODE OUTPUT, NSET=SHELL_NODE
UT
*OUTPUT, FIELD, TIME MARKS=YES, NUMBER INTERVAL=550
*ELEMENT OUTPUT, ELSET=WATER_ELEMENT
PRESS
*NODE OUTPUT, NSET=WATER_NODE
UT
*Element Output, elset=WATER_ELEMENT, directions=YES
EVF, SVAVG
*OUTPUT, HIST, FREQ=9999,filter=smooth
*ELEMENT OUTPUT, ELSET=SHELL_ELEMENT
```

```
SSAVG1,SSAVG2,SSAVG3,SSAVG4,SSAVG5,SSAVG6,S,SP,PRESS
*OUTPUT, HIST, FREQ=9999,filter=smooth
*ELEMENT OUTPUT, ELSET=WATER_ELEMENT
PRESS
*NODE OUTPUT, NSET=WATER_NODE
U3
*END STEP
```

B.2. Input file for the tank's parametric model using SPH method

```
*HEADING
ADAPTIVE MESHING EXAMPLE
WATER SLOSHING IN A BAFFLED TANK
Unit Kg,m,sec
*parameter
#
#geometric parameters (can be modified)
#
L = 0.6
W = 0.3
T = 0.05
HT = 0.36
HW =0.3
MX=15
MY=8
MZ=6
MXT=15
MYT=8
MZT=8
##
##dependent parameters (do not modify)
##
N2=1+MX
N3=(MX+1)*MZ+1
N4=N3+MX
N5=N4*MY+1
N6=N5+MX
N7=N5+(MX+1)*MZ
N8=N7+MX
MXP1=MX+1
N4P1=N4+1
N4P2=N4+2
N4PN2P2=N4+N2+2
N4PN2P1=N4+N2+1
N2P2=N2+2
N2P1=N2+1
N2M1=N2-1
E4=MX*MZ
NT1=N8+1
NT2=NT1+MXT
NT3=NT1+(MXT+1)*MYT
NT4=NT3+MXT
NT5=(MYT+1)*(MXT+1)*MZT+NT1
NT6=NT5+MXT
```

```
NT7=NT5+(MXT+1)*MYT
NT8=NT7+MXT
MXTP1=MXT+1
NDOR=(MXT+1)*(MYT+1)
ES1=MX*MZ*MY+1
NT1P1=NT1+1
NT1P2=NT1+2
NT2P1=NT2+1
NT2P2=NT2+2
NT2PNDOR=NT2+NDOR
NT2NDORMXT1=NT2PNDOR+MXT+1
NT2PMXTP1=NT2+MXT+1
ES2=ES1+MXT*MYT
ES3=ES2+MYT*MZT
NT5P1=NT5+1
NT6P2=NT6+2
NT6P1=NT6+1
ES4=ES3+MXT*MYT
NT4PMXTP2=NT4+MXT+2
NT4P1=NT4+1
ES5=ES4+MYT*MZT
NT4P2=NT4+2
NT4P1=NT4+1
ES6=ES5+MXT*MZT
NT3P1=NT3+1
NT3PNDORP1=NT3+NDOR+1
NT3PNDOR=NT3+NDOR
THICKNESS=T
WATERCO=HW
WATERPRESS=HW*(-9810)
#
#end of parameter list
#
*****************************************************************
*********WATER NODE DEFINITION
*NODE
1,0,0,0
<N2>,<L>,0,0
<N3>,0,0,<HW>
<N4>,<L>,0,<HW>
<N5>,0,<W>,0
<N6>,<L>,<W>,0
<N7>,0,<W>,<HW>
<N8>,<L>,<W>,<HW>
*NGEN,NSET=A1
1,<N3>,<MXP1>
*NGEN,NSET=A2
<N5>,<N7>,<MXP1>
*NGEN,NSET=B1
<N2>,<N4>,<MXP1>
*NGEN,NSET=B2
<N6>,<N8>,<MXP1>
*NFILL,NSET=A
A1,A2,<MY>,<N4>
*NFILL,NSET=B
B1,B2,<MY>,<N4>
```

```
*NFILL,NSET=WATER_NODE,BIAS=1
A,B,<MX>,1
**********************************************************************
*********WATER ELEMENT DEFINITION
*ELEMENT,TYPE=C3D8R
1,1,2,<N4P2>,<N4P1>,<N2P1>,<N2P2>,<N4PN2P2>,<N4PN2P1>
*ELGEN,ELSET=WATER_ELEMENT
1,<MX>,1,1,<MZ>,<N2>,<N2M1>,<MY>,<N4>,<E4>
**********************************************************************
*********SHELL NODE DEFINITION
*NODE
<NT1>,0,<W>,0
<NT2>,<L>,<W>,0
<NT3>,0,0,0
<NT4>,<L>,0,0
<NT5>,0,<W>,<HT>
<NT6>,<L>,<W>,<HT>
<NT7>,0,0,<HT>
<NT8>,<L>,0,<HT>
*NGEN,NSET=AT1
<NT1>,<NT3>,<MXTP1>
*NGEN,NSET=AT2
<NT5>,<NT7>,<MXTP1>
*NGEN,NSET=BT1
<NT2>,<NT4>,<MXTP1>
*NGEN,NSET=BT2
<NT6>,<NT8>,<MXTP1>
*NFILL,NSET=AT
AT1,AT2,<MZT>,<NDOR>
*NFILL,NSET=BT
BT1,BT2,<MZT>,<NDOR>
*NFILL,NSET=SHELL_NODE,BIAS=1
AT,BT,<MXT>,1
**********************************************************************
*********SHELL ELEMENT DEFINITION
*ELEMENT,TYPE=S4R
<ES1>,<NT1>,<NT1P1>,<NT2P2>,<NT2P1>
*ELGEN,ELSET=SHELL_ELEMENT_1
<ES1>,<MXT>,1,1,<MYT>,<MXTP1>,<MXT>
*ELEMENT,TYPE=S4R
<ES2>,<NT2>,<NT2PNDOR>,<NT2NDORMXT1>,<NT2PMXTP1>
*ELGEN,ELSET=SHELL_ELEMENT_2
<ES2>,<MZT>,<NDOR>,1,<MYT>,<MXTP1>,<MZT>
*ELEMENT,TYPE=S4R
<ES3>,<NT6P1>,<NT6P2>,<NT5P1>,<NT5>
*ELGEN,ELSET=SHELL_ELEMENT_3
<ES3>,<MXT>,1,1,<MYT>,<MXTP1>,<MXT>
*ELEMENT,TYPE=S4R
<ES4>,<NT1>,<NT2P1>,<NT4PMXTP2>,<NT4P1>
*ELGEN,ELSET=SHELL_ELEMENT_4
<ES4>,<MZT>,<NDOR>,1,<MYT>,<MXTP1>,<MZT>
*ELEMENT,TYPE=S4R
<ES5>,<NT4P1>,<NT4P2>,<NT1P1>,<NT1>
*ELGEN,ELSET=SHELL_ELEMENT_5
<ES5>,<MXT>,1,1,<MZT>,<NDOR>,<MXT>
*ELEMENT,TYPE=S4R
```

```
<ES6>,<NT3>,<NT3P1>,<NT3PNDORP1>,<NT3PNDOR>
*ELGEN,ELSET=SHELL_ELEMENT_6
<ES6>,<MXT>,1,1,<MZT>,<NDOR>,<MXT>
*ELSET,ELSET=SHELL_ELEMENT
SHELL_ELEMENT_1,SHELL_ELEMENT_2,SHELL_ELEMENT_3,SHELL_ELEMENT_4,S
HELL_ELEMENT_5,SHELL_ELEMENT_6
**************************************************************
*********MATERIAL DEFINITION
*SHELL SECTION, ELSET=SHELL_ELEMENT, MATERIAL=STEEL,offset=SNEG
<THICKNESS>
*MATERIAL,NAME=STEEL
*DENSITY
 7846,
*ELASTIC
 21000000000, 0.279
*SURFACE,TYPE=ELEMENT, NAME=SHELLSURF
SHELL_ELEMENT,SNEG
*SOLID SECTION, ELSET=WATER_ELEMENT, MATERIAL=WATER,
CONTROLS=CONVERT
*SECTION CONTROLS, NAME=CONVERT,ELEMENT CONVERSION=yes,CONVERSION
CRITERION=TIME



2,0
***K=300,K/G=1.E+6, (Actual K of water = 300000)
*MATERIAL, NAME=WATER
*VISCOSITY
1.0E-3,
*DENSITY
983.2,
*EOS, TYPE=USUP
45.85,0.,0.
**************************************************************
*********BOUNDARY DEFINITION
*NSET,NSET=EDGES,GENERATE
<NT1>,<NT4>,1
*BOUNDARY
EDGES,3,6,0.0
*INITIAL CONDITIONS, TYPE=STRESS, GEOSTATIC
WATER_ELEMENT,0.,<WATERCO>,<WATERPRESS>,0,1.,1.,
*surfaceinteraction, name=rough
*friction,rough
**************************************************************
*********AMPLITUDE DEFINITION
*INCLUDE, INPUT=AMP-TO-100.inp
**************************************************************
*********TIME OUT DEFINITION
*Filter, name=smooth, type=butterworth
2000,4
*Mass adjust, Target DT=7.528e-07
SHELL_ELEMENT, current
**************************************************************
*********STEP DEFINITION  11111111111111
*STEP
*DYNAMIC, EXPLICIT
```

```
,55
*Bulk Viscosity
0.06, 1.2
*Fixed Mass Scaling, elset=SHELL_ELEMENT, dt=7.528e-07,
type=below min
**
*contact, op=NEW
*contactinclusions,ALL EXTERIOR
*CONTACT PROPERTY ASSIGNMENT
,,rough
*DLOAD
WATER_ELEMENT, GRAV, 9.81, 0., 0.,-1.
*BOUNDARY,TYPE=ACCELERATION,AMPLITUDE=AMP-X
EDGES,1,1,1.
*BOUNDARY,TYPE=ACCELERATION,AMPLITUDE=AMP-Y
EDGES,2,2,1.
**********************************************************************
*********OUTPUT DEFINITION
*Restart, write, number interval=12, time marks=NO
*NSET, NSET=ALL_N
SHELL_NODE,WATER_NODE
*ELSET, ELSET=ALL_E
SHELL_ELEMENT,WATER_ELEMENT
*OUTPUT, FIELD, TIME MARKS=YES, NUMBER INTERVAL=550
*ELEMENT OUTPUT, ELSET=SHELL_ELEMENT
P,S,MISESMAX,SP,PRESS
*NODE OUTPUT, NSET=SHELL_NODE
UT
*OUTPUT, FIELD, TIME MARKS=YES, NUMBER INTERVAL=550
*ELEMENT OUTPUT, ELSET=WATER_ELEMENT
PRESS
*NODE OUTPUT, NSET=WATER_NODE
UT
*OUTPUT, HIST, FREQ=9999,filter=smooth
*ELEMENT OUTPUT, ELSET=SHELL_ELEMENT
SSAVG1,SSAVG2,SSAVG3,SSAVG4,SSAVG5,SSAVG6,S,SP,PRESS
*OUTPUT, HIST, FREQ=9999,filter=smooth
*ELEMENT OUTPUT, ELSET=WATER_ELEMENT
PRESS
*NODE OUTPUT, NSET=WATER_NODE
U3
*END STEP
```